SpringerBriefs in Computer Science

Mingcheng He · Huaqing Wu · Xuemin Shen

Resource Management for Satellite-Terrestrial Vehicular Networks

Springer

SpringerBriefs in Computer Science

SpringerBriefs present concise summaries of cutting-edge research and practical applications across a wide spectrum of fields. Featuring compact volumes of 50 to 125 pages, the series covers a range of content from professional to academic.

Typical topics might include:

- A timely report of state-of-the art analytical techniques
- A bridge between new research results, as published in journal articles, and a contextual literature review
- A snapshot of a hot or emerging topic
- An in-depth case study or clinical example
- A presentation of core concepts that students must understand in order to make independent contributions.

Briefs allow authors to present their ideas and readers to absorb them with minimal time investment. Briefs will be published as part of Springer's eBook collection, with millions of users worldwide. In addition, Briefs will be available for individual print and electronic purchase. Briefs are characterized by fast, global electronic dissemination, standard publishing contracts, easy-to-use manuscript preparation and formatting guidelines, and expedited production schedules. We aim for publication 8–12 weeks after acceptance. Both solicited and unsolicited manuscripts are considered for publication in this series.

**Indexing: This series is indexed in Scopus, Ei-Compendex, and zbMATH **

Mingcheng He · Huaqing Wu · Xuemin Shen

Resource Management for Satellite-Terrestrial Vehicular Networks

Springer

Mingcheng He
Waterloo, ON, Canada

Huaqing Wu
Calgary, AB, Canada

Xuemin Shen
Waterloo, ON, Canada

ISSN 2191-5768 ISSN 2191-5776 (electronic)
SpringerBriefs in Computer Science
ISBN 978-3-032-24525-0 ISBN 978-3-032-24526-7 (eBook)
https://doi.org/10.1007/978-3-032-24526-7

This Springer imprint is published by the registered company Springer Nature Switzerland AG
The registered company address is: Gewerbestrasse 11, 6330 Cham, Switzerland

Preface

Connected vehicle (CV) technology is expected to revolutionize future transportation systems by enabling real-time information exchange and content delivery through vehicular networks. By leveraging vehicle-to-everything (V2X) communication, a broad set of safety-critical and efficiency-oriented applications, such as cooperative perception, coordinated driving, remote operation, and content distribution, can be enabled to expand situational awareness, reduce response time, and smooth traffic flow. To support these advancements, vehicular networks must meet stringent requirements for global connectivity, low latency, and high reliability. Terrestrial networks, constrained by fixed infrastructure layouts, often struggle to maintain consistent network service across remote areas, rural regions, and during emergencies. Satellite-terrestrial vehicular networks (STVNs), which integrate low Earth orbit satellites to supplement terrestrial infrastructure, offer a heterogeneous architecture that provides resilient and ubiquitous connectivity. However, in STVNs, different terrestrial deployment strategies and satellite constellation designs lead to varying network availability, while inherent satellite mobility results in dynamic satellite coverage and visibility windows for CVs. These heterogeneities pose significant challenges in ensuring continuous and reliable network service in STVNs. Furthermore, in STVNs, diverse applications rely on multidimensional resources across communication, computing, and caching from both satellite and terrestrial networks, each exhibiting distinct constraints and time-varying availability. The spatiotemporal demand fluctuations driven by CV mobility further complicate the coordination of heterogeneous networks and the orchestration of multidimensional resources. As a result, effective network design and efficient resource management are essential for STVNs to operate reliably under the highly dynamic network environment and diversified service requirements.

In this monograph, we investigate resource management in STVNs, aiming to provide reliable network services for CVs and enable low-complexity and intelligent resource management. Chapter 1 provides an overview of STVN concepts, the slicing-based two-stage resource management framework, key technical challenges, and the objective of this monograph. Chapter 2 investigates state-of-the-art research work, including performance modeling and scheme design for STVN resource management at both reservation and operation stages. Chapter 3 develops theoretical communication models to characterize STVN performance under various satellite constellation configurations and terrestrial deployment strategies. The analysis evaluates key performance metrics, including service availability, outage probability, and throughput, revealing the joint impact of satellite mobility and terrestrial layout on network reliability and coverage. These results provide the analytical foundation for the design of resource management schemes in STVNs. Then, Chaps. 4 and 5 investigate resource management schemes for STVNs under a slicing-based two-stage framework. Specifically, Chap. 4 focuses on the reservation stage, studying HD map distribution in STVNs and proposing an adaptive resource slicing scheme to guarantee service-level agreements by coordinating time-varying satellite and terrestrial resources. Chapter 5 focuses on the operation stage, addressing cooperative environment sensing in STVNs and developing a real-time resource scheduling scheme under different connectivity patterns to cope with dynamic network conditions and varying service demands. Finally, Chap. 6 concludes the monograph and discusses potential future research directions. This monograph presents a systematic principle that provides a unified theoretical and practical framework for STVN design. This principle's primary value lies in its ability to: (1) boost efficiency by optimizing the use of multidimensional network resources; (2) maximize performance by fully leveraging the complementary strengths of satellite and terrestrial networks in vehicular environments; and (3) lay the groundwork for building resilient, scalable, and adaptive vehicular communication systems. By providing these essential design guidelines and analytical tools, this monograph greatly contributes to the evolution of intelligent transportation and inspires future innovations in integrated satellite-terrestrial systems.

We would like to thank Prof. Weihua Zhuang, Dr. Conghao Zhou, and Dr. Shisheng Hu from the Broadband Communications Research (BBCR) group at the University of Waterloo, for their valuable suggestions and help to this monograph. We would also like to thank all the members of the BBCR group for their support. Special thanks to the staff at Springer Nature, particularly Susan Lagerstrom-Fife and Reeshma K. P., for their invaluable help throughout the publication preparation process.

Waterloo, ON, Canada Mingcheng He
Calgary, AB, Canada Huaqing Wu
Waterloo, ON, Canada Xuemin Shen

Competing Interests The authors have no competing interests to declare that are relevant to the content of this manuscript.

Contents

Acronyms

3C	Communication, Computing, and Caching
3GPP	3rd Generation Partnership Project
5G	Fifth-Generation
AI	Artificial Intelligence
AP	Access Point
AWGN	Additive White Gaussian Noise
BS	Base Station
CAV	Connected and Automated Vehicle
CDF	Cumulative Distribution Function
CSTRS	Cooperative Satellite-Terrestrial Resource Scheduling
CV	Connected Vehicle
ECEF	Earth-Centered Earth-Fixed
ETSI	European Telecommunications Standards Institute
HD	High Definition
HPPO	Hybrid Proximal Policy Optimization
ITU	International Telecommunication Union
LEO	Low Earth Orbit
MDP	Markov Decision Process
MEC	Mobile Edge Computing
NHPP	Non-Homogeneous Poisson Process
NTN	Non-Terrestrial Network
PPO	Proximal Policy Optimization
PPP	Poisson Point Process
PSO	Particle Swarm Optimization
QoE	Quality of Experience
QoS	Quality of Service
RL	Reinforcement Learning
RoI	Range of Interest
RSU	Roadside Unit
SAGVN	Space-Air-Ground Integrated Vehicular Network
SBMA	Swap-Based Matching Algorithm

SDN	Software-Defined Networking
SSG	Satellite Service Group
STIN	Satellite-Terrestrial Integrated Network
STVN	Satellite-Terrestrial Vehicular Network
TLRS	Two-Layer Resource Slicing
TSG	Terrestrial Service Group
V2I	Vehicle-to-Infrastructure
V2N	Vehicle-to-Network
V2S	Vehicle-to-Satellite
V2V	Vehicle-to-Vehicle
V2X	Vehicle-to-Everything

Chapter 1
Introduction

Abstract Connected vehicles (CVs) are becoming a key component of intelligent transportation systems, enabling information exchange among vehicles, infrastructure, and surrounding environments to support diverse vehicular applications, such as cooperative perception, trajectory planning, and autonomous driving. These safety-critical and efficiency-oriented applications require vehicular networks with ubiquitous connectivity, low transmission latency, and high reliability. However, terrestrial vehicular networks are constrained by infrastructure deployment and geographic conditions, especially in remote or rural areas and emergency scenarios, leading to coverage gaps and unstable service. By integrating low Earth orbit (LEO) satellites with terrestrial infrastructures, satellite-terrestrial vehicular networks (STVNs) emerge as a promising architecture. Benefiting from global coverage, relatively low propagation latency, and dense constellation deployment, LEO satellites complement terrestrial networks to enable reliable, flexible, and ubiquitous service provisioning. This chapter first provides an overview of vehicular networks, representative application scenarios, and the architectural evolution from conventional terrestrial vehicular networks to STVNs. Then, a slicing-based two-stage resource management framework is presented, where large-timescale resource reservation and real-time resource orchestration design can effectively reduce decision complexity while preserving responsiveness to dynamic network conditions. Meanwhile, the key challenges for STVN resource management arising from satellite mobility, heterogeneous connectivity, and spatiotemporal service dynamics are discussed. Finally, the scope and organization of this monograph are outlined.

Keywords Resource management · Satellite-terrestrial vehicular networks · Connected vehicles · Vehicle-to-everything communications

M. He et al., *Resource Management for Satellite-Terrestrial Vehicular Networks*,
SpringerBriefs in Computer Science, https://doi.org/10.1007/978-3-032-24526-7_1

1.1 Overview of Satellite-Terrestrial Vehicular Networks

1.1.1 Connected Vehicle Applications and Service Requirements

As the number and density of vehicles continue to increase worldwide, transportation systems are facing three major challenges: traffic safety, congestion, and environmental impact. According to the U.S. National Highway Traffic Safety Administration (NHTSA), about 94% of traffic accidents are caused by human operational errors [1], and road traffic crashes result in approximately 1.19 million deaths annually worldwide [2]. Meanwhile, traffic congestion significantly prolongs commuting time, especially during rush hours, where drivers can experience dozens of hours of congestion each year. Inefficient transportation also leads to excessive fuel consumption and increased carbon emissions, which degrade air quality.

Driven by advances in sensing technologies, artificial intelligence (AI), and onboard computing platforms, modern vehicles are becoming increasingly intelligent. Specifically, vehicles can perceive surrounding environments using cameras, radar, and LiDAR sensors, and make driving decisions through embedded processing units. These capabilities enable vehicles to have faster reactions than human drivers and introduce the potential to substantially improve transportation safety and efficiency [3]. However, relying solely on single-vehicle intelligence has inherent limitations. The perception range of onboard sensors is restricted by line-of-sight conditions and extreme environments such as occlusion, heavy rain, snow, or fog. Moreover, decisions based solely on local observations cannot capture large-scale traffic dynamics, leading to suboptimal behaviors and inefficient coordination among vehicles. Therefore, relying only on standalone vehicle intelligence may struggle to accurately obtain surrounding information, compromising safety and reliability.

With the digitalization of transportation systems, vehicles are evolving from isolated transportation entities into networked information nodes to overcome the limitations of standalone perception and decision-making. Specifically, vehicles are able to continuously receive and exchange sensing information and driving intentions with surrounding vehicles and infrastructures through wireless communications. By enabling such interactions among vehicles and infrastructures, a communication network is formed on the road, referred to as a vehicular network. In this context, vehicles are transformed from standalone entities into connected vehicles (CVs). Through vehicle-to-everything (V2X) interactions, including vehicle-to-vehicle (V2V), vehicle-to-infrastructure (V2I), and vehicle-to-network (V2N) communications, CVs obtain information beyond onboard perception and cooperate with other traffic participants in vehicular networks [4, 5]. By combining local sensing with shared information, CVs enhance decision-making reliability and enable coordinated operations across the transportation system [6]. Accordingly, CVs can access diverse external information and leverage it to support a wide range of applications supporting safety-critical, efficiency-oriented, and infotainment services. Typical applications are summarized as follows [7]:

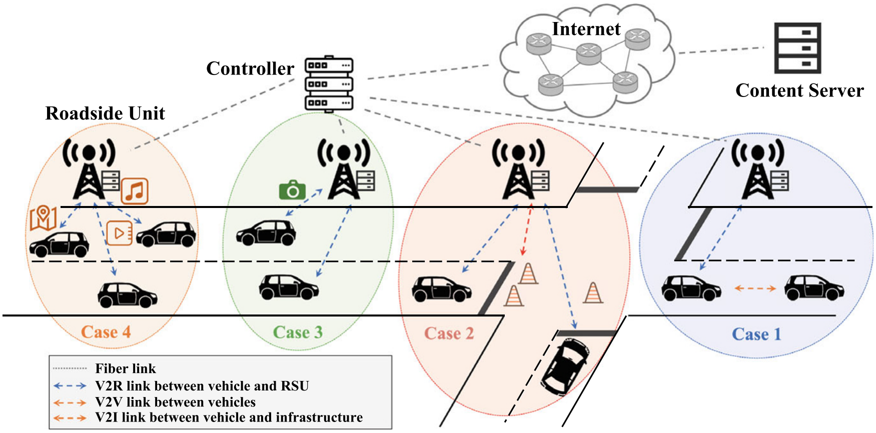

Fig. 1.1 An overview of connected vehicle applications

1. **Cooperative driving signaling**: CVs can exchange driving intentions and operation states with surrounding vehicles and infrastructures based on locally sensed and received information, shown as **Case 1** in Fig. 1.1. Such signaling enables cooperative maneuvers, e.g., lane changing, merging, and platooning, to optimize trajectories and reduce traffic disturbances. In emergency situations, such as sudden braking, warning messages can be rapidly disseminated to nearby vehicles, improving reaction timeliness and enhancing safety.
2. **Road safety warning**: Real-time safety-related warnings are of the utmost importance for connected vehicles to ensure driving safety, including collision warnings and road hazard alerts, such as signals, accidents, or roadwork, which are critical for preventing accidents. Through V2X communications, CVs can receive and disseminate warning messages, enabling early risk detection and appropriate maneuver decisions, shown as **Case 2** in Fig. 1.1.
3. **Traffic efficiency information**: To improve traffic flow efficiency, vehicles require dynamic environment information, including surrounding vehicle locations, traffic states, and road conditions. While onboard sensors provide local perception, infrastructure-assisted sensing can extend the observation range and mitigate sensing blind spots, shown as **Case 3** in Fig. 1.1. By continuously receiving such information, CVs can perform trajectory planning and navigation updates to avoid congestion and improve overall transportation efficiency.
4. **Infotainment and data services**: CVs can also obtain multimedia and data services, including high-definition (HD) maps, location-based services, and in-vehicle entertainment, by downloading from infrastructures to better support driving efficiency and provide a comfortable and convenient travel experience for passengers. Specifically, HD maps support accurate localization and navigation [8], while location-aware services enable automated parking, electronic toll collection, and personalized information services. Additionally, video streaming,

Table 1.1 CV application categories, use cases, and service requirements

Application categories	Use case examples	Transmission data rate	Delay	Reliability
Cooperative driving signaling	Cooperative maneuvers: lane changing, platooning	Low	$\leq$ 20 ms	99.99%
	Emergent situations	Low	$\leq$10 ms	99.9999%
Road safety warning	Collision warning	Low	$\leq$20 ms	99.9%
	Road hazard warning: signal violation, roadwork warning	Low	$\leq$100 ms	99.9%
Traffic efficiency information	Infrastructure-assisted environment perception	$\geq$ 10 Mbps	$\leq$100 ms	99%
Infotainment and data service	Automatic parking, electronic toll collect	Low	$\leq$500 ms	99%
	Delay-sensitive applications: live video streaming	$\geq$50 Mbps	$\leq$150 ms	90%
	Delay-tolerant applications: HD map distribution, vehicle software updating	$\sim$ 20 Mbps	Best effort	Best effort

audio, gaming, and augmented reality applications can enhance the passenger travel experience [9]. For instance, passengers may request some location-based content during their traveling to obtain updated restaurant or sight information with some audio or video content, shown as **Case 4** in Fig. 1.1.

Service requirements of CV applications vary significantly in terms of transmission data rate, delay, and reliability [7, 10–12], as summarized in Table 1.1. These metrics are commonly used to characterize the communication service quality required by CV applications and are defined as follows:

- *Transmission data rate*: The required data rate to successfully deliver application information within its delay constraint.

- *Delay*: The time from the occurrence of an event in the application scenario to the successful reception of the corresponding information, including both communication and processing latency, i.e., the end-to-end delay [7, 13].
- *Reliability*: The probability that the information is correctly delivered within a specified delay or freshness requirement [13].

Different CV applications place distinct requirements on these metrics, depending on how the transmitted information affects driving decisions and user experience. Safety-critical services, such as cooperative driving signaling and road safety warning, require ultra-low latency and extremely high reliability for a fast reaction because delayed or lost messages may directly lead to hazardous driving decisions. In contrast, traffic efficiency applications, such as navigation assistance, tolerate slightly higher latency but still demand consistent information freshness to maintain stable driving performance. Meanwhile, infotainment and map services usually involve large data volumes and flexible delay tolerance, but they still require reliable transmission to ensure user experience and service continuity. Moreover, delay and reliability requirements are often jointly constrained. Even if the average delay satisfies the requirement, an occasional large delay may still affect safety-critical decisions. Therefore, reliability essentially controls the tail distribution of latency, ensuring that time-critical information is delivered within strict deadlines, to improve driving safety and experience.

In summary, CVs improve road safety and travel experience by continuously exchanging information through V2X communications in vehicular networks to support diverse applications. Meanwhile, the heterogeneous service requirements make reliable information delivery essential, especially under high mobility and dynamic traffic conditions. Therefore, vehicular networks are expected to provide scalable and flexible network services, enabling both low-latency local interactions and global information acquisition for various CV applications.

1.1.2 Terrestrial Vehicular Networks

To support the diverse applications of CVs, wireless communication infrastructure deployed along roads forms terrestrial vehicular networks, which currently serve as the primary platform for V2X service provisioning, as shown in Fig. 1.1. By integrating direct short-range communication and cellular-based infrastructure access, terrestrial vehicular networks enable vehicles to exchange information with nearby traffic participants as well as remote network services.

At the local level, V2V communication allows nearby vehicles to directly disseminate time-critical messages within a short range. However, due to limited transmission power and communication distance, V2V links are mainly suitable for small packets and localized interactions, typically for cooperation driving and safety-related data transmission. To extend communication range and improve transmission reliability, infrastructure-assisted communication is introduced through roadside units (RSUs) and cellular base stations (BSs). With cellular V2X technologies such as LTE-V2X and NR-V2X, vehicles can access wide-area connectivity with higher data rate and more stable links [14, 15]. This enables delay-sensitive information delivery and supports data-intensive services, such as HD map updates, traffic state dissemination, and multimedia services, within the coverage area.

From a system architecture perspective, terrestrial vehicular networks are built upon heterogeneous ground communication systems, including cellular networks, Wi-Fi, and millimeter-wave communications. Modern cellular evolution toward ultra-dense small-cell deployment significantly improves spectrum efficiency and network throughput, allowing vehicles in urban areas to achieve high data rate and low latency access. Meanwhile, network nodes are interconnected through high-speed optical fiber backhaul, ensuring reliable large-volume data exchange across the network.

Meanwhile, some CV applications, such as environment sensing and video streaming, require a tremendous quantity of computing demand for data processing before transmitting the data to CVs. Traditional cloud-based computing introduces a large delay on the backhaul link, while modern terrestrial vehicular networks are increasingly integrated with mobile edge computing (MEC). By employing computing and caching resources at RSUs or BSs, data processing can be performed close to vehicles rather than in remote cloud servers. This reduces backhaul transmission delay and allows real-time processing of sensing data, which is particularly important for environment perception sharing and cooperative driving assistance. The availability of edge intelligence and caching further enables efficient content distribution and supports computation-intensive vehicular services. Overall, dense deployment of terrestrial infrastructure combined with MEC servers allows CVs to obtain low-latency communication, high data rate transmission, and local processing capability, making terrestrial vehicular networks capable of supporting most V2X applications in urban environments.

Despite these advantages, terrestrial vehicular networks still face inherent limitations in supporting CVs. First, network coverage may be geographically constrained, considering fixed terrestrial infrastructures and cost-sensitive deployment. In highways, rural regions, and sparsely populated areas, deploying and maintaining dense RSUs or BSs is costly and sometimes impractical. Consequently, vehicles may experience intermittent connectivity or even complete service interruption, which degrades CV applications requiring continuous network access. Second, terrestrial networks provide limited flexibility in highly dynamic vehicular scenarios. Traffic demand varies significantly across time and space, for example, between rush hours and off-peak periods or between urban and suburban areas. Static infrastructure capacity cannot efficiently adapt to these variations, leading to network congestion in hotspot areas and resource underutilization in low-density regions. Frequent handovers caused by high mobility further affect communication stability.

Therefore, relying solely on terrestrial vehicular networks cannot guarantee ubiquitous and reliable network availability for CVs, especially under high mobility and uneven traffic distribution conditions. To provide seamless connectivity and flexible resource provisioning, additional dimensions beyond ground infrastructure are required.

1.1.3 LEO Satellite-Assisted Vehicular Networks

Although terrestrial vehicular networks can effectively support most CV services in urban environments, their performance strongly depends on infrastructure deployment density and geographic conditions. In highways, rural regions, oceans, or mountainous areas, ground infrastructure may be sparse or unavailable, leading to service interruption and degraded application performance. To provide global connectivity and service continuity beyond the coverage of terrestrial infrastructure, satellite communication has emerged as an important complementary networking paradigm for future wireless networks [16].

Satellite networks consist of satellites operating at different orbital altitudes, including geostationary Earth orbit (GEO), medium Earth orbit (MEO), and low Earth orbit (LEO) [17]. Although GEO and MEO satellites provide extremely large coverage footprints and relatively stable links, their high orbit altitude introduces substantial long propagation delay, which cannot meet the stringent delay requirements of most CV applications. In contrast, LEO satellites operate at much lower altitudes, typically from hundreds to a few thousand kilometers [18], significantly reducing signal propagation delay and enabling latency comparable to terrestrial communications. In addition, satellite infrastructure is less affected by local disasters or infrastructure failures, providing robust communication support for safety-related services. With dense constellation deployment and steerable beams, LEO satellites can provide large-scale and continuous connectivity to CVs over broad regions [19].

Modern LEO satellites are evolving from traditional relay nodes operated in transparent modes into space network access platforms capable of directly serving CVs. Operating in regenerative communication modes, satellites can process and route signals onboard and provide wide-area V2N connectivity. Through large-scale constellation deployment, LEO satellite networks enable near-continuous connectivity over wide geographical regions, supporting vehicles traveling across cities, highways, and remote areas. Meanwhile, satellite communication naturally supports broadcast and multicast transmissions due to its top-down feature, enabling efficient large-scale information dissemination, such as traffic information dissemination, software updates, and map distribution.

In addition to communication capability, LEO satellites can also carry MEC servers, enabling onboard computing and caching capabilities. By processing or caching data directly in space, part of the service workload can be handled closer to CVs compared with remote cloud centers or ground stations, reducing backhaul dependency and improving responsiveness for CV applications [20]. In this case, LEO satellites have attracted substantial attention from academia and industry due to the global network availability and flexible resource provisioning.

Despite these advantages, LEO satellite-assisted vehicular networks also exhibit inherent characteristics that differentiate them from terrestrial networks. Due to the high velocity of LEO satellites, which can be 7.56 km/s, the coverage area of satellites changes over time, resulting in a highly dynamic satellite network topology. In this case, satellite–CV links vary continuously over time, resulting in dynamic link quality and periodic service availability. Furthermore, due to the constrained power and high-cost MEC servers on LEO satellites, onboard resources, including bandwidth, computing, and caching capacity, are limited compared with terrestrial infrastructure. In addition, although the propagation delay of LEO satellites is much smaller than that of satellites in higher orbits, it remains non-negligible for real-time interactive applications.

Overall, satellite networks are particularly suitable for providing global connectivity and large-scale information support, rather than replacing local and low-latency terrestrial communications. Consequently, LEO satellite networks serve as an indispensable integration to vehicular networking by complementing terrestrial coverage and enabling ubiquitous connectivity for CVs.

1.1.4 Integrated Architecture of Satellite-Terrestrial Vehicular Networks

Neither terrestrial vehicular networks nor LEO satellite networks alone can fully satisfy the heterogeneous service requirements of CVs. Terrestrial infrastructure provides low-latency and high-capacity communication in local regions but suffers from limited coverage and deployment cost. Conversely, LEO satellite networks offer global connectivity and efficient large-scale data dissemination, which however exhibit dynamic connectivity and constrained onboard resources. Therefore, integrating satellite and terrestrial networks into a unified vehicular communication architecture becomes a potential approach to enable seamless, flexible, and cost-effective network services [21, 22], which form satellite-terrestrial vehicular networks (STVNs).

In STVNs, ground infrastructure and satellite systems jointly serve CVs through coordinated access and resource provisioning [23], as shown in Fig. 1.2. Vehicles can connect to RSUs, cellular BSs, and LEO satellites via heterogeneous wireless links, and may operate in single-connectivity or multi-connectivity modes depending on service requirements and link conditions [24]. Meanwhile, terrestrial nodes are interconnected through high-capacity wired backhaul, and satellite feeder links connect ground stations to satellite constellations, enabling data exchange across network segments. Through such hierarchical connectivity, CVs can access both nearby low-latency terrestrial networks and wide-reaching satellite networks within a unified networking framework.

From a service perspective, the integrated architecture leverages the complementary characteristics of the two network segments. Local and delay-critical interac-

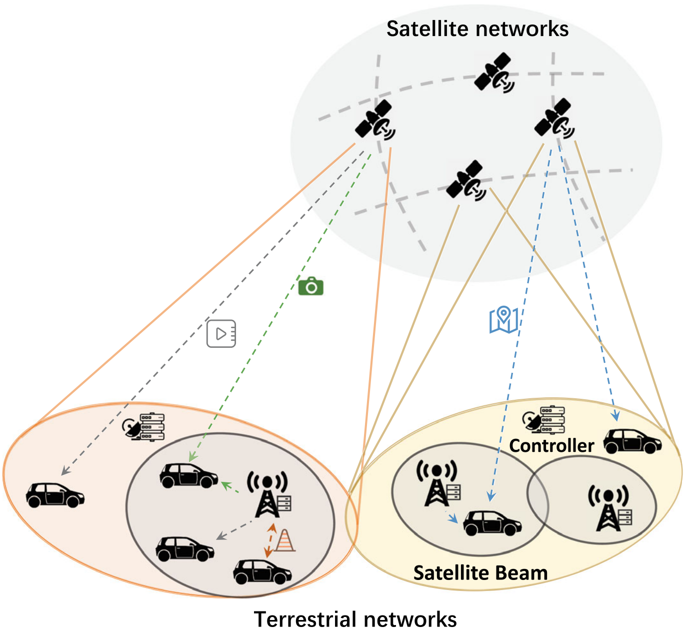

Fig. 1.2 Satellite-terrestrial vehicular network architecture

tions, such as cooperative driving signaling and safety warning, are mainly supported by terrestrial communications. In contrast, popular information dissemination, large-volume content delivery, and connectivity continuity are efficiently supported by LEO satellites. Moreover, satellite multicast transmission and terrestrial unicast transmission can be jointly utilized to improve spectrum efficiency and reduce redundant transmissions.

The integrated architecture also enables flexible resource provisioning across heterogeneous network domains. When terrestrial infrastructure experiences congestion or limited coverage, traffic can be offloaded to satellites to maintain service continuity. Conversely, when vehicles are located in dense urban regions, terrestrial networks can provide high-rate and low-latency communication, while satellites offer supplementary support such as backup connectivity. Through coordinated operation, STVNs can adapt to spatially and temporally varying traffic demands.

Overall, the satellite–terrestrial integrated architecture forms a unified vehicular networking paradigm that combines local responsiveness with global accessibility. By jointly exploiting complementary communication characteristics, STVNs provide the foundation for scalable, reliable, and flexible service provisioning for diverse CV applications.

1.2 Two-Stage Resource Management Technology

Although the integrated satellite–terrestrial architecture enables ubiquitous connectivity, efficient service provisioning in STVNs remains challenging due to heterogeneous service requirements and highly dynamic network conditions. Different CV applications demand distinct delay, reliability, and data-rate guarantees, while available communication, computing, and caching resources vary over time because of satellite mobility. Consequently, treating all services and users in a unified manner leads to inefficient utilization and unstable quality of service.

To systematically organize diversified services over shared infrastructures, resource slicing is introduced as a service-oriented network management paradigm [25, 26]. By logically partitioning physical resources into multiple customized virtual service networks, referred to as slices, different application categories can be supported with isolated resources tailored to differentiated performance provisioning. Such a structured abstraction simplifies service orchestration over heterogeneous satellite–terrestrial resources while maintaining isolation among applications.

However, due to the high complexity of multi-dimensional resource orchestration and the coexistence of slow-varying network characteristics, such as traffic demand evolution and satellite visibility, and fast-varying dynamics, including channel variation and instantaneous vehicle access, resource management in STVNs naturally involves decisions at different timescales. To handle such multi-timescale characteristics, a slicing-based two-stage resource management paradigm is proposed. In the large-timescale reservation stage, network resources are reserved for different slices according to predicted demand and network conditions. In the real-time operation stage, reserved resources are then allocated to individual CVs to adapt to instantaneous variations. This hierarchical design significantly reduces management complexity while maintaining service performance.

1.2.1 STVN Resource Management Framework

To support heterogeneous CV applications over STVNs, multi-dimensional resources must be coordinated across different network segments and domains. In STVNs, communication, computing, and caching (3C) resources are distributed among LEO satellites, RSUs, and BSs, and their availability varies over time due to satellite mobility and dynamic traffic. Meanwhile, CV task requests arrive at fine time granularity and require an instantaneous response. The coexistence of long-term resource variation and short-term service dynamics makes direct per-CV resource management highly complex.

To address this issue, a slicing-based resource management framework is adopted in STVNs, illustrated in Fig. 1.3, which separates service-level orchestration from real-time execution, enabling scalable control and fast adaptation under highly dynamic environments [27]. Instead of directly scheduling resources for individual

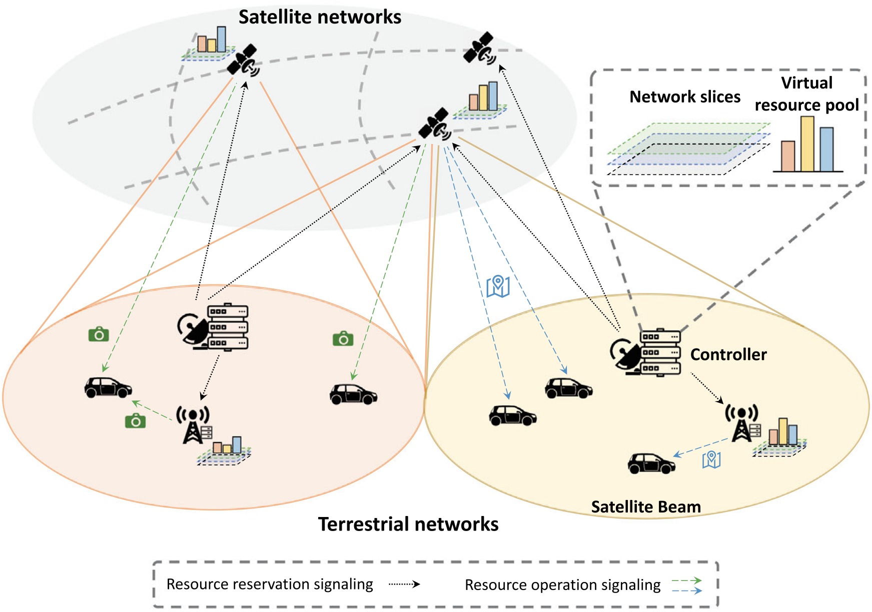

Fig. 1.3 Slicing-based two-stage resource management framework in STVNs

CVs across all network entities, multi-dimensional resources from both terrestrial and satellite segments are first abstracted into a unified virtual resource pool and partitioned into multiple network slices. Each slice corresponds to a class of CV applications with similar service requirements, enabling aggregated service-level control rather than vehicle-level global optimization. Different slices coexist on the same physical network but operate independently with isolated resources, enabling customized performance provisioning and satisfactory service requirements. For example, as shown in Fig. 1.3, three different slices are established with specified service requirements. The three slices are built on the same physical network, but manage multi-dimensional resources separately and independently in each slice. This resource abstraction reduces decision dimensionality and allows differentiated service provisioning.

Based on the resource abstraction, the resource management framework follows a hierarchical control structure, consisting of a central controller responsible for the reservation stage management and distributed local controllers responsible for the operation stage in real-time [28, 29].

The central controller, deployed in the terrestrial network, is responsible for global resource orchestration across RSUs, BSs, and LEO satellites. By collecting network status and predicted demand, the controller constructs a time-varying virtual resource pool and partitions resources for each slice by reserving resources in each network component. This mechanism allows safety-critical services, traffic information services, and infotainment services to coexist while satisfying distinct service requirements through resource isolation without mutual interference. Generally, the slicing decisions should be adjusted from time to time to guarantee high performance of service provisioning, which is referred to as a slicing window, related to the variation of available resources and service demand. The resource reservation focuses on service-level provisioning rather than resource scheduling for individual CV, allowing the system to adapt resource distribution to traffic evolution and satellite mobility.

The local controllers, located at RSUs and LEO satellites, perform real-time resource allocation according to the reserved slice resources. Given instantaneous network conditions, including channel states, vehicle mobility, and task requests, local controllers allocate multi-dimensional resources to individual CVs to satisfy different service requirements. Since different services exhibit distinct latency and reliability demands, scheduling policies are slice-dependent. For example, safety-critical services prioritize reliable and low-latency transmission, while data-intensive services emphasize throughput efficiency. Meanwhile, each local controller continuously reports resource utilization and service satisfaction to the central controller, enabling future slice adjustment.

Through this hierarchical architecture, the central controller performs slice-oriented resource reservation based on global information, whereas local controllers execute real-time allocation to cope with rapid network dynamics. Such a slicing-based architecture enables scalable and flexible resource management across satellite and terrestrial networks while satisfying differentiated service requirements for diverse CV applications.

1.2.2 Slicing-Based Two-Stage Resource Management Workflow

Based on the hierarchical slicing-based architecture, resource management in STVNs operates through a two-stage workflow, consisting of a large-timescale reservation stage and a real-time operation stage, illustrated in Fig. 1.4. The two stages operate at different timescales and cooperate to handle the coexistence of resource variation and service dynamics in vehicular environments.

The reservation stage performs service-level resource provisioning over a relatively large timescale (e.g., minutes to hours). The objective is to determine how much multi-dimensional resource should be reserved for each slice according to predicted service demand and time-varying resource availability. During each slicing window, the following procedures are executed:

- *Global information collection*: The central controller aggregates system-wide information from RSUs, BSs, and LEO satellites, including available communication, computing, caching capacity, satellite visibility duration, and slice resource utilization. Meanwhile, CVs periodically report mobility statistics, service request history, and QoS satisfaction level, forming the basis for resource planning.

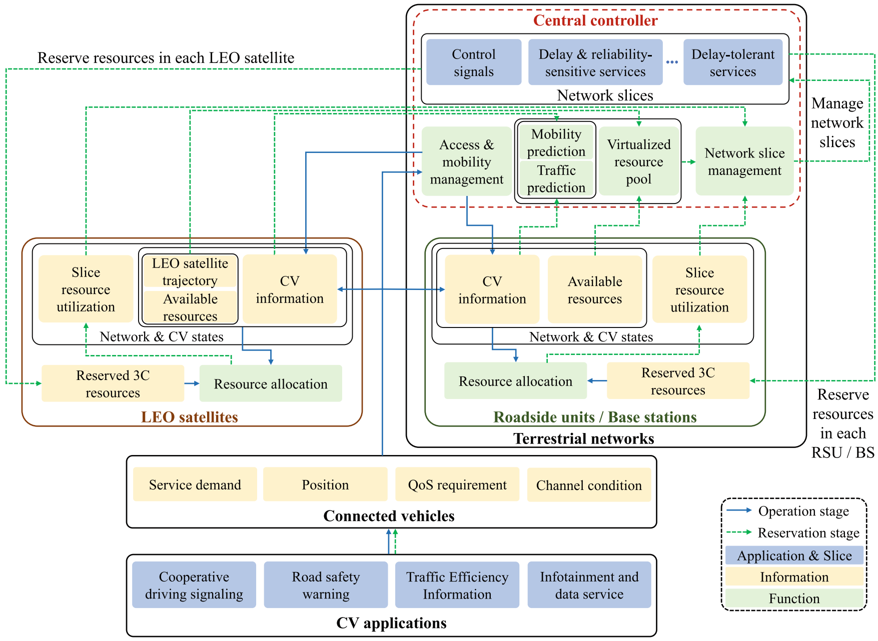

Fig. 1.4 Slicing-based resource management workflow in STVNs

- *Mobility and traffic prediction*: Using historical vehicle trajectories and application request patterns, the controller predicts time-varying satellite coverage, spatial vehicle distribution, and aggregated service demand for each slice.
- *Virtualized resource pool construction*: Multi-dimensional resources from satellite and terrestrial networks are abstracted into a unified virtual resource pool. Because satellite coverage varies over time, the pool is time-varying and reflects expected resource availability over time windows.
- *Network slice management*: Based on predicted demand and available virtual resources, the controller updates the slice configuration by partitioning the resource pool into multiple slices corresponding to different application classes. Specifically, for each slice, the controller determines the reserved proportion of 3C resources, maps virtual resources onto physical resources across terrestrial and satellite entities, and reserves resources for the upcoming slicing window.

The reservation stage determines the service capacity of each slice rather than scheduling individual CVs, and it is periodically updated to adapt to traffic evolution and satellite visibility variation.

The operation stage executes fine-grained resource allocation for individual CVs over a short timescale (e.g., milliseconds). Given the reserved slice resources, local controllers at RSUs and LEO satellites dynamically allocate communication, computing, and caching resources according to instantaneous network conditions. For each service request, the following procedures are executed:

- *Session creation*: When a CV initiates sensing, data transmission, or content retrieval, a service session is established and associated with a corresponding network slice based on its QoS requirement.
- *State information collection*: When the session is created, the network entities collect instantaneous state information, including channel quality, CV mobility state, slice resource utilization, and satellite coverage status.
- *Access and mobility management*: According to service type and network conditions, the system determines the appropriate access node serving the CV. For a mobile CV, handover or multi-connectivity decisions may be performed to maintain service continuity [30].
- *Real-time resource allocation*: Within the reserved slice resources, the network entity allocates communication, computing, and caching resources to individual CVs. Allocation decisions dynamically adapt to dynamic STVN environments to satisfy delay and reliability requirements.
- *Monitoring and feedback*: Different metrics such as delay, reliability, and resource utilization are measured and reported to the central controller, forming feedback for future slice adjustment and demand prediction refinement.

To summarize, from the slicing-based two-stage resource management workflow, the reservation stage performs service-level provisioning, and the operation stage serves for QoS satisfaction for each CV through real-time adaptation under dynamic STVN environments.

1.3 Technical Challenges

Despite the proposed slicing-based two-stage architecture providing a systematic framework for resource management in STVNs, efficient resource management and practical realization are still not sufficiently studied. Specifically, STVNs are fundamentally different from conventional terrestrial vehicular networks, where network topology is time-varying, service demand evolves dynamically, resource dimensions are tightly coupled, and connectivity patterns differ across infrastructures. These characteristics prevent the direct application of traditional resource slicing or resource scheduling methods, with the following essential challenges:

1. **Geometry-dependent network availability**: In STVNs, communication availability is determined not only by wireless channel conditions but also by satellite orbital geometry. Due to satellite movement and Earth rotation, the network topology itself becomes time-varying at the scale of resource management, where link duration, service continuity, and achievable throughput vary over time and location. Unlike terrestrial vehicular networks, where connectivity is almost stable during scheduling, STVN resource provisioning depends on predicting when a satellite is visible and how long the connection persists. Therefore, resource management cannot be designed independently of network modeling, which makes analytical performance characterization non-trivial and fundamental.

2. **Dynamic network environments**: In vehicular environments, traffic density and application requests change rapidly across time and space, while satellite visibility simultaneously affects resource availability. As a result, both service demand and available resources in STVNs fluctuate concurrently. Such dual dynamics make resource provisioning and slice configuration different from terrestrial networks, where a fixed slicing window length is inadequate for STVNs. Specifically, resource reservation cannot directly rely on traffic statistics in a long slicing window, which may risk a mismatch once satellite resources or vehicle density change, resulting in degraded service performance. Frequent slice reconfiguration, however, introduces high overhead and instability. Therefore, the STVNs must continuously balance slice stability and adaptability under jointly time-varying demand and resource conditions.
3. **Complicated multi-dimensional decision-making**: In STVNs, 3C resources are jointly provided by satellite and terrestrial infrastructures, and their effects on service performance are tightly coupled. For instance, increasing transmission bandwidth without sufficient computing resources does not reduce end-to-end delay, while executing the same task over satellite and terrestrial networks leads to different optimal 3C resource coupling because of their heterogeneous propagation delay, processing capabilities, and resource costs. Moreover, resource allocation decisions also affect future system states, such as queue evolution, resource availability, and service satisfaction. Therefore, resource management is regarded as a sequential decision-making problem, where current actions influence long-term performance. Solving such a problem to manage multi-dimensional resources under uncertainty and dynamic environments is complicated.
4. **Heterogeneous connectivity patterns**: In STVNs, satellite and terrestrial networks exhibit different connectivity behaviors. Specifically, satellites offer continuous availability over a service duration with their extensive coverage, but usually involve higher propagation delay and resource cost. In contrast, terrestrial links provide low latency and efficient unicast transmission, while the network connectivity is affected by vehicle mobility with frequent handovers. Meanwhile, different services may prefer different transmission mechanisms. For example, large-scale common information is efficiently delivered via satellite multicast, while delay-sensitive or customized data primarily relies on terrestrial unicast communication. Consequently, resource scheduling must adapt to distinct service demands, changing connectivity conditions, and transmission modes to maintain service continuity and pursue resource efficiency, which significantly complicates real-time control design.

Given the above challenges, supporting diverse CV applications over STVNs necessitates the study of resource management under dynamic and heterogeneous network environments to improve resource efficiency while satisfying distinct service requirements of CV applications in STVNs.

1.4 Aim of the Monograph

In this monograph, we focus on efficient resource management for STVNs that support diverse CV applications under highly dynamic environments to tackle the above-mentioned challenges. In particular, we investigate theoretical modeling for STVN performance analysis under diverse satellite constellation configurations and terrestrial deployment strategies, which lay the foundation of resource management in STVNs. Furthermore, we present model-data co-driven resource management schemes for the reservation stage and the operation stage orchestration in STVNs, respectively. These works efficiently manage multi-dimensional resources across satellite and terrestrial networks, aiming to provide reliable network services for CVs and enable low-complexity and intelligent resource management.

In Chap. 2, we provide state-of-the-art research related to the monograph. First, performance modeling methods for STVN resource management evaluation are introduced. Then, existing resource management schemes in terms of reservation-stage resource slicing and operation-stage resource scheduling are discussed.

In Chap. 3, we develop tractable theoretical models for performance analysis for STVNs. By explicitly evaluating satellite orbital characteristics, constellation parameters, and terrestrial deployment strategies, analytical expressions of service availability, outage probability, and system throughput are derived. The analysis reveals the joint impact of satellite mobility and terrestrial layout on network reliability and coverage, providing theoretical guidelines for resource management.

Under the theoretical performance modeling for STVN resource management, Chaps. 4 and 5 investigate resource management schemes under the slicing-based two-stage framework for STVNs. In Chap. 4, we focus on reservation-stage resource management for HD map distribution in STVNs. Leveraging both multicast and unicast transmissions that can support map delivery with different characteristics from satellite and terrestrial networks, a two-slice architecture is designed to cooperatively support the service. To cope with spatiotemporal demand fluctuations, time-varying satellite availability, and multi-dimensional resource coupling, the resource slicing problem is formulated as a sequential decision-making problem. Aiming to minimize the long-term system cost, a hybrid data-model co-driven approach-based two-layer resource slicing scheme is proposed, with the integration of reinforcement learning-based adaptive slice management in the outer layer and optimization-based caching and multicast determination in the inner layer. The proposed scheme can effectively balance flexibility and computational efficiency in dynamic and heterogeneous STVNs.

In Chap. 5, we investigate operation-stage resource scheduling for infrastructure-assisted environment sensing. To satisfy stringent sensing freshness and reliability requirements under dynamic network conditions, a cooperative satellite–terrestrial resource scheduling scheme is proposed that jointly optimizes sensing decisions and real-time resource allocation for efficient resource consumption. By exploiting satellite multicast capability, CV clustering and sensing interval determination are first exploited by leveraging the coalition game optimization-based algorithm to reduce resource consumption and scheduling complexity, while a reinforcement learning-based algorithm is then employed to allocate computing and communication resources in real time to adapt to CV dynamics.

Finally, we conclude this monograph and discuss potential future research directions of resource management in STVNs in Chap. 6.

References

1. Singh, S.: Critical reasons for crashes investigated in the national motor vehicle crash causation survey. NHTSA, US Department of Transportation 2, 1–2 (2015)
2. Global status report on road safety, World Health Organization (2023)
3. J. Van Brummelen, M. O'Brien, D. Gruyer, H. Najjaran: Autonomous vehicle perception: The technology of today and tomorrow. Transp. Res. C, Emerg. Technol. **89**, 384–406 (2018)
4. Montanaro, U., Dixit, S., Fallah, S., Dianati, M., Stevens, A., Oxtoby, D., Mouzakitis, A.: Towards connected autonomous driving: review of use-cases. Veh. Syst. dynamics **57**(6), 779–814 (2019)
5. Wang, H., Liu, T., Kim, B., Lin, C.W., Shiraishi, S., Xie, J., Han, Z.: Architectural design alternatives based on cloud/edge/fog computing for connected vehicles. IEEE Commun. Surveys Tuts. **22**(4), 2349–2377 (2020)
6. Wang, Z., Zhu, H., He, M., Zhou, Y., Luo, X., Zhang, N.: GAN and multi-agent DRL based decentralized traffic light signal control. IEEE Trans. Veh. Technol. **71**(2), 1333–1348 (2021)
7. 5GAA: C-V2X Use Cases Volume II: Examples and Service Level Requirements, (2020). White paper
8. He, M., Luo, X., Wang, Z., Yang, F., Qian, H., C.: Hua: Global traffic state recovery via local observations with generative adversarial networks. In: IEEE ICASSP, pp. 3767–3771. (2020)
9. Zhou, C., Gao, J., Li, M., Cheng, N., Shen, X., Zhuang, W.: Digital twin-based 3D map management for edge-assisted device pose tracking in mobile AR. IEEE Internet Things J. **11**(10), 17812–17826 (2024)
10. ETSI: Intelligent transport systems (ITS); vehicular communications; basic set of applications; definitions, p. 638. (2009). Technical Report
11. Wang, J., Liu, J., Kato, N.: Networking and communications in autonomous driving: A survey. IEEE Commun. Surveys Tuts. **21**(2), 1243–1274 (2018)
12. Amjad, Z., Sikora, A., Hilt, B., Lauffenburger, J.P.: Low latency V2X applications and network requirements: Performance evaluation. In: Proc. IEEE IV, pp. 220–225. (2018)
13. 3GPP: Service requirements for enhanced V2X scenarios, (2025). Technical Specification version 19.0.0, release 19
14. 3GPP: NR and NG-RAN overall description, (2026). Technical Specification version 19.1.0, release 19
15. Shen, X., Gao, J., Li, M., Zhou, C., Hu, S., He, M., Zhuang, W.: Toward immersive communications in 6G. Front. Comput. Sci. **4**, 1068478 (2023)
16. Cheng, N., He, J., Yin, Z., Zhou, C., Wu, H., Lyu, F., Zhou, H., Shen, X.: 6G service-oriented space-air-ground integrated network: A survey. Chinese J. Aeronaut. **35**(9), 1–18 (2022)
17. Su, Y., Liu, Y., Zhou, Y., Yuan, J., Cao, H., Shi, J.: Broadband LEO satellite communications: Architectures and key technologies. IEEE Wireless Commun. **26**(2), 55–61 (2019)
18. 3GPP: Study on new radio (NR) to support non-terrestrial networks, (2020). version 15.4.0, release 15
19. Wu, H., He, M., Shen, X., Zhuang, W., Dao, N., Shi, W.: Network performance analysis of satellite-terrestrial vehicular network. IEEE Internet Things J. **11**(9), 16829–16844 (2024)
20. He, M., Zhou, C., Wu, H., Shen, X.: Learning-based cache placement and content delivery for satellite-terrestrial integrated networks. In: Proc. IEEE GLOBECOM, pp. 1–6. (2021)

21. Zhang, N., Zhang, S., Yang, P., Alhussein, O., Zhuang, W., Shen, X.: Software defined space-air-ground integrated vehicular networks: Challenges and solutions. IEEE Commun. Mag. **55**(7), 101–109 (2017)
22. Hong, T., Zhao, W., Liu, R., Kadoch, M.: Space-air-ground IoT network and related key technologies. IEEE Wireless Commun. **27**(2), 96–104 (2020)
23. C. Zhou, H. Wu, M. He, W. Wu, N. Cheng, X. Shen: Adaptive access mode selection in space-ground integrated vehicular networks. In: Proc. IEEE GLOBECOM, pp. 1–6 (2021)
24. He, M., Hua, C., Xu, W., Gu, P., Shen, X.: Delay optimal concurrent transmissions with raptor codes in dual connectivity networks. IEEE Trans. Netw. Sci. Eng. **8**(2), 1478–1491 (2021)
25. Wijethilaka, S., Liyanage, M.: Survey on network slicing for Internet of things realization in 5G networks. IEEE Commun. Surveys Tuts. **23**(2), 957–994 (2021)
26. Zhou, C., Gao, J., Li, M., Shen, X., Zhuang, W., Li, X., Shi, W.: AI-assisted slicing-based resource management for two-tier radio access networks. IEEE Trans. Cogn. Commun. Netw. **9**(6), 1691–1706 (2023)
27. He, M., Wu, H., Zhou, C., Hu, S., Shen, X., Zhuang, W.: Adaptive multi-dimensional resource slicing in cognitive satellite-terrestrial vehicular networks. IEEE Trans. Cogn. Commun. Netw. **12**, 3191–3208 (2026)
28. Shen, X., Gao, J., Wu, W., Lyu, K., Li, M., Zhuang, W., Li, X., Rao, J.: AI-assisted network-slicing based next-generation wireless networks. IEEE Open J. Veh. Technol. **1**, 45–66 (2020)
29. Zhou, C., Gao, J., Li, M., Shen, X., Zhuang, W.: Digital twin-empowered network planning for multi-tier computing. J. Commun. Inf. Netw. **7**(3), 221–238 (2022)
30. He, M., Hua, C., Gu, P.: Design and analysis for dual connectivity and raptor codes assisted handover in vehicular networks. In: IEEE WCNC, pp. 1–7. (2020)

Chapter 2
State-of-the-Art Research for STVN Resource Management

Abstract This chapter reviews state-of-the-art research on resource management for satellite–terrestrial vehicular networks (STVNs). We first summarize representative performance modeling studies characterizing the time-varying communication conditions from Low Earth Orbit (LEO) satellite operation, which provide quantitative foundations for resource management. Then, we review existing resource management schemes from a two-timescale perspective, covering reservation-stage resource slicing for long-term planning and operation-stage resource scheduling for real-time adaptation. Overall, this chapter organizes the current literature into a coherent view of performance model and scheme design for resource management in STVNs.

Keywords Satellite-terrestrial vehicular networks · Low Earth orbit satellites · Resource slicing · Resource scheduling

2.1 Performance Modeling Research

Motivated by the increasing demand for ubiquitous and reliable connectivity, Low Earth Orbit (LEO) satellite networks have become an important complement to traditional terrestrial communication infrastructures. By extending coverage to remote and underserved areas and providing significantly lower propagation latency than legacy satellite systems, LEO constellations form a fundamental enabler of satellite-terrestrial vehicular networks (STVNs). In STVNs, network performance is closely related to satellite motion, service operation requirements, and network organization across heterogeneous segments. Quantifying such coupled and time-varying communication behavior is essential for resource management, which relies on the achievable service reliability over time and space. This section briefly summarizes the communication characteristics in STVNs that motivate performance modeling, and reviews representative analytical modeling studies for STVN resource management.

Communication behavior in STVNs is influenced by the physical and communication properties of satellite systems, which are generally categorized by different orbital altitudes. While Geostationary Earth Orbit (35,786 km) and Medium Earth

M. He et al., *Resource Management for Satellite-Terrestrial Vehicular Networks*, SpringerBriefs in Computer Science, https://doi.org/10.1007/978-3-032-24526-7_2

Orbit (7,000–20,000 km) satellites provide wide coverage, their round-trip propagation delays may exceed 100 ms [1], struggling to meet the stringent latency requirements of vehicular services. In contrast, LEO satellites, orbiting at altitudes between 600 and 1,500 km, can reduce propagation delays to less than 10 ms, making them more suitable for diverse CV applications.

Modern LEO constellations typically operate in transparent or regenerative relaying modes [2], and their communication conditions exhibit strong spatiotemporal variations due to several key factors. First, the spectrum in Ku-band (12–18 GHz) and Ka-band (26–40 GHz) are primarily utilized in LEO systems, which can improve satellite communication throughput but introduce higher sensitivity to atmospheric attenuation and cross-system interference, especially under spectrum coexistence with terrestrial networks [3, 4]. Second, to achieve global coverage, LEO satellites are organized into specific constellations, most commonly Walker Delta or Walker Star topologies [5], which differ in orbital arrangement and coverage characteristics and directly influence link dynamics and network connectivity, yet also bring time-varying link availability under satellite mobility and line-of-sight constraints [5]. Third, unlike the fixed beams of traditional systems, modern LEO satellites employ phased-array technology to dynamically shape and track beams [2]. This allows the satellite to compensate for its high-speed motion and maintain focus on specific geographical areas or high-priority vehicular clusters. On the other hand, dynamic beam footprints, as well as frequent satellite and beam handovers, lead to rapidly changing channel quality and service duration for ground users [2, 6–8].

In practice, STVNs are expected to provide continuous connectivity across moving coverage areas and heterogeneous access segments. Standardization efforts from the 3rd Generation Partnership Project (3GPP) on non-terrestrial networks emphasize global connectivity and service continuity in integrated satellite-terrestrial operation [1, 2, 9], while convergence principles and system-level frameworks are also discussed in the International Telecommunication Union (ITU) recommendations [10, 11]. Therefore, LEO-induced mobility and dynamic coverage make both link quality and connectivity duration highly time-dependent communication performance in STVNs, which should be characterized over a spatiotemporal modeling beyond instantaneous link evaluations.

Motivated by this requirement, a range of analytical modeling approaches has been developed to quantify the performance of satellite and satellite-terrestrial integrated networks. Stochastic geometry has been widely adopted to characterize link reliability and system throughput under satellite mobility and heterogeneous interference [12]. The outage probability and throughput of LEO satellite and satellite-terrestrial downlink systems are analyzed in [13, 14], respectively. Signal quality distributions in relay-assisted integrated networks are further investigated in [15]. To capture the effects of satellite motion, non-stationary channel models describing time-varying distances between satellites and ground users are proposed in [16], while terrestrial-satellite interference is examined in [17]. In addition, protocol-layer impacts of satellite channel characteristics are discussed in [18].

These studies indicate that communication performance in STVNs depends jointly on satellite dynamics and terrestrial deployment to capture spatiotemporal variability and cross-segment interactions, which can provide system-level evaluation of service availability and reliability and are regarded as an essential basis for STVN resource management. While existing performance modeling provides tractable insights, some satellite-related motion, constellation-parameter-dependent geometry, and the resulting time-varying topologies in practical LEO satellite systems are rarely considered. To bridge this gap and support resource management evaluation, Chap. 3 develops theoretical modeling for STVN performance analysis under realistic constellation settings by explicitly accounting for key constellation parameters and further examines how terrestrial deployment strategies jointly shape service availability, outage probability, and throughput.

2.2 Reservation-Stage Resource Slicing

STVNs support diverse CV applications with heterogeneous delay, reliability, and data-rate requirements. These services coexist over a shared satellite–terrestrial infrastructure where communication, computing, and caching resources are distributed across satellites, roadside units, and base stations. Directly scheduling resources to individual users in such a large-scale heterogeneous system leads to high orchestration complexity and unstable service provisioning. Therefore, resource slicing is required to organize network resources according to service categories rather than instantaneous user demands. Reservation-stage resource management performs this slicing process over a large timescale. Instead of reacting to real-time channel variations, STVNs need to determine the resource capacity prepared for different service types under predicted traffic demand and satellite availability. To realize this objective, resource slicing has become a widely adopted paradigm, where heterogeneous physical resources are abstracted into virtual slices and allocated to service classes with differentiated performance targets.

A number of studies investigate centralized or hierarchical slicing architectures to enable resource reservation. For instance, a satellite–terrestrial integrated network architecture with a global controller for slice decision-making is proposed in [19], while adaptive slicing window mechanisms are developed in [20] to accommodate time-varying service demands and dynamic network environments. To improve flexibility and resilience, extensible slicing frameworks designed, including the definition, modeling, orchestration, and deployment of multiple slices and infrastructures, are discussed in [21]. SDN-based, AI-assisted, and digital twin-assisted slicing frameworks for future wireless networks and space–air–ground integrated networks are further explored in [22–24], highlighting the role of intelligent control in efficient resource provisioning.

Beyond architectural design, several works focus on reservation-stage slicing strategies for multi-domain and multi-service scenarios with a shared physical network infrastructure. For example, multi-domain dynamic slicing models tailored for delay-sensitive applications are studied in [25, 26], while resilient slicing designs incorporating redundant resource provisioning are proposed in [27] to mitigate potential failures. Quality of service (QoS)-aware reservation schemes for enhanced Mobile Broadband (eMBB) services in STVNs are investigated in [28] with the adaptive network selection design, and joint admission control and slicing frameworks supporting heterogeneous services are developed in [29].

To cope with non-stationary service demands and satellite mobility, learning-based [30] and digital-twin-assisted reservation mechanisms are introduced in [31, 32], enabling adaptive and robust long-term resource planning. Hybrid data–model-driven slicing approaches that explicitly account for spatiotemporal demand variations are extensively investigated, where statistical modeling is combined with data-driven learning to improve long-term reservation decisions under multi-beam coverage constraints [33], or for a cooperative slicing scenario [26]. In [34], low-delay, high-throughput, and wide-coverage slices are constructed for space–air–ground integrated networks by jointly optimizing service delay, throughput, and coverage area using centralized and distributed multi-agent deep deterministic policy gradient (DDPG)-based algorithms. Furthermore, [35] proposes a reconfigurable radio access network slicing scheme that dynamically adjusts reserved resources for heterogeneous services with the objective of maximizing long-term system revenue.

Overall, reservation-stage resource slicing organizes heterogeneous network resources at the service level and reduces orchestration complexity by decoupling long-term planning from instantaneous scheduling. However, since reserved resources cannot fully capture fast variations in connectivity and traffic, real-time adaptation mechanisms are still required. This motivates operation-stage resource scheduling, which is discussed in the following section.

2.3 Operation-Stage Resource Scheduling

While reservation-stage resource slicing plans resources at the service level, instantaneous connectivity and traffic conditions in STVNs still vary due to CV mobility, channel fluctuation, and intermittent satellite visibility. Therefore, reserved resources must be dynamically adjusted in real time to support individual CVs. Operation-stage resource scheduling performs fine-grained decisions over small timescales, which determine the resource allocation to users and tasks at each moment in STVNs. The objective is to maintain service continuity and low latency under rapidly changing network conditions. In the following, we review representative operation-stage mechanisms in STVNs and related integrated networks, including user association, radio resource allocation, and joint communication, computing, and caching (3C) resource orchestration.

User Association and Access Mode Selection: Due to the heterogeneous characteristics of satellite and terrestrial networks, user association and access mode selection constitute fundamental operation-stage decisions. Existing studies investigate adaptive association strategies that exploit the complementary advantages of terrestrial networks, such as low propagation delay, and satellite networks, such as wide coverage and reduced handover frequency. Learning-based access mode selection schemes are proposed in [36, 37], enabling flexible and reliable connectivity for diverse vehicular services under highly dynamic channel conditions and mobility patterns. When direct satellite–user links are unavailable or exhibit poor channel quality, relay-assisted association and backhaul-aware access strategies are explored, where satellites serve as part of the backhaul infrastructure to extend coverage and enhance network capacity [38]. Such approaches are further extended to IoT-oriented STIN scenarios, where joint association and resource management decisions are optimized using reinforcement learning-based mechanisms to improve long-term utility and spectrum efficiency [39, 40].

Radio Resource Allocation: A substantial body of work addresses radio resource management in STVNs to improve spectrum efficiency, reliability, and fairness under heterogeneous access conditions. Representative studies focus on the joint optimization of power allocation, beamforming, and interference management, considering cooperative satellite–terrestrial transmission and non-orthogonal multiple access schemes [41, 42]. To cope with rapid network dynamics and incomplete system information in STVNs, intelligent radio resource management frameworks based on SDN architectures and AI techniques have been proposed, enabling centralized control, predictive optimization, and adaptive configuration of heterogeneous resources [43–45]. In parallel, analytical modeling and stochastic performance analysis provide theoretical guidance for delay-aware and reliability-aware radio resource allocation, capturing the impact of satellite mobility, intermittent connectivity, and hybrid interference in integrated networks [46, 47].

Joint Communication, Computing, and Caching Resource Orchestration: Beyond radio resource allocation, effective management of communication, computing, and caching (3C) resources in STVNs requires tightly coupled and real-time decision-making across heterogeneous network segments. Rather than treating different resource types in isolation, recent studies emphasize integrated control and optimization paradigms that jointly coordinate multi-dimensional resources under satellite mobility, intermittent connectivity, and rapidly varying traffic demands.

From a control and architectural perspective, SDN has been widely adopted to enable unified and programmable management of 3C resources across satellite and terrestrial networks. An SDN-based STIN architecture assisted by learning algorithms is proposed in [48, 49], where a centralized controller coordinates communication and computing resources to adapt to dynamic network conditions. Similar SDN-enabled and learning-assisted frameworks further support real-time orchestration of multi-dimensional resources in integrated networks [50, 51], particularly in scenarios involving task offloading and edge computing [52, 53]. Such architectures provide a flexible foundation for real-time 3C orchestration by decoupling control and data planes and enabling global network visibility.

Building on these architectural foundations, a variety of integrated optimization frameworks have been developed to jointly manage 3C resources. Matching-based optimization methods are proposed to minimize service delay and improve resource utilization in integrated networks [54], while game-theoretic approaches, such as Nash bargaining formulations, are adopted to enhance system throughput while ensuring fairness among users [55]. These studies demonstrate that coordinated multi-resource optimization can effectively balance efficiency, fairness, and service quality in dynamic STVN environments. To cope with uncertainty and fast system dynamics, data-driven and learning-assisted paradigms have been increasingly explored for operation-stage 3C resource orchestration. In caching-enabled STINs, learning-based approaches dynamically adapt cache placement and content delivery decisions to time-varying user demands and satellite visibility, reducing content delivery latency and backhaul load [56, 57]. In addition, learning-based and hybrid optimization methods are extended to jointly schedule 3C resources, enabling adaptive task offloading [58], content delivery [59], and user-centric service provisioning under limited system information [60].

Overall, operation-stage mechanisms determine how reserved resources are utilized in real time under fast-varying network conditions. Compared with the reservation-stage resource slicing, which operates at the service level, the operation-stage resource scheduling focuses on instantaneous adaptation at the user and task level. The interaction between the two stages forms a slicing-based two-stage resource management framework, which is the basis of the resource orchestration strategies developed in the subsequent chapters.

2.4 Summary of State-of-the-Art Research

In this chapter, we reviewed state-of-the-art research on resource management in STVNs from a multi-timescale perspective. We first summarized representative performance modeling studies and key system characteristics that motivate system-level performance characterization for resource management evaluation. Then, we reviewed resource management schemes in both reservation-stage resource slicing for large timescale resource planning and operation-stage resource scheduling for real-time resource adaptation.

Despite the research endeavors, substantial studies still remain in addressing several fundamental challenges in STVN resource management, including the challenges from geometry-dependent network availability, network dynamics in highly dynamic vehicular environments, multi-dimensional decision coupling across 3C resources, and heterogeneous connectivity patterns across satellite and terrestrial segments. To tackle these gaps, in this monograph, we investigate resource management for STVNs. Specifically, Chap. 3 develops theoretical performance models that explicitly capture practical constellation geometry and terrestrial deployment effects, providing system-level metrics for resource management evaluation. Building on these theoretical performance modeling, Chaps. 4 and 5 design reservation-stage resource slicing and operation-stage resource scheduling schemes, respectively, to coordinate time-varying heterogeneous resources under diverse connectivity patterns and service requirements.

References

1. 3GPP: Study on new radio (NR) to support non-terrestrial networks, (2020). version 15.4.0, release 15
2. 3GPP: Solutions for NR to support non-terrestrial networks (NTN), vol. 16, (2023). Technical Report version 16.2.0, release
3. Kodheli, O., et al.: Satellite communications in the new space era: A survey and future challenges. IEEE Commun. Surveys Tuts. **23**(1), 70–109 (2020)
4. Heydarishahreza, N., Han, T., Ansari, N.: Spectrum sharing and interference management for 6g leo satellite-terrestrial network integration. IEEE Commun. Surveys Tuts. **27**(5), 2794–2825 (2025)
5. Guo, L., Liu, J., Sheng, M., Li, J.: Constellation topology design for maximum capacity of leo satellite networks. IEEE Trans. Commun. **73**(6), 4321–4334 (2025)
6. Del Portillo, I., Cameron, B.G., Crawley, E.F.: A technical comparison of three low earth orbit satellite constellation systems to provide global broadband. Acta Astronaut. **159**, 123–135 (2019)
7. Lin, X.: 5G new radio evolution meets satellite communications: Opportunities, challenges, and solutions. 5G and beyond: Fundamentals and standards pp, pp. 517–531. (2021)
8. Wu, J., Su, S., Wang, X., Zhang, J., Gao, Y.: Accelerating handover in mobile satellite network. In: Proc. IEEE INFOCOM, pp. 531–540. (2024)
9. 3GPP: Study on scenarios and requirements for next generation access technologies, (2025). Technical Report version 19.0.0, release 19
10. ITU-T: Fixed, mobile and satellite convergence-requirements for IMT-2020 networks and beyond. Tech. Rep. Y 3200, (2022)
11. ITU-T: Fixed, mobile and satellite convergence-framework for IMT-2020 networks and beyond. Tech. Rep. Y 3201, (2023)
12. Wu, H., He, M., Shen, X., Zhuang, W., Dao, N., Shi, W.: Network performance analysis of satellite-terrestrial vehicular network. IEEE Internet Things J. **11**(9), 16829–16844 (2024)
13. Jung, D.H., Ryu, J.G., Byun, W.J., Choi, J.: Performance analysis of satellite communication system under the shadowed-rician fading: A stochastic geometry approach. IEEE Trans. Commun. **70**(4), 2707–2721 (2022)
14. Guo, K., Lin, M., Zhang, B., Wang, J.B., Wu, Y., Zhu, W.P., Cheng, J.: Performance analysis of hybrid satellite-terrestrial cooperative networks with relay selection. IEEE Trans. Veh. Technol. **69**(8), 9053–9067 (2020)
15. Lin, H., Zhang, C., Huang, Y., Zhao, R., Yang, L.: Fine-grained analysis on downlink LEO satellite-terrestrial mmwave relay networks. IEEE Wireless Commun. Lett. **10**(9), 1871–1875 (2021)
16. Ye, J., Pan, G., Alouini, M.S.: Earth rotation-aware non-stationary satellite communication systems: Modeling and analysis. IEEE Trans. Wireless Commun. **20**(9), 5942–5956 (2021)
17. Sharma, P.K., Yogesh, B., Gupta, D., Kim, D.I.: Performance analysis of IoT-based overlay satellite-terrestrial networks under interference. IEEE Trans. Cogn. Commun. Netw. **7**(3), 985–1001 (2021)
18. Guidotti, A., et al.: Architectures and key technical challenges for 5G systems incorporating satellites. IEEE Trans. Veh. Technol. **68**(3), 2624–2639 (2019)
19. Ma, T., Qian, B., Qin, X., Liu, X., Zhou, H., Zhao, L.: Satellite-terrestrial integrated 6G: An ultra-dense LEO networking management architecture. IEEE Wireless Commun. **31**(1), 62–69 (2022)
20. Shen, H., Tian, Y., Wang, T., Bai, G.: Slicing-based task offloading in space-air-ground integrated vehicular networks. IEEE Trans. Mobile Comput. **23**(5), 4009–4024 (2023)
21. Drif, Y., Chaput, E., Lavinal, E., Berthou, P., Tiomela Jou, B., Gremillet, O., Arnal, F.: An extensible network slicing framework for satellite integration into 5G. Int. J. Satellite Commun. Netw. **39**(4), 339–357 (2021)

22. Huang, X., Yang, H., Zhou, C., He, M., Shen, X., Zhuang, W.: When digital twin meets generative AI: Intelligent closed-loop network management. IEEE Netw. **39**(5), 272–279 (2025)
23. Wu, H., Chen, J., Zhou, C., Shi, W., Cheng, N., Xu, W., Zhuang, W., Shen, X.: Resource management in space-air-ground integrated vehicular networks: SDN control and AI algorithm design. IEEE Wireless Commun. **27**(6), 52–60 (2020)
24. Zhou, C., Hu, S., Gao, J., Huang, X., Zhuang, W., Shen, X.: User-centric immersive communications in 6G: A data-oriented framework via digital twin. IEEE Wireless Commun. **32**(3), 122–129 (2025)
25. Kovacevic, I., Shafigh, A.S., Glisic, S., Lorenzo, B., Hossain, E.: Multi-domain network slicing with latency equalization. IEEE Trans. Netw. Service Manag. **17**(4), 2182–2196 (2020)
26. He, M., Pei, Y., Hu, S., Tang, Z., Zhuang, W., Shen, X.: Adaptive resource provisioning in satellite networks via VAE-assisted contextual bandit learning. In: Proc. WCSP, pp. 1–6. IEEE (2025)
27. Esmat, H.H., Lorenzo, B., Shi, W.: Toward resilient network slicing for satellite-terrestrial edge computing iot. IEEE Internet Things J. **10**(16), 14621–14645 (2023)
28. De Cola, T., Bisio, I.: QoS optimisation of eMBB services in converged 5G-satellite networks. IEEE Trans. Veh. Technol. **69**(10), 12098–12110 (2020)
29. Lyu, F., Yang, P., Wu, H., Zhou, C., Ren, J., Zhang, Y., Shen, X.: Service-oriented dynamic resource slicing and optimization for space-air-ground integrated vehicular networks. IEEE Trans. Intell. Transp. Syst. **23**(7), 7469–7483 (2021)
30. Li, J., He, M., Zhou, C., Huang, X., Liu, Z., Zhao, L., Wang, C.X., Wu, H.: Integration of generative AI and mobile networking: A comprehensive survey. IEEE Trans. Netw. Sci. Eng. **13**, 4369–4405 (2025)
31. Wu, H., Chen, J., Zhou, C., Li, J., Shen, X.: Learning-based joint resource slicing and scheduling in space-terrestrial integrated vehicular networks. J. Commun. Inf. Nets. **6**(3), 208–223 (2021)
32. He, M., Wu, H., Zhou, C., Hu, S., Tang, Z., W.: Zhuang: Digital twin-assisted robust and adaptive resource slicing in LEO satellite networks. In: Proc. IEEE GLOBECOM, pp. 3261–3266. (2024)
33. He, M., Wu, H., Zhou, C., Shen, X.: Resource slicing with cross-cell coordination in satellite-terrestrial integrated networks. In: Proc. IEEE ICC, (2024)
34. Zhou, G., Zhao, L., Zheng, G., Song, S., Zhang, J., Hanzo, L.: Multiobjective optimization of space-air-ground-integrated network slicing relying on a pair of central and distributed learning algorithms. IEEE Internet Things J. **11**(5), 8327–8344 (2024)
35. Liu, Y., Ma, T., Qin, X., Zhou, H., Shen, X.: Reconfigurable RAN slicing for ultra-dense LEO satellite networks via DRL. IEEE Trans. Cogn. Commun. Netw. **11**(1), 566–580 (2025)
36. Zhou, C., Wu, H., He, M., Wu, W., Cheng, N., Shen, X.: Adaptive access mode selection in space-ground integrated vehicular networks. In: Proc. IEEE GLOBECOM, pp. 1–6 (2021)
37. Yan, L., Fang, X., Hao, L., Fang, Y.: Safety-oriented resource allocation for space-ground integrated cloud networks of high-speed railways. IEEE J. Sel. Areas Commun. **38**(12), 2747–2759 (2020)
38. Di, B., Zhang, H., Song, L., Li, Y., Li, G.Y.: Ultra-dense LEO: Integrating terrestrial-satellite networks into 5G and beyond for data offloading. IEEE Trans. Wireless Commun. **18**(1), 47–62 (2018)
39. Hong, T., Ni, Y., Li, Z., Xu, L., Zhang, G.: A dynamic load balancing access control scheme for massive IoT in space-terrestrial integrated network. IEEE Internet Things J. **12**(9), 12562–12578 (2025)
40. Shah, H.A., Zhao, L., Kim, I.M.: Joint network control and resource allocation for space-terrestrial integrated network through hierarchical deep actor-critic reinforcement learning. IEEE Trans. Veh. Technol. **70**(5), 4943–4954 (2021)
41. Chu, J., Chen, X.: Robust design for integrated satellite-terrestrial internet of things. IEEE Internet Things J. **8**(11), 9072–9083 (2021)
42. Wang, L., Wu, Y., Zhang, H., Choi, S., Leung, V.C.: Resource allocation for NOMA based space-terrestrial satellite networks. IEEE Trans. Wireless Commun. **20**(2), 1065–1075 (2020)

43. Liang, Y.C., Tan, J., Jia, H., Zhang, J., Zhao, L.: Realizing intelligent spectrum management for integrated satellite and terrestrial networks. J. Commun. Inf. Nets. **6**(1), 32–43 (2021)
44. Wu, H., Chen, J., Zhou, C., Lyu, F., Zhang, N., Wang, L., Shen, X.: Load- and mobility-aware cooperative content delivery in sag integrated vehicular networks. In: Proc. IEEE ICC, (2021)
45. Zhang, X., Qian, B., Qin, X., Ma, T., Chen, J., Zhou, H., Shen, X.: Cybertwin-assisted mode selection in ultra-dense LEO integrated satellite-terrestrial network. J. Commun. Inf. Netw. **7**(4), 360–374 (2022)
46. Zhu, Y., Zhou, D., Sheng, M., Li, J., Han, Z.: Stochastic delay analysis for satellite data relay networks with heterogeneous traffic and transmission links. IEEE Trans. Wireless Commun. **20**(1), 156–170 (2021)
47. Chen, L., Tang, F., Liu, J., Li, X., Zhu, Y., Yu, J., Yang, L.T., Li, Z., Yao, B., Yu, Y.: Time-varying resource graph based processing on the way for space-terrestrial integrated vehicle networks. IEEE Trans. Mobile Comput. **23**(2), 1985–2002 (2023)
48. Shi, Y., Cao, Y., Liu, J., Kato, N.: A cross-domain SDN architecture for multi-layered space-terrestrial integrated networks. IEEE Netw. **33**(1), 29–35 (2019)
49. Kafle, V.P., Sekiguchi, M., Asaeda, H., Harai, H.: Integrated network control architecture for terrestrial and non-terrestrial network convergence. IEEE Commun. Standards Mag. **8**(1), 12–19 (2024)
50. Li, J., Shi, W., Wu, H., Zhang, S., Shen, X.: Cost-aware dynamic SFC mapping and scheduling in SDN/NFV-enabled space-air-ground-integrated networks for internet of vehicles. IEEE Internet Things J. **9**(8), 5824–5838 (2021)
51. Qiu, C., Yao, H., Yu, F.R., Xu, F., Zhao, C.: Deep Q-learning aided networking, caching, and computing resources allocation in software-defined satellite-terrestrial networks. IEEE Trans. Veh. Technol. **68**(6), 5871–5883 (2019)
52. Zhang, X., Liu, J., Xiong, Z., Huang, Y., Zhang, R., Mao, S., Han, Z.: Cost-effective hybrid computation offloading in satellite-terrestrial integrated networks. IEEE Internet Things J. **11**(22), 36786–36800 (2024)
53. Han, D., Ye, Q., Peng, H., Wu, W., Wu, H., Liao, W., Shen, X.: Two-timescale learning-based task offloading for remote iot in integrated satellite-terrestrial networks. IEEE Internet Things J. **10**(12), 10131–10145 (2023)
54. Chen, D., Yang, C., Gong, P., Chang, L., Shao, J., Ni, Q., Anpalagan, A., Guizani, M.: Resource cube: Multi-virtual resource management for integrated satellite-terrestrial industrial IoT networks. IEEE Trans. Veh. Technol. **69**(10), 11963–11974 (2020)
55. Fu, S., Wu, B., Wu, S., Fang, F.: Multi-resources management in 6G-oriented terrestrial-satellite network. China Commun. **18**(9), 24–36 (2021)
56. He, M., Zhou, C., Wu, H., Shen, X.: Learning-based cache placement and content delivery for satellite-terrestrial integrated networks. In: Proc. IEEE GLOBECOM, pp. 1–6. (2021)
57. Tang, J., Li, J., Chen, X., Xue, K., Zhang, L., Sun, Q., Lu, J.: Cooperative caching in satellite-terrestrial integrated networks: A region features aware approach. IEEE Trans. Veh. Technol. **73**(7), 10602–10616 (2024)
58. Shang, B., Li, C., Ma, J., Fan, P.: Inter-satellite links-enabled cooperative edge computing in satellite-terrestrial networks. IEEE Trans. Wireless Commun. **25**, 1223–1239 (2026)
59. He, M., Wu, H., Shen, X., Zhuang, W.: Cooperative resource scheduling for environment sensing in satellite-terrestrial vehicular networks. IEEE Internet Things J. **12**(6), 6734–6748 (2025)
60. Zhou, C., Gao, J., Hu, S., Cheng, N., Zhuang, W., Shen, X.: User-centric communication service provision for edge-assisted mobile augmented reality. IEEE Trans. Mobile Comput. **25**(3), 3435–3449 (2026)

Chapter 3
Theoretical Modeling for STVN Performance Analysis

Abstract Low Earth orbit (LEO) satellite-assisted communications have emerged as a promising solution for enabling reliable, flexible, and globally seamless service provisioning in next-generation vehicular networks. This chapter focuses on the theoretical modeling for satellite–terrestrial vehicular network (STVN) performance analysis, supporting connected vehicle (CV) applications. We first establish a tractable architectural modeling for LEO satellite–CV communication systems by explicitly accounting for satellite orbital characteristics and constellation parameters. Then, the analytical modeling of LEO satellite–CV communication performance is analyzed in terms of service availability, outage probability, and system throughput under practical satellite constellation settings. Furthermore, the impact of different terrestrial network deployments on the overall STVN performance is investigated to reveal the interplay between satellite and terrestrial infrastructures. Extensive numerical results are provided to validate the analytical findings and to illustrate how system parameters and deployment choices affect the network performance of STVNs.

Keywords Network architecture modeling · Satellite constellation configuration · Communication performance analysis · Infrastructure deployment

To fully realize the potential of CVs, ubiquitous vehicle-to-everything (V2X) connectivity is required to support a wide range of applications, from safety-critical collision avoidance to high-bandwidth infotainment services. Although terrestrial networks can provide high data rates, their coverage gaps, caused by the deployment cost of roadside units (RSUs) and geographical constraints, motivate the integration of low Earth orbit (LEO) satellites to enable globally flexible and reliable connectivity [1]. By combining the high-capacity terrestrial segment with the wide-area coverage and robustness of LEO constellations, satellite–terrestrial vehicular networks (STVNs) are able to provide seamless service continuity for CV applications [2]. However, the inherent heterogeneity of STVNs, including disparate propagation delays and highly dynamic network topologies induced by satellite mobility, poses significant challenges to service provisioning. Understanding the fundamental performance limits of STVNs is therefore essential for effective network design and resource management [3].

M. He et al., *Resource Management for Satellite-Terrestrial Vehicular Networks*, SpringerBriefs in Computer Science, https://doi.org/10.1007/978-3-032-24526-7_3

In this chapter, we conduct a comprehensive performance analysis of STVNs in which both LEO satellites and RSUs cooperatively serve CVs within their respective coverage areas. RSUs are connected to the core network through terrestrial backhaul links, while satellites operate in a regenerative mode, analogous to a distributed unit in the 3GPP radio access network architecture [4]. Each satellite communicates with CVs via service links and connects to ground stations through feeder links. Note that we primarily focus on the performance of service links, which directly determine the communication quality experienced by CVs.

To this end, we establish a practical LEO satellite constellation model for communication performance analysis. Based on this model, we investigate the key constellation parameters that affect propagation delay and network coverage in satellite–terrestrial communications. The analytical modeling of LEO satellite–CV communication performance is then developed in terms of service availability, outage probability, and system throughput. Furthermore, the impact of different terrestrial infrastructure deployment strategies on the overall STVN performance is examined to reveal the interplay between satellite constellation design and terrestrial network layout. Extensive numerical results are presented to illustrate the analytical findings and to demonstrate the performance benefits of integrating LEO satellites with terrestrial vehicular networks. The main contribution of this chapter can be summarized as follows:

- A practical LEO satellite constellation model is developed to capture the impact of satellite orbital parameters on satellite–CV communication performance.
- The analytical modeling of LEO satellite–CV communication is comprehensively investigated in terms of service availability, outage probability, and throughput under practical constellation configurations.
- The impacts of terrestrial infrastructure deployment strategies on STVN performance are investigated to evaluate the benefits of satellite–terrestrial integration for CV services.

The remainder of this chapter is organized as follows. Section 3.1 presents the LEO satellite constellation model and analyzes the impact of constellation parameters. Section 3.2 investigates the analytical modeling of LEO satellite–CV communication performance in terms of service availability, outage probability, and throughput. Section 3.3 examines the impact of different satellite constellation designs and terrestrial network deployment strategies on STVN performance. Finally, Sect. 3.4 summarizes this chapter.

3.1 Architectural Modeling of LEO Satellite Constellation

This section establishes an architectural model for low Earth orbit (LEO) satellite constellations, which serves as the foundation for the performance analysis. Key physical and geometric factors that fundamentally affect satellite–CV communications are explicitly considered, including Earth rotation as well as the constraints

Table 3.1 Summary of notations

Notation	Definition
r_{E}, r	Earth radius and LEO satellite orbit radius
α, h	Satellite orbit inclination angle and orbit altitude
ϕ	Angle between a satellite and the ascending node
ω	Angle between the x-axis and the line from the origin to the ascending node
(β_u, γ_u)	(latitude, longitude) of a CV
d	The distance between a CV and its associated access point (LEO satellite or RSU)
θ_{th}	The minimum elevation angle constraint
μ_{th}	The maximum satellite boresight angle constraint
$d_{\max}$	The maximum satellite-CV distance to satisfy elevation and boresight angle constraints
N, M	Number of satellite orbits and number of satellites per orbit
P_a^o	Probability of an LEO orbit being feasible for CVs
P_a^s	Probability of at least one satellite on an orbit being available to provide CV services
$P_{a,1}$	Probability of satellite-CV service being available
$R_{t,1}, R_{t,2}$	Required throughput for satellite and terrestrial communications
$\lambda_{\mathbf{x}}$	RSU deployment intensity in terrestrial RSU deployment **Case x**
$P_{o,1}$	Satellite communication service outage probability
$P_{o,2}^{\mathbf{x}}$	Terrestrial service outage probability in RSU deployment **Case x**
$T_{1,\max}$	Maximum achievable satellite system throughput
$T_{2,\max}^{\mathbf{x}}$	Maximum achievable terrestrial system throughput in RSU deployment **Case x**

imposed by elevation angle and boresight angle. Based on this modeling framework, we analyze the constellation design requirements, focusing on the number of satellites per orbit and the number of orbits needed to ensure continuous satellite coverage over the service area. The primary notations used throughout this chapter are summarized in Table 3.1.

3.1.1 Satellite Movement with Earth Rotation

Due to the rotation of the Earth, the movement of LEO satellites relative to the ground deviates from a simple circular trajectory, as illustrated in Fig. 3.1a. The Earth rotation causes satellite tracks continuously shift over time, which directly affects satellite visibility and link dynamics for ground users.

To characterize satellite motion and its impact on communication performance, we adopt an Earth-centered Earth-fixed (ECEF) coordinate system, as shown in Fig. 3.1b,

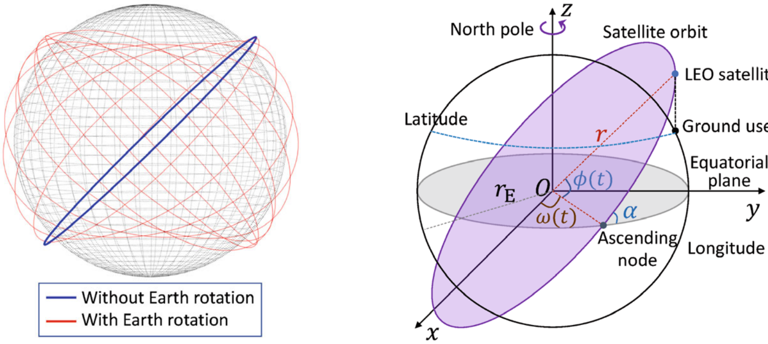

(a) Satellite orbits with and without Earth rotation. (b) Earth-centered Earth-fixed coordinate system.

Fig. 3.1 An illustration of satellite orbits

where the Earth is modeled as a perfect sphere.[1] The origin of the coordinate system is located at the Earth center. The $+x$-axis passes through the intersection of the Equator and the Prime Meridian, the $+z$-axis points toward the North Pole, and the $+y$-axis is orthogonal to both the x- and z-axes. This coordinate system rotates with the Earth.

As shown in Fig. 3.1b, the satellite orbit radius is denoted by $r = r_E + h$, where r_E is the Earth radius and h is the satellite orbit altitude. The orbit inclination angle is denoted by α. Let $\omega(t)$ denote the time-varying angle between the x-axis and the line connecting the Earth's center to the ascending node, given by

$$\omega(t) = \omega_0 + \Delta\omega_E \cdot t, \tag{3.1}$$

where ω_0 is the initial angle of the ascending node, and $\Delta\omega_E$ is the Earth rotation angular velocity. Let $\phi(t)$ denote the angular position of the satellite along its orbit relative to the ascending node at time t, which is given by

$$\phi(t) = \phi_0 + \Delta\phi_S \cdot t, \tag{3.2}$$

where ϕ_0 is the initial angle between the satellite and ascending node and $\Delta\phi_S$ represents the satellite's angular velocity along the orbit.

[1] More accurate Earth models, such as the WGS84 ellipsoidal model, can be adopted for high-precision positioning. However, numerical comparisons indicate that the difference in satellite–CV distance between the spherical model and the WGS84 model can be negligible for LEO satellite communications. Even in extreme cases, such as ground terminals located near the poles or near the equator, the relative error remains below 0.01%. Therefore, the spherical Earth model is adopted for simplicity.

Consider a CV located on the Earth's surface with latitude β_u and longitude γ_u. The position of the CV in the ECEF coordinate system can be expressed as

$$\begin{cases} x_u = r_{\mathrm{E}} \cos\beta_u \cos\gamma_u, \\ y_u = r_{\mathrm{E}} \cos\beta_u \sin\gamma_u, \\ z_u = r_{\mathrm{E}} \sin\beta_u. \end{cases} \tag{3.3}$$

The position of the LEO satellite at time t is determined jointly by Earth rotation and satellite orbital movement, and can be expressed as

$$\begin{cases} x_s(t) = r\cos\phi(t)\cos\omega(t) - r\sin\phi(t)\sin\omega(t)\cos\alpha, \\ y_s(t) = r\cos\phi(t)\sin\omega(t) + r\sin\phi(t)\cos\omega(t)\cos\alpha, \\ z_s(t) = r\sin\phi(t)\sin\alpha. \end{cases} \tag{3.4}$$

Based on the satellite and CV positions, the instantaneous distance between the LEO satellite and the CV is given by

$$d(t) = \sqrt{(x_s(t) - x_u)^2 + (y_s(t) - y_u)^2 + (z_s(t) - z_u)^2}. \tag{3.5}$$

3.1.2 Impact of Elevation Angle and Boresight Angle

The feasibility of a satellite–CV communication link is fundamentally constrained by geometric factors, including the minimum elevation angle required at the ground terminal and the maximum satellite boresight angle supported by the satellite antenna. These constraints jointly determine the effective coverage region of a LEO satellite and directly affect link availability and service continuity.

To ensure a feasible satellite–CV link, the distance $d(t)$ between the satellite and the CV must satisfy both the minimum elevation angle constraint and the maximum boresight angle constraint, given by

$$d(t) \le \sqrt{r^2 - r_{\mathrm{E}}^2 + r_{\mathrm{E}}^2\sin^2\theta_{\mathrm{th}}} - r_{\mathrm{E}}\sin\theta_{\mathrm{th}}, \tag{3.6a}$$

$$d(t) \le r\cos\mu_{\mathrm{th}} - \sqrt{r_{\mathrm{E}}^2 - r^2 + r^2\cos^2\mu_{\mathrm{th}}}, \tag{3.6b}$$

where θ_{th} denotes the minimum elevation angle at the CV and μ_{th} denotes the maximum satellite boresight angle.

In scenarios where satellite links are not obstructed by surrounding objects, such as rural or open areas, the elevation angle constraint in Eq. (3.6a) and the boresight angle constraint in Eq. (3.6b) are interrelated. As illustrated in Fig. 3.2a, the minimum elevation angle can be determined by the maximum boresight angle, given by

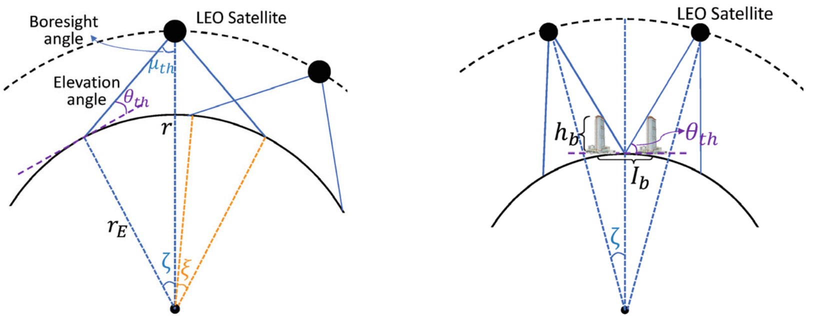

(a) Elevation angle and boresight angle constraints. (b) High-rise building blockage constraints.

Fig. 3.2 Illustration of LEO satellite coverage

$$\sin(\mu_{\text{th}}) = \frac{r_{\text{E}} \cos(\theta_{\text{th}})}{r}. \tag{3.7}$$

In contrast, in urban environments with dense high-rise buildings, satellite links may be blocked by surrounding structures, and the minimum elevation angle is mainly affected by the building height and inter-building distance rather than by satellite boresight angle. Consider an urban scenario with a maximum building height h_d and a minimum inter-building distance I_d, as illustrated in Fig. 3.2b, the minimum elevation angle should satisfy

$$\theta_{\text{th}} = \arctan(h_d/(0.5I_d)) \tag{3.8}$$

to guarantee that CVs between the buildings can be covered by LEO satellites.

3.1.3 Number of Satellites on One Orbit

To ensure continuous satellite coverage along each orbit, the number of LEO satellites deployed on a single orbit must be sufficiently large to avoid coverage gaps between adjacent satellites. This subsection derives the minimum number of satellites per orbit required to guarantee uninterrupted coverage under the elevation angle constraint introduced in the previous subsection.

Given the minimum elevation angle θ_{th}, the effective coverage of a single satellite along the Earth's surface can be characterized by the Earth central angle ζ, as illustrated in Fig. 3.2a. The angle ζ is defined as the angle subtended at the Earth's center between the satellite and a CV located at the edge of the satellite coverage region, and is given by

$$\zeta = \arcsin\left(d_{\max} \cos\theta_{\text{th}}/r\right). \tag{3.9}$$

Here, $d_{\max}$ denotes the maximum allowable satellite–CV distance constrained jointly by the minimum elevation angle and the maximum satellite boresight angle, expressed as

$$d_{\max} = \min\left(\sqrt{r^2 - r_E^2 + r_E^2 \sin^2\theta_{\text{th}}} - r_E \sin\theta_{\text{th}}, r\cos\mu_{\text{th}} - \sqrt{r_E^2 - r^2 + r^2\cos^2\mu_{\text{th}}}\right)$$

is the maximum allowable satellite-CV distance under elevation angle and boresight angle constraints.

Then, the coverage area of one LEO satellite can be expressed as

$$S = 2\pi r_E^2(1 - \cos\zeta). \tag{3.10}$$

To avoid coverage gaps along an orbit, the minimum number of satellites required on one orbit is given by

$$M_{\min} = \lceil \pi/\zeta \rceil . \tag{3.11}$$

When the actual number of satellites deployed on an orbit exceeds $M_{\min}$, the coverage regions of adjacent satellites overlap, where the overlapped coverage angle, denoted by ξ, can be expressed as

$$\xi = 2\zeta - \frac{2\pi}{M_{\min}}, \tag{3.12}$$

quantifying the redundancy in satellite coverage along the orbit. This overlap plays an important role in improving service availability and robustness, and will be exploited in the subsequent performance analysis.

3.1.4 Number of Orbits in Satellite Constellation

In this subsection, we investigate the minimum number of orbits required in a LEO satellite constellation to guarantee seamless global coverage. Unlike the number of satellites per orbit, which determines coverage continuity along an orbit, the number of orbits directly governs coverage continuity across different longitudes, which varies with the orbit inclination angle.

We first consider polar-orbit constellations with an inclination angle of $\alpha = \pi/2$, as illustrated in Fig. 3.3a. Due to the symmetry of polar orbits, seamless global coverage can be ensured by guaranteeing uninterrupted service for CVs located on the equator, which represents the worst-case coverage scenario. Consider a CV located at point A on the equator. As derived in Sect. 3.1.3, the angle between two adjacent satellites on the same orbit is $2\pi/M_{\min}$. Accordingly, the Earth-centered angles between point A and two adjacent satellites s_1 and s_2 satisfy $\angle s_1OA = \angle s_2OA = \pi/M_{\min}$.

To avoid coverage gaps, the coverage regions of satellites s_1, s_2, and a satellite s_3 on the adjacent orbit must intersect at a common point I or exhibit sufficient overlap. In this case, the condition of satellite s_3 should satisfy

$$\angle s_3 OA \le \Delta + \zeta = \arccos\left(1 - \left[\cos(\frac{\pi}{M_{\min}}) + \cos\zeta\right]\right) + \arcsin\left(\frac{d_{\max}}{r}\cos\theta_{\text{th}}\right). \tag{3.13}$$

Considering the inherent symmetry of polar orbits, if one hemisphere is seamlessly covered by ascending satellites, the opposite hemisphere will be covered by descending satellites on the same orbits. As a result, the minimum number of orbits required for seamless global coverage in a polar-orbit constellation is given by

$$N_{\min} = \left\lceil \frac{\pi}{\arccos\left(1 - \left[\cos(\frac{\pi}{M_{\min}}) + \cos\zeta\right]\right) + \arcsin\left(\frac{d_{\max}}{r}\cos\theta_{\text{th}}\right)} \right\rceil. \tag{3.14}$$

We next consider general inclined-orbit constellations with inclination angle $\alpha \neq \pi/2$, as illustrated in Fig. 3.3b. In this case, both ascending and descending satellites can simultaneously provide coverage for the same geographic region. Consider a constellation characterized by inclination angle α, number of orbits N, number of satellites per orbit M, and inter-orbit phasing parameter F. At a given time instant, the position of a reference satellite in the ECEF coordinate system can be denoted by (ω_0, ϕ_0), $\omega_0 \in [0, 2\pi)$, $\phi_0 \in [0, 2\pi)$, as shown in Fig. 3.1b. Accordingly, the position of satellite S in the constellation is given by

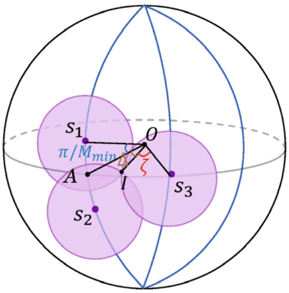

(a) Polar orbits ($\alpha = \frac{\pi}{2}$) (O: the Earth center. s_1, s_2, and s_3: LEO satellites. A: the center of the coverage overlap area of s_1 and s_2. I: the intersection of three satellites' coverage areas. The blue curves represent the satellite orbits, and the pink circles represent satellite coverage areas.)

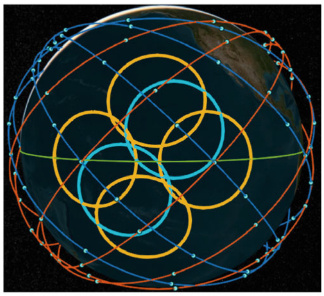

(b) Inclined orbits ($\alpha \neq \frac{\pi}{2}$) (Orange lines: ascending satellite orbits. Blue lines: descending satellite orbits. Green line: the Earth Equator. Yellow circles: the coverage areas of ascending satellites. Cyan circles: the coverage areas of descending satellites.)

Fig. 3.3 LEO satellite coverage with different inclination angles

$$(\omega_s, \phi_s) = \left(\left(\omega_0 + n \cdot \frac{2\pi}{N}\right) \bmod 2\pi, \left(\phi_0 + n \cdot \frac{2\pi F}{MN} + m \cdot \frac{2\pi}{M}\right) \bmod 2\pi \right), \tag{3.15}$$

where $n \in \{0, \ldots, N-1\}$ and $m \in \{0, \ldots, M-1\}$ index the orbit and satellite in the orbit, respectively.

For an arbitrary point A on the Earth with ECEF coordinates (ω_A, ϕ_A), $\omega_A \in [0, 2\pi)$, $\phi_A \in [0, 2\pi)$, the Earth-centered angle between point A and a satellite S is

$$\angle AOS = \arccos\left(\frac{x_A x_s + y_A y_s + z_A z_s}{r r_{\mathrm{E}}}\right), \tag{3.16}$$

where (x_A, y_A, z_A) and (x_s, y_s, z_s) are obtained from (3.4) for point A and satellite S.

Seamless coverage is achieved if, for any (ω_0, ϕ_0) and any point A, the Earth-centered angle to the closest satellite is no greater than ζ. This condition can be expressed as the optimization problem to find the minimum number of orbits $N_{\min}$. Mathematically, this is represented as:

$$\max_{\omega_0, \phi_0, \omega_A, \phi_A} \min_{\omega_s, \phi_s} \angle AOS \le \zeta \quad \equiv \quad \min_{\omega_0, \phi_0, \omega_A, \phi_A} \max_{\omega_s, \phi_s} f(\omega_s, \phi_s) \ge \cos\zeta, \tag{3.17}$$

where

$$\begin{aligned} f &= (x_A x_s + y_A y_s + z_A z_s)/(r r_{\mathrm{E}}) \\ &= \cos\alpha \sin(\omega_A - \omega_s) \sin(\phi_s - \phi_A) + \sin^2\alpha \sin\phi_s \sin\phi_A \\ &\quad + \cos(\omega_A - \omega_s)\left(\cos\phi_s \cos\phi_A + \cos^2\alpha \sin\phi_s \sin\phi_A\right). \end{aligned} \tag{3.18}$$

By analyzing the first-order optimality conditions, the ideal position (ω_s^*, ϕ_s^*) of the closest satellite to point A can be derived, given by

$$\phi_s^* = \phi_A \ \text{ or } \ \pi - \phi_A + 2k\pi, k \in \{0, 1\},$$

$$\omega_s^* = \begin{cases} \omega_A + 2k\pi, & \text{if } \phi_s^* = \phi_A, \\ \omega_A - \arcsin \frac{\cos\alpha \sin(2\phi_A)}{1 - \sin^2\phi_A \sin^2\alpha} + 2k\pi, & \text{if } \phi_s^* = \pi - \phi_A + 2k\pi \text{ and} \\ & \quad \cos^2\alpha \sin^2\phi_A - \cos^2\phi_A \ge 0, \\ \omega_A - \left(\pi - \arcsin \frac{\cos\alpha \sin(2\phi_A)}{1 - \sin^2\phi_A \sin^2\alpha}\right) + 2k\pi, & \text{if } \phi_s^* = \pi - \phi_A + 2k\pi \text{ and} \\ & \quad \cos^2\alpha \sin^2\phi_A - \cos^2\phi_A < 0. \end{cases}$$

Since satellite positions are discrete, the actual closest satellite (ω_s', ϕ_s') is selected as the nearest feasible point in the constellation, given by

$$
\begin{aligned}
n' &= \mathrm{round}\left(\frac{(\omega_s^* - \omega_0)N}{2\pi}\right), \\
m' &= \mathrm{round}\left(\frac{(\phi_s^* - \phi_0 - n' \cdot \frac{2\pi F}{MN})M}{2\pi}\right), \\
\omega_s' &= (\omega_0 + n' \cdot \frac{2\pi}{N}) \bmod 2\pi, \\
\phi_s' &= (\phi_0 + n' \cdot \frac{2\pi F}{MN} + m' \cdot \frac{2\pi}{M}) \bmod 2\pi.
\end{aligned}
\tag{3.19}
$$

The subsequent step involves determining $\min_{\omega_0,\phi_0,\omega_A,\phi_A} f|_{(\omega_s',\phi_s')}$. Due to the rounding operations in (3.19), the optimization problem does not admit a closed-form solution. Therefore, a linear search over $(\omega_0, \phi_0, \omega_A, \phi_A)$ is employed to obtain the minimum value of $f|_{(\omega_s',\phi_s')}$, denoted as f^*. By ensuring that $f^* \geq \cos\zeta$, the minimum number of orbits $N_{\min}$ required for seamless coverage can be determined.

3.1.5 *Performance Evaluation Under Different Satellite Constellation Parameters*

In this subsection, we evaluate the impact of key satellite constellation parameters on the propagation delay and coverage characteristics of LEO satellite–CV communications. The default satellite orbital parameters are listed in Table 3.2.

We first examine the impact of Earth rotation on propagation delay and satellite coverage duration, where CVs are always associated with the closest available satellite. Figure 3.4a illustrates the propagation delay experienced by a CV located at $(\beta_u, \gamma_u) = (0, 0)$. When Earth rotation is ignored, successive satellites on the same orbit yield identical delay performances, as their relative motion with respect to the CV is periodic and symmetric. Since 20 satellites on one orbit can guarantee no coverage gap between adjacent satellites in both cases with elevation angles equal to 10° and 20°, the elevation angle threshold does not affect the experienced propagation delay. In contrast, when Earth rotation is considered, the relative geometry between the CV and satellites continuously evolves, resulting in distinct delay performances

Table 3.2 LEO satellite orbital parameters

Orbit altitude	550 km
Number of satellites on one orbit	20
Initial angles (ω_0, ϕ_0)	(0,0)
Earth rotation angular velocity $\Delta\omega_E$	7.292×10^{-5} rad/s
Velocity of the satellite on its orbit	7.62 km/s
Default CV location	$(\beta_u, \gamma_u) = (0, 0)$

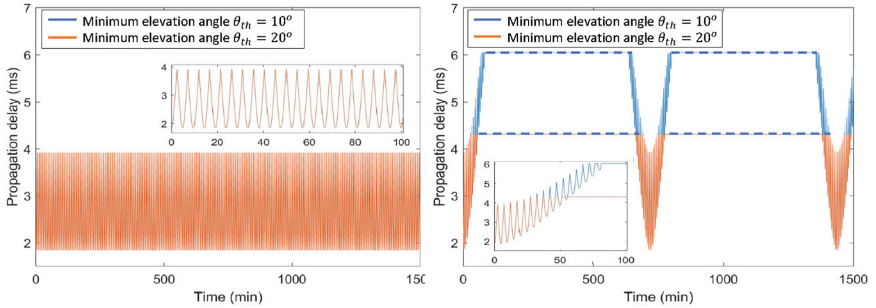

(1) Without Earth rotation (2) With Earth rotation

(a) CV location: $(\beta_u, \gamma_u) = (0, 0)$.

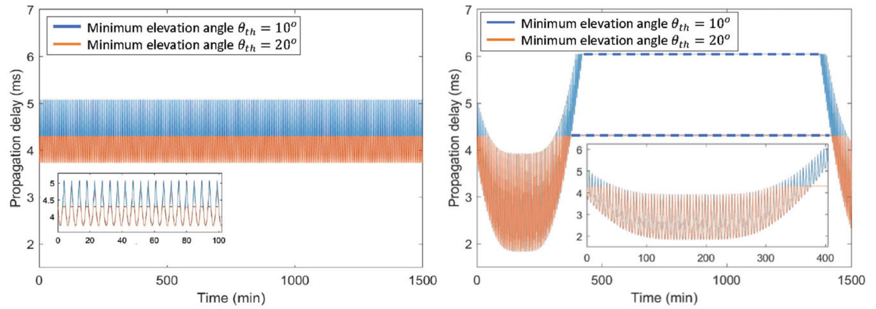

(1) Without Earth rotation (2) With Earth rotation

(b) CV location: $(\beta_u, \gamma_u) = (\pi/4, \pi/4)$.

Fig. 3.4 LEO satellite-CV communication propagation delay with and without Earth rotation (with inclination angle of $\pi/4$)

for different satellites on the same orbit. The dashed segments in Fig. 3.4a indicate time intervals during which the CV is not covered by any satellite on the given orbit, revealing that Earth rotation can introduce intermittent coverage loss even when orbit-level coverage is guaranteed. Moreover, reducing the elevation angle threshold increases the satellite coverage duration by enlarging the effective coverage region. Similar trends are observed for a CV located at $(\beta_u, \gamma_u) = (\pi/4, \pi/4)$, as shown in Fig. 3.4b. In this case, Earth rotation induces a daily periodic variation in propagation delay, highlighting its non-negligible impact on satellite–CV link dynamics.

Figure 3.5 illustrates the joint impact of orbit inclination and propagation delay constraints on satellite coverage duration. Here, the term "connected" indicates that a CV is covered by a LEO satellite when the elevation angle and boresight angle constraints are satisfied. The terms "< 5 ms" and "< 3 ms" further impose additional propagation delay requirements, meaning that a satellite service is considered available only when the propagation delay is less than 5 ms or 3 ms, respectively. These thresholds reflect the diverse delay requirements of different CV services. The results indicate that coverage duration varies significantly with CV location under

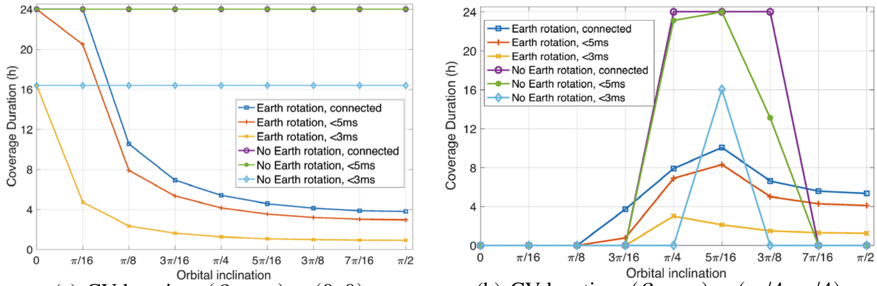

(a) CV location: $(\beta_u, \gamma_u) = (0, 0)$. (b) CV location: $(\beta_u, \gamma_u) = (\pi/4, \pi/4)$.

Fig. 3.5 Satellite coverage duration affected by Earth rotation

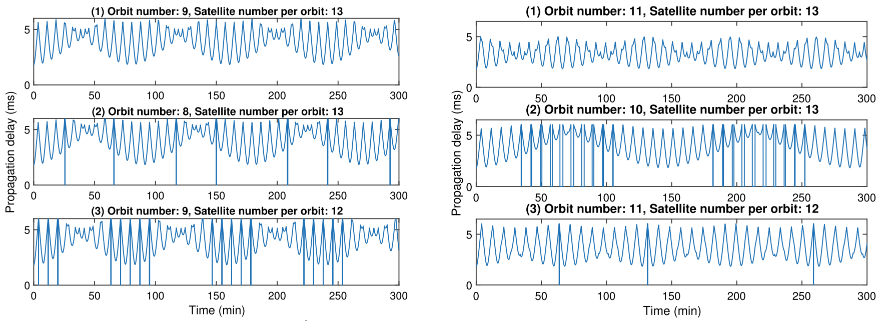

(a) Polar orbits $\alpha = \pi/2$. (b) Inclined orbits $\alpha = \pi/4$.

Fig. 3.6 Validation on the required number of orbits and satellites per orbit (CV location: $(\beta_u, \gamma_u) = (0, 0)$)

the same satellite constellation. For a CV located at $(0, 0)$, the coverage duration generally decreases as the inclination angle increases when Earth rotation is taken into account. In contrast, for a CV located at $(\pi/4, \pi/4)$, satellite coverage is achievable only for specific inclination angles. Overall, accounting for Earth rotation substantially reduces the practical coverage duration compared with idealized scenarios that neglect Earth rotation, underscoring the importance of realistic constellation modeling.

Figure 3.6 demonstrates how the number of orbits and the number of satellites per orbit jointly affect the propagation delay performance. For polar-orbit constellations, seamless coverage is achieved with 9 orbits and 13 satellites per orbit, whereas inclined-orbit constellations with $\alpha = \pi/4$ require seven orbits with thirteen satellites per orbit. When the constellation parameters fall below these thresholds, time intervals with zero propagation delay appear, indicating loss of satellite connectivity. These observations validate our analysis on the required number of orbits and satellites per orbit for seamless coverage.

Figure 3.7 illustrates the relationship between elevation angle constraints, coverage overlap, required satellite density, and propagation delay. Specifically, the

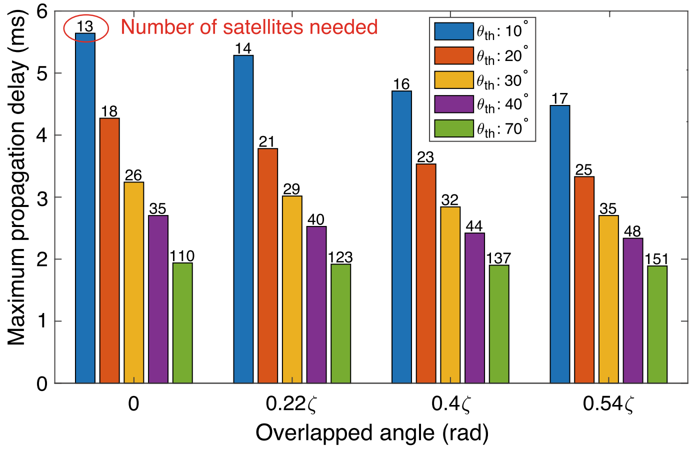

Fig. 3.7 Required number of satellites per orbit and the corresponding maximum propagation delay under different elevation angle thresholds and coverage overlap angles, with an orbit inclination angle of $\pi/2$

required number of satellites on each orbit to avoid a coverage gap is shown on top of each bar in the figure. When the elevation angle threshold θ_{th} is small, as in rural or open environments with minimal blockage, each satellite covers a larger area, leading to larger maximum propagation delays but requiring fewer satellites per orbit. As θ_{th} increases, which may occur in urban environments, the satellite coverage area decreases, resulting in more satellites required on each orbit with a smaller propagation delay. Similarly, increasing the coverage overlap angle ξ improves link robustness and reduces propagation delay at the cost of deploying more satellites.

Finally, Fig. 3.8 indicates the impact of constellation size on the coverage duration in each day under a strict propagation delay constraint of 3 ms. The results show that when the number of orbits is small, adding an orbit is more effective in extending coverage duration than adding satellites within an orbit. For example, in Fig. 3.8a,

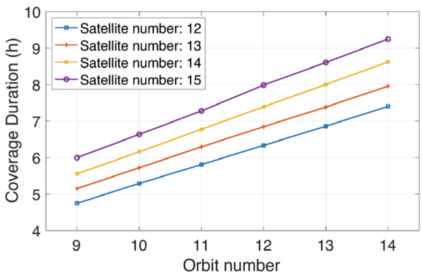

(a) Polar orbits $\alpha = \pi/2$.

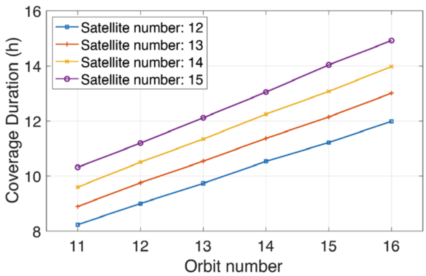

(b) Inclined orbits $\alpha = \pi/4$.

Fig. 3.8 LEO satellite coverage duration with different orbits and satellite numbers when the orbit number is 9, increasing the orbit number leads to a larger coverage duration enhancement than adding one satellite on the same orbit. Nevertheless, when the number of orbits is relatively large, increasing the number of satellites per orbit becomes the dominant factor in enhancing coverage duration.

3.2 Analytical Modeling of Communication Performance

In this section, we investigate the analytical model of communication performance in STVNs by quantifying the impact of satellite orbital parameters on key performance metrics, including service availability, outage probability, and system throughput. Building on the constellation modeling and coverage analysis in Sect. 3.1, we focus on how satellite mobility shapes the time-varying link characteristics experienced by CVs. Since vehicle mobility is relatively slow compared with the orbital motion of LEO satellites, we mainly focus on the impact of satellite mobility in the performance analysis, allowing us to isolate and highlight the dominant effects of satellite dynamics.

3.2.1 LEO Satellite-CV Service Availability

In this subsection, we analyze the service availability of LEO satellite–CV communications by characterizing the probability that at least one satellite can satisfy the communication distance constraint at a given time instant. Based on the satellite motion model in Sect. 3.1.1, the satellite position can be expressed as a function of $\omega(t)$ and $\phi(t)$. For notational simplicity, the explicit dependence on time is omitted, and the satellite–CV distance is rewritten as a function of ϕ and ω, given by

$$\begin{aligned} d(\phi, \omega) = \Big(r^2 + r_{\mathrm{E}}^2 - 2r\big[&x_u(\cos\phi\cos\omega - \sin\phi\sin\omega\cos\alpha) \\ &+ y_u(\cos\phi\sin\omega + \sin\phi\cos\omega\cos\alpha) + z_u\sin\phi\sin\alpha\big]\Big)^{\frac{1}{2}}. \end{aligned} \tag{3.20}$$

For a given orbit inclination angle α and Earth rotation angle ω, the satellite orbit is fixed. Different satellites on the same orbit correspond to different values of ϕ, leading to different satellite–CV distances. The minimum distance between the CV and any satellite on the orbit can be obtained by solving

$$\partial \frac{d(\phi, \omega)}{\partial \phi} = 0, \tag{3.21}$$

which yields

$$\sin^2\phi = \frac{1}{1+\left(\frac{x_u\cos\omega+y_u\sin\omega}{z_u\sin\alpha-x_u\sin\omega\cos\alpha+y_u\cos\omega\cos\alpha}\right)^2}. \tag{3.22}$$

Letting $U = x_u\cos\omega + y_u\sin\omega$ and $Q = z_u\sin\alpha - x_u\sin\omega\cos\alpha + y_u\cos\omega\cos\alpha$, we have

$$\phi = \arcsin\left(Q/\sqrt{Q^2+U^2}\right). \tag{3.23}$$

The minimum satellite–CV distance for a given ϕ and ω is

$$d_{\alpha,\omega}^{\min} = \sqrt{r^2+r_E^2-2r\,(U\cos\phi+Q\sin\phi)} = \sqrt{r^2+r_E^2-2r\sqrt{Q^2+U^2}}. \tag{3.24}$$

If $d_{\alpha,\omega}^{\min} > d_{\max}$, no satellite on the orbit can satisfy the communication distance constraint, and the orbit is not feasible. We then characterize the probability that a satellite orbit is feasible, i.e., the minimum satellite–CV distance on the orbit does not exceed $d_{\max}$. This probability is denoted by P_a^o and given by

$$P_a^o = \Pr\left(d_{\alpha,\omega}^{\min} \le d_{\max}\right). \tag{3.25}$$

The following proposition characterizes P_a^o for both polar and inclined orbits.

Proposition 3.1 *Define $U = x_u\cos\omega + y_u\sin\omega$ and $Q = z_u\sin\alpha - x_u\sin\omega\cos\alpha + y_u\cos\omega\cos\alpha$, as functions of ω. Let ω_1 and ω_2 be the two solutions to $Q^2+U^2 = \left(\frac{r^2+r_{\mathrm{E}}^2-d_{\max}^2}{2r}\right)^2$. For a constellation with N evenly spaced satellite orbits, the probability that at least one orbit is feasible is given by*

$$P_a^o = \begin{cases} \frac{N*|\omega_1-\omega_2|}{\pi}, & \text{if } \alpha = \frac{\pi}{2} \text{ and } |\omega_1-\omega_2| \le \frac{\pi}{N}, \\ 1, & \text{if } \alpha = \frac{\pi}{2} \text{ and } |\omega_1-\omega_2| > \frac{\pi}{N}, \\ \frac{N*|\omega_1-\omega_2|}{2\pi}, & \text{if } \alpha < \frac{\pi}{2} \text{ and } |\omega_1-\omega_2| \le \frac{2\pi}{N}, \\ 1, & \text{if } \alpha < \frac{\pi}{2} \text{ and } |\omega_1-\omega_2| > \frac{2\pi}{N}. \end{cases} \tag{3.26}$$

Proof The probability of a satellite orbit being feasible (i.e., the minimum satellite-CV distance can satisfy the maximum allowable distance constraint) is given by

$$P_a^o = \Pr(d_{\alpha,\omega}^{\min} \le d_{\max}) = \Pr\left(Q^2+U^2 \ge \left(\frac{r^2+r_{\mathrm{E}}^2-d_{\max}^2}{2r}\right)^2\right).$$

When $\alpha = \frac{\pi}{2}$, we have $U = x_u \cos\omega + y_u \sin\omega$ and $Q = z_u$. Therefore, we have

$$\begin{aligned} U^2 + Q^2 &= x_u^2 - x_u^2 \sin^2\omega + y_u^2 \sin^2\omega + 2x_u y_u \cos\omega \sin\omega + z_u^2 \\ &= x_u y_u \sin 2\omega + \frac{x_u^2 - y_u^2}{2} \cos 2\omega + \frac{r_{\mathrm{E}}^2 + z_u^2}{2} \geq \left(\frac{r^2 + r_{\mathrm{E}}^2 - d_{\max}^2}{2r}\right)^2. \end{aligned}$$

Note that the solution to $\mu \sin x + \nu \cos x = \kappa$ is

$$x = 2n\pi \pm \arccos\left(\frac{\kappa}{\sqrt{\mu^2 + \nu^2}}\right) + \arctan(\frac{\mu}{\nu}).$$

Letting $\mu = x_u y_u, \nu = \frac{x_u^2 - y_u^2}{2}, \kappa = \left(\frac{r^2 + r_{\mathrm{E}}^2 - d_{\max}^2}{2r}\right)^2 - \frac{r_{\mathrm{E}}^2 + z_u^2}{2}$, we can derive the two solutions ω_1 and ω_2 to the equation $Q^2 + U^2 = \left(\frac{r^2 + r_{\mathrm{E}}^2 - d_{\max}^2}{2r}\right)^2$ as

$$\begin{aligned} \omega_1 &= -\frac{1}{2}\left(\arccos\left(\frac{\kappa}{\sqrt{\mu^2 + \nu^2}}\right) + \arctan\left(\frac{\mu}{\nu}\right)\right) \\ \omega_2 &= \frac{1}{2}\left(\arccos\left(\frac{\kappa}{\sqrt{\mu^2 + \nu^2}}\right) + \arctan\left(\frac{\mu}{\nu}\right)\right). \end{aligned}$$

In general, for inclined orbits with $\alpha < \pi/2$, equation $Q^2 + U^2 = \left(\frac{r^2 + r_{\mathrm{E}}^2 - d_{\max}^2}{2r}\right)^2$ also has two solutions ω_1 and ω_2. Only when $\omega \in [\min(\omega_1, \omega_2), \max(\omega_1, \omega_2)]$, it is possible that satellites on the orbit can satisfy the communication distance constraint to provide CV services. Therefore, we have

$$P_a^o = \Pr\left(Q^2 + U^2 \geq \left(\frac{r^2 + r_{\mathrm{E}}^2 - d_{\max}^2}{2r}\right)^2\right) = \frac{|\omega_1 - \omega_2|}{2\pi} = \frac{\arccos\left(\frac{\kappa}{\sqrt{\mu^2+\nu^2}}\right)}{2\pi}.$$

When there are N satellite orbits, we consider the maximum orbit separation, i.e., the adjacent two orbits are separated by π/N for polar orbits and $2\pi/N$ for inclined orbits. Therefore, the probability of having at least one feasible satellite orbit can be obtained. ■

When an orbit is feasible, i.e., $\omega \in [\min(\omega_1, \omega_2), \max(\omega_1, \omega_2)]$, a satellite on the orbit is available for the CV only when its orbital angle ϕ satisfies

$$d(\phi, \omega) \leq d_{\max}. \tag{3.27}$$

Letting $\mu = -x_u \sin\omega \cos\alpha + y_u \cos\omega \cos\alpha + z_u \sin\alpha$, $\nu = x_u \cos\omega + y_u \sin\omega$, and $\kappa = \frac{r^2 + r_{\mathrm{E}}^2 - d_{\max}^2}{2r}$, the above condition can be rewritten as

$$\mu \sin\phi + \nu \cos\phi \leq \kappa. \tag{3.28}$$

With M satellites uniformly distributed on the orbit, the probability that at least one satellite on the feasible orbit satisfies the distance constraint is given by

$$P_a^s = \Pr\left(d(\phi, \omega) \leq d_{\max} \mid \omega\right) = \begin{cases} \dfrac{M|\phi_1 - \phi_2|}{2\pi}, & |\phi_1 - \phi_2| \leq \frac{2\pi}{M}, \\ 1, & |\phi_1 - \phi_2| > \frac{2\pi}{M}, \end{cases} \tag{3.29}$$

where

$$\phi_1 = -\arccos\left(\frac{\kappa}{\sqrt{\mu^2 + \nu^2}}\right) + \arctan\left(\frac{\mu}{\nu}\right),$$
$$\phi_2 = \arccos\left(\frac{\kappa}{\sqrt{\mu^2 + \nu^2}}\right) + \arctan\left(\frac{\mu}{\nu}\right).$$

Combining the orbit-level feasibility and the satellite-level availability probabilities, the overall service availability of LEO satellite–CV communication is given by

$$P_{a,1} = P_a^o \cdot P_a^s. \tag{3.30}$$

3.2.2 LEO Satellite-CV Outage Probability

When the satellite-CV distance is smaller than $d_{\max}$, the elevation angle and boresight angle constraints are satisfied, and the satellite service is considered available in the geometric sense. Beyond link availability, CV services must satisfy minimum throughput requirements. A service outage occurs when the achievable link capacity falls below the required throughput. Considering satellite-CV communications over an additive white Gaussian noise (AWGN) channel with free-space path loss, the link capacity can be calculated using the Shannon formula, given by

$$C_1 = B_1 \log_2\left(1 + \frac{G_{t,1} G_{r,1} p_1 c^2}{(4\pi f_1)^2 \sigma^2 d^2}\right), \tag{3.31}$$

where $G_{t,1}$ and $G_{r,1}$ are the transmit and receive antenna gains, B_1 is the bandwidth, p_1 is the transmit power, c is the light speed, f_1 is the carrier frequency, and σ^2 is the noise power.

Proposition 3.2 *Denote by $R_{t,1}$ the required LEO satellite-CV throughput. Conditioned on the satellite-CV distance being smaller than $d_{\max}$, the service outage probability is*

$$P_{o,1} = \min\left(1,\ \max\left(0,\ \frac{d_{\max}^2 - \frac{G_{t,1}G_{r,1}p_1c^2}{(4\pi f_1)^2\sigma^2\left(2^{R_{t,1}/B_1}-1\right)}}{d_{\max}^2 - h^2}\right)\right).$$

Proof service outage occurs when $C_1 \leq R_{t,1}$. Conditioned on $d \leq d_{\max}$, we have

$$P_{o,1} = \Pr\left(C_1 \leq R_{t,1} \,\middle|\, d \leq d_{\max}\right) = \Pr\left(d \geq d_{t,1} \,\middle|\, d \leq d_{\max}\right), \tag{3.32}$$

where the distance threshold $d_{t,1}$ is obtained by solving $C_1 = R_{t,1}$, yielding

$$d_{t,1} = \sqrt{\frac{A_1}{2^{R_{t,1}/B_1} - 1}}, \qquad A_1 = \frac{G_{t,1}G_{r,1}p_1c^2}{(4\pi f_1)^2\sigma^2}. \tag{3.33}$$

Thus, the throughput requirement is satisfied only if the satellite-CV distance $d \leq d_{t,1}$ to avoid service outage. Under the spherical geometry model, the set of satellite positions satisfying $d \leq x$ forms a spherical cap on the satellite orbit sphere. Let $\mathcal{S}(x)$ denote the area of this spherical cap for a distance threshold x, given by

$$\mathcal{S}(x) = \frac{\pi(r_{\mathrm{E}} + h)(x^2 - h^2)}{r_{\mathrm{E}}} \tag{3.34}$$

Then, conditioned on $d \leq d_{\max}$, the outage probability equals the fraction of the geometrically available region that does not satisfy the throughput constraint, given by

$$P_{o,1} = \frac{\mathcal{S}(d_{\max}) - \mathcal{S}(d_{t,1})}{\mathcal{S}(d_{\max})} = \frac{d_{\max}^2 - d_{t,1}^2}{d_{\max}^2 - h^2}. \tag{3.35}$$

Finally, boundary cases are handled as follows. If $d_{t,1} < h$, even the closest satellite (at distance h) cannot satisfy the throughput requirement, and thus $P_{o,1} = 1$. If $d_{t,1} \geq d_{\max}$, the throughput requirement is satisfied whenever the geometric constraints are met, and thus $P_{o,1} = 0$. Overall, the satellite-CV service outage probability is

$$P_{o,1} = \min\left(1, \max\left(0, \frac{d_{\max}^2 - d_{t,1}^2}{d_{\max}^2 - h^2}\right)\right). \tag{3.36}$$

■

3.2.3 LEO Satellite-CV Throughput

Building on the service availability analysis in Sect. 3.2.1 and the outage probability characterization in Sect. 3.2.2, we define the achievable LEO satellite-CV throughput as the data rate that can be successfully delivered without service outage. Specifically, for a satellite-CV link with transmission rate R, the achievable throughput is given by

$$T_1 = P_{a,1}\,(1 - P_{o,1})\,R = \begin{cases} P_{a,1}\ R, & R \in \left[0,\ R_{\max}^1\right], \\ P_{a,1}\ \frac{\frac{A_1}{2^{R/B_1}-1} - h^2}{d_{\max}^2 - h^2}\ R, & R \in \left[R_{\max}^1,\ R_{\max}^2\right], \\ 0, & R \in \left[R_{\max}^2,\ \infty\right], \end{cases} \tag{3.37}$$

where $R_{\max}^1 = B_1 \log_2\left(1 + \frac{A_1}{d_{\max}^2}\right)$ and $R_{\max}^2 = B_1 \log_2\left(1 + \frac{A_1}{h^2}\right)$. The expression reflects the tradeoff between increasing the transmission rate and the resulting outage probability.

Proposition 3.3 *For a LEO satellite-CV link with transmission rate R, the maximum achievable throughput is obtained when $R = B_1 \log_2(1 + \frac{A_1}{d_{\max}^2})$, yielding*

$$T_{1,\max} = P_{a,1} B_1 \log_2\left(1 + \frac{A_1}{d_{\max}^2}\right).$$

Proof or $R \in [0,\ R_{\max}^1]$, the outage probability is zero and T_1 increases linearly with R. For $R \in [R_{\max}^1,\ R_{\max}^2]$, differentiating (3.37) with respect to R, we can have

$$\frac{\partial T_1}{\partial R} = \frac{P_{a,1}}{d_{\max}^2 - h^2}\left[\frac{A_1}{2^{R/B_1} - 1}\left(1 - \frac{R \ln 2}{B_1}\frac{2^{R/B_1}}{2^{R/B_1} - 1}\right) - h^2\right]. \tag{3.38}$$

By analyzing the monotonicity of the term $f(x) = \frac{x 2^x}{2^x - 1}$, where $x = \frac{R}{B_1}$, we have

$$f'(x) = \frac{2^x}{(2^x - 1)^2}\left(2^x - 1 - x \ln 2\right).$$

Since $(2^x - 1 - x \ln 2)' = 2^x \ln 2 - \ln 2 \geq 0$ when $x \geq 0$, we have f monotonically increases with x. When x is approached to 0, we have

$$f(x) = \frac{x\,(1 + x \ln 2 + o(x))}{x \ln 2 + o(x)} \longrightarrow [x \to 0]\frac{1}{\ln 2}. \tag{3.39}$$

In this case, it can be shown that

$$\frac{\partial T_1}{\partial R} = \frac{P_{a,1}}{d_{max}^2 - h^2} \cdot \left[\frac{A_1}{2^{R/B_1} - 1} \left(1 - \frac{R \ln 2}{B_1} \frac{2^{R/B_1}}{(2^{R/B_1} - 1)} \right) - h^2 \right]$$
$$\leq \frac{P_{a,1}}{d_{\max}^2 - h^2} \cdot \left[\frac{A_1}{2^{R/B_1} - 1} \left(1 - \ln 2 \cdot \frac{1}{\ln 2} \right) - h^2 \right] < 0.$$

Therefore, T_1 decreases monotonically with R when $R \geq R_{\max}^1$, and the maximum throughput is achieved at $R = R_{\max}^1$. ■

When n CVs are simultaneously served by the same LEO satellite using orthogonal channel resources, the overall achievable throughput is

$$T_{1,n} = nP_{a,1} \left(1 - \min \left(1, \max \left(0, \frac{d_{\max}^2 - d_{t,n}^2}{d_{\max}^2 - h^2} \right) \right) \right) R, \tag{3.40}$$

where

$$d_{t,n} = \sqrt{\frac{A_1}{2^{nR_{t,1}/B_1} - 1}}. \tag{3.41}$$

In this case, the satellite-CV distance must be no greater than $d_{t,n}$ to avoid service outage. Similar to the single-user case, the maximum overall throughput is achieved when $nR = B_1 \log_2\left(1 + \frac{A_1}{d_{\max}^2}\right)$, given by

$$T_{1,\max} = P_{a,1} B_1 \log_2 \left(1 + \frac{A_1}{d_{\max}^2} \right). \tag{3.42}$$

3.2.4 Performance Evaluation of LEO Satellite-CV Communications

We evaluate the performance of LEO satellite–CV communications in terms of service availability, outage probability, and system throughput under different satellite constellation parameters. The default satellite communication parameters are listed in Table 3.3.

Table 3.3 LEO satellite communication parameters [5]

Carrier frequency f_1	20 GHz	Transmission power p_1	10 W
Bandwidth B_1	500 MHz	Noise power σ^2	–117 dBW
Transmission antenna gains $G_{t,1}$	32 dBi	Receiving antenna gains $G_{r,1}$	34 dBi

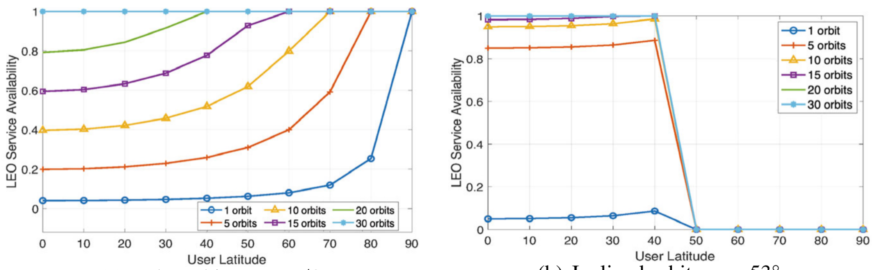

(a) Polar orbits $\alpha = \pi/2$.

(b) Inclined orbits $\alpha = 53°$.

Fig. 3.9 LEO satellite-CV communication service availability with different orbit inclination angles and CV latitudes

Figure 3.9 illustrates the LEO satellite–CV service availability for different orbit inclination angles and CV latitudes. As shown in Fig. 3.9a, polar orbits provide superior coverage for CVs located at high latitudes. Moreover, increasing the number of orbits can significantly improve the service availability. In contrast, with the orbit inclination angle of 53° as shown in Fig. 3.9b, inclined orbits offer better coverage for CVs at low latitudes compared with polar orbits. These results indicate that, to achieve uniformly high service availability across both high- and low-latitude regions, a hybrid constellation design combining polar and inclined orbits should be adopted.

Figure 3.10 depicts the impact of the minimum elevation angle θ_{th} and the required satellite communication data rate $R_{t,1}$ on the service outage probability. For a given θ_{th}, the outage probability increases with $R_{t,1}$, since a higher data rate represents a stricter constraint on the maximum allowable satellite–CV distance. On the other hand, for a fixed $R_{t,1}$, increasing θ_{th} leads to both reduced service availability and higher outage probability. When $R_{t,1}$ is below a certain threshold, the outage probability remains 0, whereas excessively large values of $R_{t,1}$ result in an outage probability of 1.

Figure 3.11 presents the achievable LEO satellite–CV throughput for different values of θ_{th} and transmission rate R. The throughput first increases and then decreases with R, which is consistent with the theoretical analysis in Sect. 3.2.3. Specifically, a small R limits the data rate, while a large R significantly increases the outage probability, both leading to a low throughput. When θ_{th} is small, the outage probability is high, as observed in Fig. 3.10; when θ_{th} is large, the satellite availability probability decreases, as reflected by the reduced slope of the increasing portion of the throughput curve. Both cases degrade the overall throughput. Comparing Fig. 3.11a, b, increasing the number of orbits enhances the satellite availability probability and mitigates the impact of θ_{th} on service availability, thereby improving the achievable throughput. These results suggest that the transmission rate R and the elevation angle threshold θ_{th} should be jointly optimized to maximize the overall LEO satellite–CV throughput.

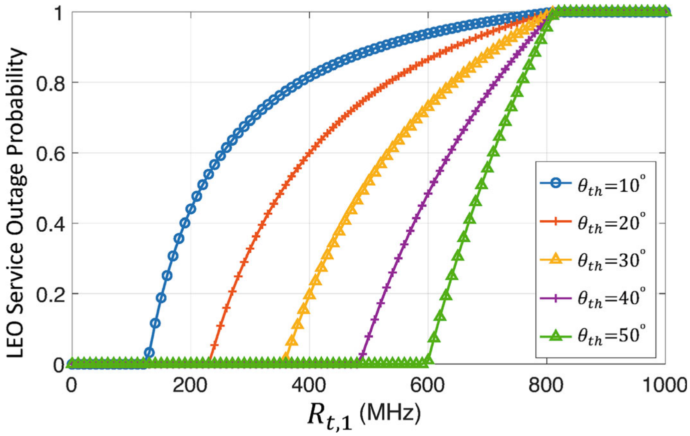

Fig. 3.10 LEO satellite-CV outage probability with different elevation angle and data rate requirements ($\alpha = 53°$)

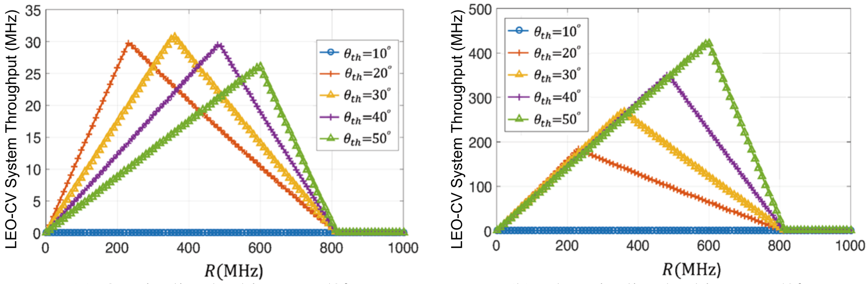

(a) One inclined orbits $\alpha = 53°$ (b) Three inclined orbits $\alpha = 53°$

Fig. 3.11 LEO satellite-CV communication throughput with different θ_{th} and R

3.3 Impacts of Terrestrial Deployment on STVNs

Building on the analytical modeling of LEO satellite–CV communication performance, we extend the study to STVNs by examining the impact of different terrestrial network deployment strategies on STVN performance.

3.3.1 Terrestrial Network Deployment Strategies

In terrestrial CV networks, the deployment of RSUs is closely related to road layouts. To capture this dependency, we consider two representative road geometries, as illustrated in Fig. 3.12. Specifically, Fig. 3.12a depicts a parallel-road layout with an inter-road spacing of ϱ, while Fig. 3.12b shows a crossed-road layout with the same

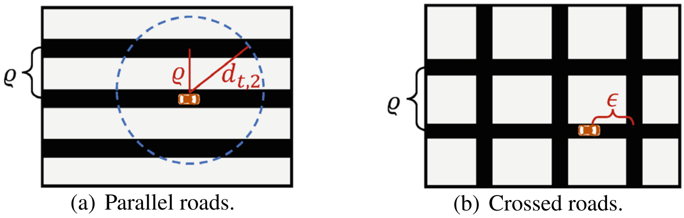

Fig. 3.12 Two different road layouts

spacing ϱ. Based on these road layouts, we consider three typical terrestrial RSU deployment strategies:

- **1D Poisson point process (PPP):** RSUs are deployed along roads according to a one-dimensional PPP.
- **1D equal-interval:** RSUs are deployed along roads with equal distance separations.
- **2D PPP:** For comparison, we further consider a scenario where RSUs or cellular base stations (BSs) are deployed over a two-dimensional area following a PPP, independent of the road layout [6]. For notational consistency, the term RSU is used to represent both RSUs and BSs.

By combining the road layouts and RSU deployment strategies, five terrestrial deployment cases are considered:

- **Case a**: 2D PPP RSU deployment with intensity $\lambda_{\mathbf{a}}$.
- **Case b**: 1D PPP RSU deployment on parallel roads with intensity $\lambda_{\mathbf{b}}$.
- **Case c**: 1D PPP RSU deployment on crossed roads with intensity $\lambda_{\mathbf{c}}$.
- **Case d**: 1D equal-interval RSU deployment on parallel roads with intensity $\lambda_{\mathbf{d}}$.
- **Case e**: 1D equal-interval RSU deployment on crossed roads with intensity $\lambda_{\mathbf{e}}$.

In **Case a**, the number of RSUs in a unit area follows a Poisson distribution with parameter $\lambda_{\mathbf{a}}$, and the probability that no RSU exists within an area of size ς is given by $e^{-\lambda_{\mathbf{a}}\varsigma}$. In **Case b** and **Case c**, where RSUs are deployed along roads according to a 1D PPP, the probabilities that no RSU exists within a road segment of length l are $e^{-\lambda_{\mathbf{b}}l}$ and $e^{-\lambda_{\mathbf{c}}l}$, respectively.

In **Case d** and **Case e**, RSUs are deployed with equal intervals, where the inter-RSU distances are $I_{\mathbf{d}} = 1/\lambda_{\mathbf{d}}$ and $I_{\mathbf{e}} = 1/\lambda_{\mathbf{e}}$, respectively. In this case, the probability that no RSU exists within a road segment of length l can be expressed as

$$f_{\mathrm{N}}(\lambda, l) = \max\left(0, \frac{1/\lambda - l}{1/\lambda}\right), \tag{3.43}$$

which yields $f_{\mathrm{N}}(\lambda_{\mathbf{d}}, l)$ and $f_{\mathrm{N}}(\lambda_{\mathbf{e}}, l)$ for **Case d** and **Case e**, respectively.

3.3.2 Service Outage Probability and Throughput

For terrestrial RSU-CV communications over an AWGN channel, the achievable link capacity calculated by the Shannon formula can be given by

$$C_2 = B_2 \log_2 \left(1 + \frac{G_{t,2} G_{r,2} p_2 c^2}{(4\pi f_2)^2 \sigma^2 d^{\alpha_\mathrm{P}}}\right), \tag{3.44}$$

where $G_{t,2}$, $G_{r,2}$, B_2, p_2, f_2, α_P, and σ^2 denote the transmit antenna gain, receive antenna gain, channel bandwidth, transmit power, carrier frequency, path-loss exponent, and noise power, respectively.

To satisfy a target terrestrial data rate $R_{t,2}$, the condition $C_2 \geq R_{t,2}$ must hold, which leads to the maximum allowable RSU–CV communication distance, given by

$$d \leq d_{t,2} = \left(\frac{A_2}{2^{R_{t,2}/B_2} - 1}\right)^{\frac{1}{\alpha_\mathrm{P}}}, \tag{3.45}$$

where

$$A_2 = \frac{G_{t,2} G_{r,2} p_2 c^2}{(4\pi f_2)^2 \sigma^2}. \tag{3.46}$$

For a CV, a terrestrial service outage occurs when no RSU is available within a distance of $d_{t,2}$ from the CV. Note that for 1D RSU deployments along roads, RSUs on adjacent roads should also be taken into account. Accordingly, the service outage probabilities for different RSU deployment cases are derived as

$$P_{o,2}^{\mathbf{a}} = e^{-\lambda_\mathbf{a} \pi d_{t,2}{}^2}, \tag{3.47a}$$

$$P_{o,2}^{\mathbf{b}} = e^{-2\lambda_\mathbf{b} d_{t,2}} \prod_{i=1}^{\lfloor d_{t,2}/\varrho \rfloor} e^{-4\lambda_\mathbf{b} \sqrt{d_{t,2}^2 - (i\varrho)^2}}, \tag{3.47b}$$

$$\begin{aligned} P_{o,2}^{\mathbf{c}} = {} & e^{-2\lambda_\mathbf{c} d_{t,2}} \prod_{i=1}^{\lfloor d_{t,2}/\varrho \rfloor} e^{-4\lambda_\mathbf{c} \sqrt{d_{t,2}^2 - (i\varrho)^2}} \\ & \times \int_0^\varrho \frac{1}{\varrho} \left(\prod_{i=0}^{\lfloor \frac{d_{t,2}-\epsilon}{\varrho} \rfloor} e^{-2\lambda_\mathbf{c} \sqrt{d_{t,2}^2 - (i\varrho+\epsilon)^2}} \times \prod_{i=1}^{\lfloor \frac{d_{t,2}+\epsilon}{\varrho} \rfloor} e^{-2\lambda_\mathbf{c} \sqrt{d_{t,2}^2 - (i\varrho-\epsilon)^2}} \right) \mathrm{d}\epsilon, \end{aligned} \tag{3.47c}$$

$$P_{o,2}^{\mathbf{d}} = f_\mathrm{N}(\lambda_\mathbf{d}, 2d_{t,2}) \prod_{i=1}^{\lfloor \frac{d_{t,2}}{\varrho} \rfloor} \left(f_\mathrm{N} \left(\lambda_\mathbf{d}, 2\sqrt{d_{t,2}^2 - (i\varrho)^2} \right) \right)^2, \tag{3.47d}$$

$$\begin{aligned} P_{o,2}^{\mathbf{e}} = {} & f_\mathrm{N}\left(\lambda_\mathbf{e}, 2d_{t,2}\right) \prod_{i=1}^{\lfloor \frac{d_{t,2}}{\varrho} \rfloor} \left(f_\mathrm{N} \left(\lambda_\mathbf{e}, 2\sqrt{d_{t,2}^2 - (i\varrho)^2} \right) \right)^2 \\ & \times \int_0^\varrho \frac{1}{\varrho} \left(\prod_{i=0}^{\lfloor \frac{d_{t,2}-\epsilon}{\varrho} \rfloor} f_\mathrm{N} \left(\lambda_\mathbf{e}, 2\sqrt{d_{t,2}^2 - (i\varrho+\epsilon)^2} \right) \right. \\ & \left. \times \prod_{i=1}^{\lfloor \frac{d_{t,2}+\epsilon}{\varrho} \rfloor} f_\mathrm{N} \left(\lambda_\mathbf{e}, 2\sqrt{d_{t,2}^2 - (i\varrho-\epsilon)^2} \right) \right) \mathrm{d}\epsilon. \end{aligned} \tag{3.47e}$$

The average throughput of a terrestrial RSU-CV link is defined as the data rate from RSUs to the CV without service outage. In **Case a**, suppose that an RSU simultaneously serves n CVs with a transmission rate R for each CV. The resulting average aggregate throughput can be expressed as

$$T_2^{\mathbf{a}} = nR\left(1 - e^{-\lambda_{\mathbf{a}}\pi\left(\frac{A_2}{2^{nR/B_2}-1}\right)^{2/\alpha_P}}\right). \tag{3.48}$$

By letting $x = nR$, $T_2^{\mathbf{a}}$ becomes a concave function of x. Therefore, the optimal value of x that maximizes the terrestrial throughput can be obtained by solving the first-order optimality condition

$$\frac{\partial T_2^{\mathbf{a}}}{\partial x} = 1 - e^{-\lambda_{\mathbf{a}}\pi\left(\frac{A_2}{2^{x/B_2}-1}\right)^{2/\alpha_P}}\left(1 + \frac{x 2\lambda_{\mathbf{a}}\pi A_2^{2/\alpha_P}\ln 2}{\alpha_P B_2}\frac{2^{x/B_2}}{\left(2^{x/B_2}-1\right)^{2/\alpha_P+1}}\right) = 0, \tag{3.49}$$

which can be efficiently solved using computing software tools such as MATLAB toolboxes. The corresponding maximum achievable terrestrial throughput is denoted by $T_{2,\max}^{\mathbf{a}}$. The maximum achievable terrestrial throughput in **Cases b–e** can be obtained following the same procedure.

Assuming that satellite and terrestrial networks operate over orthogonal frequency bands, the overall service availability of STVNs under terrestrial deployment **Case x** ($\mathbf{x} \in \{\mathbf{a}, \mathbf{b}, \mathbf{c}, \mathbf{d}, \mathbf{e}\}$) is given by

$$P_a = 1 - P_{o,2}^{\mathbf{x}} \cdot \left(1 - P_{a,1} \cdot (1 - P_{o,1})\right). \tag{3.50}$$

Accordingly, the overall achievable STVN throughput is the sum of the satellite and terrestrial throughputs for deployment **Case x**, expressed as

$$T = T_{1,\max} + T_{2,\max}^{\mathbf{x}}. \tag{3.51}$$

3.3.3 Performance Evaluation of Different Terrestrial Network Deployment Strategies

We investigate the impact of terrestrial network deployment strategies on the communication performance of STVNs through simulations. The number of LEO satellite orbits is set to three, the orbit inclination angle is 53°, and the minimum elevation angle is 30°. The default terrestrial communication parameters are listed in Table 3.4.

Figure 3.13 illustrates the terrestrial CV network throughput for different transmission rates R and numbers of CVs n served by a single RSU. As shown in Fig. 3.13a–c, although the optimal transmission rate per CV varies with the number of served CVs,

Table 3.4 Terrestrial communication parameters [7]

Carrier frequency f_2	28 GHz	Transmission power p_2	28 dBm
Bandwidth B_2	200 MHz	Path-loss exponent α_P	3
Transmission antenna gains $G_{t,2}$	3 dBi	Receiving antenna gains $G_{r,2}$	3 dBi

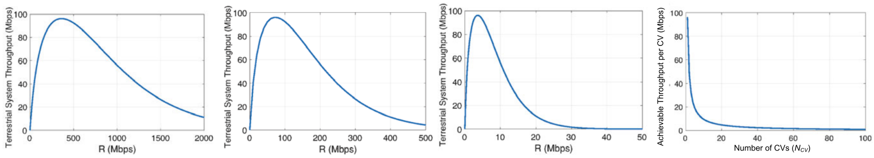

(a) $n = 1$. (b) $n = 5$. (c) $n = 100$. (d) Throughput per CV.

Fig. 3.13 Terrestrial CV network throughput performance (**Case a:** 2D PPP RSU deployment with intensity $\lambda_{\mathbf{a}} = 5 * 10^{-5}$)

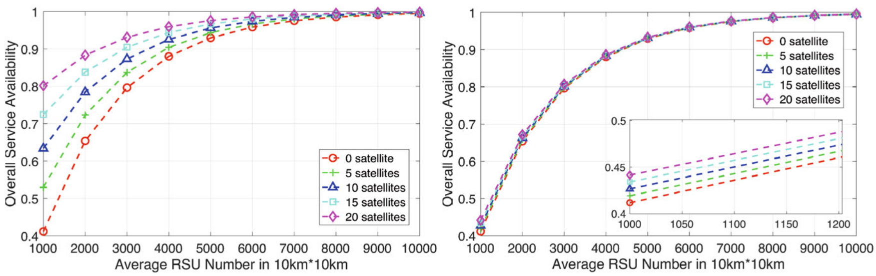

(a) Elevation angle constraint $\theta_{\text{th}} = 30°$. (b) Elevation angle constraint $\theta_{\text{th}} = 70°$.

Fig. 3.14 Impact of RSU deployment intensities (**Case a**), numbers of satellites, and elevation angle constraints on the overall service availability in STVNs

the maximum achievable aggregate terrestrial throughput remains the same, which is consistent with the analytical results in Sect. 3.3.2. As shown in Fig. 3.13d, serving more CVs with one RSU leads to a reduced achievable throughput per CV, reflecting the resource-sharing tradeoff among multiple users.

Figure 3.14 depicts the STVN service availability under different RSU deployment intensities, satellite numbers, and elevation angle constraints. With more RSUs deployed or more satellites per orbit, the overall service availability improves. Notably, when the RSU deployment intensity is low and the elevation angle threshold θ_{th} is small, corresponding to rural scenarios with sparse terrestrial infrastructure, the service availability improvement introduced by LEO satellites is substantial. In contrast, in dense RSU deployment scenarios with large θ_{th}, which can be regarded as urban environments, the additional benefit provided by LEO satellites becomes marginal.

Next, we compare the STVN performance under different RSU deployment cases (i.e., **Cases a–e**). For a fair comparison, we fix the average number of RSUs within

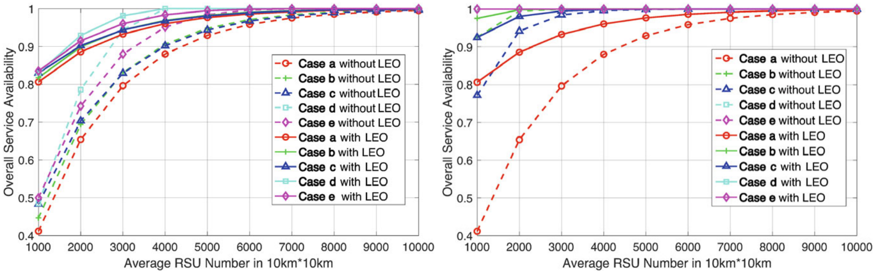

(a) Road interval ϱ = 100 m. (b) Road interval ϱ = 1000 m.

Fig. 3.15 Overall service availability in STVNs with different RSU deployment strategies and intensities (CVs are always on roads, LEO satellite orbit number: 20)

a target square area of size s^2 to n_R for all deployment strategies. Accordingly, the RSU deployment intensities are given by

$$\lambda_{\mathbf{a}} = \frac{n_R}{s^2},\ \lambda_{\mathbf{b}} = \lambda_{\mathbf{d}} = \frac{n_R \varrho}{s^2},\ \lambda_{\mathbf{c}} = \lambda_{\mathbf{e}} = \frac{n_R \varrho}{s^2}.$$

Figure 3.15 shows the overall service availability in STVNs when all CVs are located on roads. Specifically, Fig. 3.15a corresponds to a high road-density scenario with an inter-road distance of 100 m, which can be regarded as a typical urban layout, while Fig. 3.15b represents a low road-density scenario with an inter-road distance of 1000 m. Without LEO satellites, the service availability varies significantly with the RSU deployment intensity for all deployment cases. By integrating LEO satellites, the service availability can be substantially improved, especially in scenarios with sparse RSU deployment. Among different deployment strategies, 1D PPP RSU deployments (i.e., **Cases b–e**) achieve higher service availability than the 2D PPP deployment (**Case a**), since RSUs are deployed along roads to more effectively serve on-road vehicles. In contrast, the 2D PPP deployment achieves low service availability, particularly in low road-density scenarios, as some RSUs may be located far from road segments.

Finally, we consider more general scenarios where CVs are not necessarily confined to roads, such as parking areas, airports, or dense urban environments where RSUs are only deployed along major roads. As shown in Fig. 3.16a, when the road density is high, 1D on-road deployments (**Cases b–e**) outperform the 2D PPP deployment in terms of service availability, since most CVs remain within the coverage of RSUs. However, in low road-density scenarios, as shown in Fig. 3.16b, the 2D PPP deployment provides better service availability, since RSUs with 2D PPP deployment can more effectively serve off-road CVs, whereas 1D on-road deployments only cover limited areas near roads.

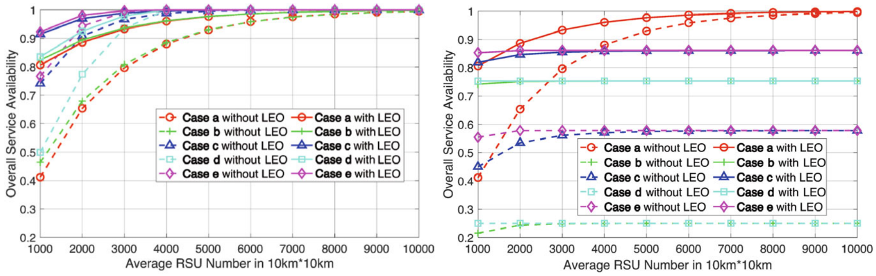

(a) Road interval ϱ = 100 m. (b) Road interval ϱ = 1000 m.

Fig. 3.16 Overall service availability in STVNs with different RSU deployment strategies and intensities (CVs are not always on roads, LEO satellite orbit number: 20)

3.4 Summary

In this chapter, theoretical models for LEO satellite–CV communications were developed. By considering practical satellite constellation parameters and terrestrial infrastructure deployment strategies, we model key performance metrics for performance analysis, including service availability, outage probability, and achievable throughput. The analytical modeling and numerical results reveal how satellite orbital configurations and RSU deployment patterns jointly shape the performance of STVNs, and demonstrate the performance gains enabled by LEO satellites, especially in scenarios with limited terrestrial coverage. The modeling in this chapter provides a fundamental baseline and serves as the analytical foundation for STVN resource management studied in the subsequent chapters.

References

1. Shen, X., Cheng, N., Zhou, H., Lyu, F., Quan, W., Shi, W., Wu, H., Zhou, C.: Space-air-ground integrated networks: review and prospect. Chinese J. Internet Things **4**(3), 3–19 (2020)
2. Zhu, X., Jiang, C.: Creating efficient integrated satellite-terrestrial networks in the 6G era. IEEE Wireless Commun. **29**(4), 154–160 (2022)
3. Wu, H., He, M., Shen, X., Zhuang, W., Dao, N., Shi, W.: Network performance analysis of satellite-terrestrial vehicular network. IEEE Internet Things J. **11**(9), 16829–16844 (2024)
4. 3GPP: Solutions for NR to support non-terrestrial networks (NTN), vol. 16, (2023). Technical Report version 16.2.0, release
5. Leyva-Mayorga, I., Soret, B., Matthiesen, B., Röper, M., Wübben, D., Dekorsy, A., Popovski, P.: Non-geostationary orbit constellation design for global connectivity. Chap. **10**, 237–267 (2024)
6. Zheng, T.X., Wen, Y., Liu, H.W., Ju, Y., Wang, H.M., Wong, K.K., Yuan, J.: Physical-layer security of uplink mmwave transmissions in cellular V2X networks. IEEE Trans. Wireless Commun. , (2022)
7. 3GPP: Base station (BS) radio transmission and reception, (2026). Technical Specification version 19.3.0, release 19

Chapter 4
Adaptive Resource Slicing for HD Map Distribution in STVNs

Abstract Building on the theoretical modelings for satellite–terrestrial vehicular network (STVN) performance analysis, this chapter investigates reservation-stage resource slicing for High-Definition (HD) map distribution in STVNs. Under the slicing-based two-stage resource management framework, large-timescale resource reservation is essential for ensuring service continuity and efficiency under time-varying satellite availability and heterogeneous terrestrial deployment. A joint management of communication and caching resources is considered across Low Earth orbit (LEO) satellites and terrestrial base stations (BSs). To exploit the heterogeneity of satellite and terrestrial networks, two slices are established to support multicast and unicast transmissions with distinct requirements. Specifically, multicast transmissions are enabled by LEO satellites to efficiently disseminate popular HD map contents, while unicast transmissions are jointly supported by both satellite and terrestrial networks to serve individualized demands. To cope with spatiotemporal demand fluctuations, time-varying satellite availability, and multi-dimensional resource coupling, the resource slicing problem is formulated as a long-term optimization problem, and a hybrid data-model co-driven approach-based two-layer resource slicing (TLRS) scheme is proposed. In the inner layer, multicast transmission and caching decisions within each slicing window are determined using a swap-based matching algorithm. In the outer layer, a hybrid proximal policy optimization (HPPO)-based reinforcement learning algorithm is employed to dynamically adjust the slicing window length and reserve communication resources in response to network dynamics. Simulation results demonstrate that the proposed TLRS scheme can effectively satisfy HD map service requirements while improving resource utilization and reducing average delay in STVNs.

Keywords Adaptive resource slicing · High-definition map distribution · Many-to-many matching · Deep reinforcement learning

Driven by the rapid evolution of intelligent transportation systems, the advancement of connected vehicles (CVs) necessitates the integration of HD maps as a fundamental infrastructure. Specifically, High-Definition (HD) maps provide decimeter-level geographic information, including lane models, traffic signals, and road geometry, which is essential for precise localization and safe navigation. However, compared

M. He et al., *Resource Management for Satellite-Terrestrial Vehicular Networks*, SpringerBriefs in Computer Science, https://doi.org/10.1007/978-3-032-24526-7_4

to traditional digital maps, HD maps involve massive data volumes, making onboard storage impractical, which necessitates robust and real-time delivery through vehicular networks to fully unlock their potential [1].

As established in previous chapters, although terrestrial networks can effectively support HD map distribution in urban areas, satellite-terrestrial vehicular networks (STVNs) are indispensable for achieving ubiquitous coverage in suburban and remote regions. By integrating low Earth orbit (LEO) satellites with terrestrial base stations (BSs) and deploying edge servers, STVNs enable low-latency and wide-area data access for CVs [2]. To guarantee the stringent service requirements of HD map distribution, resource slicing, as a key technique for service-oriented resource management, continues to play a pivotal role in STVNs [3, 4]. Specifically, resource slicing allows multiple virtual networks, referred to as network slices, to be constructed over shared physical infrastructure, enabling resource isolation and differentiated service provisioning. In reservation-stage resource management, network slices are configured by reserving resources over large timescales, which simplifies network management and mitigates competition among slices. To adapt to time-varying service demands while maintaining efficient resource utilization, slices must be periodically reconfigured, where the reconfiguration interval is referred to as the slicing window. Therefore, this chapter focuses on adaptive resource slicing in STVNs by jointly reserving communication and caching resources to support HD map distribution for CVs.

Although resource slicing has attracted substantial research interest, as reviewed in Chap. 2, several critical challenges remain insufficiently studied in dynamic STVN environments, particularly for reserving multi-dimensional resources. First, satellite and terrestrial networks differ in transmission modes and resource utilization, complementing each other in HD map distribution. The top-down multicast capability of LEO satellites enables efficient distribution of popular HD map contents to multiple CVs with similar channel conditions, significantly reducing resource consumption compared to request–response-based unicast transmission. However, multicast transmission of HD map contents is inherently periodic and may introduce additional waiting time, making unicast transmission still necessary for individual demands. By contrast, terrestrial networks primarily rely on unicast transmission, which offers higher flexibility in adapting to heterogeneous channel conditions within a BS's coverage. Consequently, jointly managing communication and caching resources for both multicast and unicast transmissions across satellite and terrestrial networks becomes highly challenging. Second, STVNs exhibit significantly higher system dynamics and uncertainty compared to purely terrestrial networks, which fundamentally complicates reservation-stage slice management. Service demands generated by CVs vary over both space and time due to vehicle mobility, while satellite mobility introduces additional dynamics through time-varying visibility windows and intermittent connectivity, resulting in fluctuating available resources. As a result, the resource state in STVNs evolves much faster and more heterogeneous conditions than in terrestrial networks with relatively stable resources, which enhances the difficulties in long-term resource reservation and slice configuration. Third, beyond the increased system dynamics, determining an appropriate slicing window length becomes a critical problem in STVNs. A long slicing window may lead to resource underutilization during off-peak periods, whereas a short window improves adaptability but incurs higher reconfiguration overhead. Although exploiting time-varying resources can enhance efficiency and reduce operational costs, striking an appropriate balance between reserved resources and slicing window length remains a key challenge.

In this chapter, we investigate the multi-dimensional resource slicing problem for HD map distribution in STVNs, aiming to reserve resources across satellite and terrestrial networks to minimize delay and resource usage while maximizing service fulfillment. Motivated by the distinct characteristics of multicast and unicast transmissions, we design a novel resource slicing architecture that establishes two collaborative slices to support HD map distribution. To address the complexity arising from interdependent multi-dimensional resources and slicing window optimization, we propose a two-layer resource slicing (TLRS) scheme based on a data–model co-driven approach. Specifically, in the outer layer, a reinforcement learning (RL)-based algorithm is developed to jointly determine the slicing window length and reserved communication resources, capturing long-term time-varying resources and spatiotemporal service demand dynamics. In the inner layer, given the reserved communication resources and slicing window length, a swap-based matching algorithm is designed to optimize multicast and caching decisions within each slicing window. The main contributions of this chapter are summarized as follows:

- We investigate reservation-stage resource management in STVNs, where LEO satellites and terrestrial BSs collaboratively support HD map distribution. Leveraging the complementary characteristics of multicast and unicast transmissions, we design a resource slicing architecture with two cooperative slices and formulate a multi-dimensional resource slicing problem that jointly optimizes communication resources, caching decisions, and slicing window length.
- We propose a TLRS scheme to enable adaptive multi-dimensional resource slicing in STVNs. By decoupling the original problem into two subproblems, the outer layer focuses on long-term slicing window and resource reservation decisions, while the inner layer optimizes multicast and caching decisions within each slicing window, which reduces the complexity of sequential decision-making.
- We develop a hybrid proximal policy optimization (HPPO)-based RL algorithm to jointly determine the discrete slicing window length and continuous communication resource reservation at the beginning of each slicing window to minimize the long-term system cost. Based on these decisions, a swap-based matching algorithm is further designed to efficiently optimize multicast and caching strategies within each window.

The remainder of this chapter is organized as follows. Section 4.1 introduces the network scenario, slicing architecture, and system models. The problem formulation and the proposed TLRS scheme are presented in Sect. 4.2. Section 4.3 develops the swap-based matching algorithm for multicast and caching decisions, followed by the HPPO-based RL algorithm for resource reservation and slicing window determination in Sect. 4.4. Performance evaluation is provided in Sects. 4.5, and 4.6 concludes this chapter.

4.1 Network Scenario and System Model

4.1.1 Scenario Description

In this chapter, we consider an STVN scenario that includes urban and suburban environments. CVs in the target area can be served by either terrestrial BSs or LEO satellites to receive HD map files [5]. Each CV generates location-specific requests for HD map files, and the demands may vary across different vehicles. The overall delay for receiving an HD map file is required to be no greater than $D^{\max}$, with the service violation probability constrained by a predefined threshold ε. Let $\mathcal{F} = \{1, \ldots, F\}$ denote the set of all HD map files associated with the target area, where each file has a data size of κ. A content server, located remotely, stores all HD maps for the area.

Denote the sets of terrestrial BSs and LEO satellites by $\mathcal{BS}$ and $\mathcal{S}$, respectively. LEO satellites are equipped with steerable antennas and can direct beams toward the target area when the elevation angle constraint is satisfied. Let $\mathcal{AP} = \mathcal{BS} \cup \mathcal{S}$ represent the set of all access points (APs), where each AP is equipped with an edge server with caching capabilities for data storage. For each AP $ap \in \mathcal{AP}$, the available resources are characterized by B_{ap}^{r}, where $r \in \mathbf{r} = \{\text{cm}, \text{ch}\}$ denotes communication bandwidth and caching capacity, respectively. An SDN controller is deployed to centrally and adaptively manage the multi-dimensional resources of all APs serving the target area in STVNs.

4.1.2 Slicing Architecture for STVNs

To efficiently distribute HD map files in STVNs while satisfying heterogeneous service requirements, a resource slicing architecture is adopted to enable service-oriented resource isolation. Due to the intrinsic heterogeneity between multicast and unicast transmissions in terms of delay sensitivity and resource utilization, sharing resources within a single slice may lead to inefficient allocation and performance degradation. Therefore, as illustrated in Fig. 4.1, we construct two isolated network slices by leveraging the complementary characteristics of satellite and terrestrial networks. Specifically, a multicast slice (MS) is established to exploit the multicast nature and wide-area coverage of LEO satellites, utilizing only satellite resources to efficiently distribute popular HD map files. In contrast, a unicast slice (US) is designed to support individualized and delay-sensitive HD map delivery, leveraging both satellite and terrestrial BS resources to flexibly adapt to heterogeneous channel conditions and service demands.

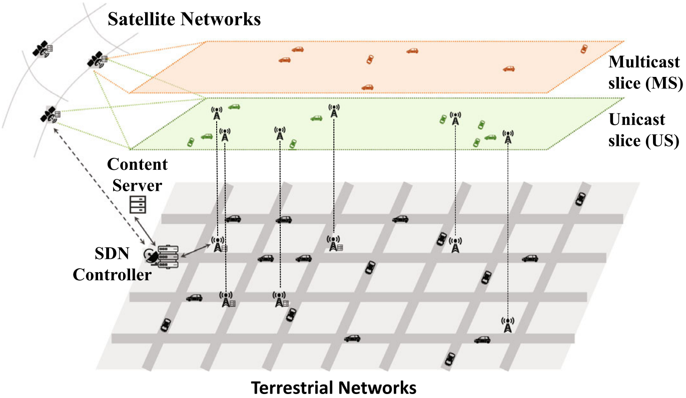

Fig. 4.1 Resource slicing architecture for STVNs

Resource slicing in STVNs operates in a time-slotted manner. To capture long-term resource dynamics while avoiding excessive reconfiguration overhead, slicing decisions are updated over slicing windows indexed by $k \in \{1, 2, \ldots\}$. Each slicing window consists of ω_k time slots, where each slot $t \in \{1, 2, \ldots, \omega_k\}$ has a fixed duration τ, where $\omega_k \leq \omega_{\max}$. We denote the t-th time slot in slicing window k by (k, t). Due to satellite mobility and spatiotemporally varying service demands, the slicing window length ω_k is adaptively adjusted across windows.

Let $P_{ap}^{k,t}$ denote the position of AP ap at time (k, t) in an Earth-centered Earth-fixed (ECEF) coordinate system. The positions of terrestrial BSs remain fixed, while the positions of LEO satellites vary across time slots. Let $a_{ap}^{k,t} \in \{0, 1\}$ denote the accessibility indicator, where $a_{ap}^{k,t} = 1$ indicates that AP ap can serve the target area at time (k, t), and $a_{ap}^{k,t} = 0$ otherwise. Accordingly, let $\mathcal{S}^k = \{ap \mid \sum_{t=1}^{\omega_k} a_{ap}^{k,t} > 0, \forall ap \in \mathcal{S}\}$ denote the set of satellites that can cover the target area during slicing window k, and let $\mathcal{AP}^k = \mathcal{BS} \cup \mathcal{S}^k$ represent the set of APs participating in resource slicing in window k. Slicing decisions for window k are made by the ground controller at the beginning of the window for all $ap \in \mathcal{AP}^k$, while the actual deployment of slices depends on instantaneous satellite visibility.

Service requests for HD map files are modeled as a non-homogeneous Poisson process (NHPP) [6], where the request intensity (in packets per second) varies over time to capture peak and non-rush traffic periods but remains constant within each time slot. Let $\lambda_f^{k,t}$ denote the aggregate request intensity for file f at time (k, t), given by $\lambda_f^{k,t} = \sum_{b \in \mathcal{BS} \cup \{0\}} \lambda_{b,f}^{k,t}$, where $\lambda_{b,f}^{k,t}$ represents the request intensity for file f within the coverage of BS b, and $\lambda_{0,f}^{k,t}$ corresponds to requests not within the coverage of any BS.

At the beginning of each slicing window, the SDN controller predicts future service demands[1] and determines resource reservation decisions for both slices. These decisions remain fixed within the slicing window. Let $\upsilon^k_{ap,x} \in [0, 1]$ denote the fraction of communication resources reserved at AP ap for slice $x \in \mathbf{x} = \{0, 1\}$ in window k, where $x = 0$ and $x = 1$ correspond to the MS and US, respectively. Let $u^k_{ap,f} \in \{0, 1\}$ indicate the caching decision, where $u^k_{ap,f} = 1$ if file f is cached in AP ap and $u^k_{ap,f} = 0$ otherwise.

Given the reserved communication resources, the packet transmission rate from AP ap to CV g under slice x at time (k, t) is

$$\xi^{k,t}_{ap,x,g} = \frac{a^{k,t}_{ap} \upsilon^k_{ap,x} B^{\mathrm{cm}}_{ap}}{\kappa} \log_2 \left(1 + \frac{p_{ap} G_{ap,g} (l^{k,t}_{ap,g})^{-\rho} |h^{k,t}_{ap,g}|^2}{\sigma^2}\right), \tag{4.1}$$

where p_{ap} is the transmit power, $G_{ap,g}$ is the antenna gain, $l^{k,t}_{ap,g}$ is the distance between AP ap and CV g, ρ is the path-loss exponent, and σ^2 is the noise power. Considering urban and suburban deployment environments, where line-of-sight satellite links may be obstructed, Rayleigh fading is adopted as a simplified model for small-scale fading in both satellite and terrestrial links, with $h^{k,t}_{ap,g} \sim \mathcal{CN}(0, 1)$.

4.1.3 Performance Modeling of Network Slices

To characterize HD map delivery in each slice, we model the service process at each AP as a queueing system. For a requested HD map file, if the file is cached at an AP, the request is directly handled by a transmission queue [9]. Otherwise, the file must first be fetched from the remote content server through the backhaul link, followed by transmission to CVs via the corresponding transmission queue.

Let $m^k_{ap,f}$ denote the multicast indicator, where $m^k_{ap,f} = 1$ indicates that file f is multicast by satellite ap in slicing window k, and $m^k_{ap,f} = 0$ otherwise. Considering the periodic nature of multicast transmission, let T^{M} denote the interval between two consecutive multicast events. When a CV generates a request, it will be served at the next multicast event, resulting in an average waiting delay of $T^{\mathrm{M}}/2$. Moreover, since the MS is only established over satellites, propagation delay cannot be neglected. In this case, the average overall delay for delivering file f from satellite ap through the MS at time slot (k, t) is given by

$$D^{k,t}_{ap,0,f} = \begin{cases} D^{\mathrm{Q},k,t}_{\mathrm{C},ap,0} + \frac{T^{\mathrm{M}}}{2} + D^{\mathrm{P},k,t}_{ap}, & \text{if } u^k_{ap,f} = 1, \\ D^{\mathrm{Q},k,t}_{\mathrm{NC},ap,0} + \frac{T^{\mathrm{M}}}{2} + D^{\mathrm{P},k,t}_{ap} + D^{\mathrm{BH}}, & \text{otherwise,} \end{cases} \tag{4.2}$$

[1] Service demand prediction is not the primary focus of this chapter. We assume that the demand in the next $\omega_{\max}$ time slots can be estimated using existing methods, such as RNN [7] or LSTM [8].

where $D^{\mathrm{Q},k,t}_{\mathrm{C},ap,x}$ and $D^{\mathrm{Q},k,t}_{\mathrm{NC},ap,x}$ denote the queueing and transmission delays for cached and non-cached files, respectively. Meanwhile, $D^{\mathrm{P},k,t}_{ap}$ and D^{BH} represent the propagation delay and backhaul delay.

For the US, demands are served in a request–response manner without multicast waiting. The overall delay for delivering file f from AP ap to CVs at time slot (k,t) is given by

$$D^{k,t}_{ap,1,f} = \begin{cases} D^{\mathrm{Q},k,t}_{\mathrm{C},ap,1} + \mathbb{1}_{ap\in\mathcal{S}} D^{\mathrm{P},k,t}_{ap}, & \text{if } u^{k}_{ap,f} = 1, \\ D^{\mathrm{Q},k,t}_{\mathrm{NC},ap,1} + \mathbb{1}_{ap\in\mathcal{S}} D^{\mathrm{P},k,t}_{ap} + D^{\mathrm{BH}}, & \text{otherwise,} \end{cases} \tag{4.3}$$

where $\mathbb{1}_{cond} = 1$ if $cond$ is true and $\mathbb{1}_{cond} = 0$ otherwise.

Due to stochastic service arrivals and time-varying wireless channels, it is difficult to guarantee queueing and transmission delays. Moreover, average delay alone is insufficient to characterize service requirement satisfaction within each slice. In this case, to model the statistical delay performance, the large deviation theory can be employed to evaluate the delay-bounded violation probability [10]. Specifically, the violation probability of delay D exceeding the maximum allowable queueing and transmission delay should be less than ε, approximated as

$$\begin{cases} P(D \geq D^{\mathrm{Q_M},k,t}_{\mathrm{C},ap,x}) \approx e^{-\theta A^{k,t}_{\mathrm{C},ap,x} D^{\mathrm{Q_M},k,t}_{\mathrm{C},ap,x}} \leq \varepsilon, \\ P(D \geq D^{\mathrm{Q_M},k,t}_{\mathrm{NC},ap,x}) \approx e^{-\theta A^{k,t}_{\mathrm{NC},ap,x} D^{\mathrm{Q_M},k,t}_{\mathrm{NC},ap,x}} \leq \varepsilon. \end{cases} \tag{4.4}$$

where θ denotes the exponential decay rate, and the same value of θ is applied to all queues. Here, the maximum allowable queueing and transmission delays for cached and non-cached files can be expressed as

$$D^{\mathrm{Q_M},k,t}_{\mathrm{C},ap,x} = \begin{cases} D^{\max} - T^{\mathrm{M}} - D^{\mathrm{P},k,t}_{ap}, & x = 0, \\ D^{\max} - \mathbb{1}_{ap\in\mathcal{S}} D^{\mathrm{P},k,t}_{ap}, & x = 1, \end{cases} \tag{4.5}$$

$$D^{\mathrm{Q_M},k,t}_{\mathrm{NC},ap,x} = \begin{cases} D^{\max} - T^{\mathrm{M}} - D^{\mathrm{P},k,t}_{ap} - D^{\mathrm{BH}}, & x = 0, \\ D^{\max} - \mathbb{1}_{ap\in\mathcal{S}} D^{\mathrm{P},k,t}_{ap} - D^{\mathrm{BH}}, & x = 1. \end{cases} \tag{4.6}$$

To satisfy the delay violation constraint, the minimum required service rates are given by

$$A^{\min,k,t}_{\mathrm{C},ap,x} = -\frac{\log(\varepsilon)}{\theta D^{\mathrm{Q_M},k,t}_{\mathrm{C},ap,x}}, \quad A^{\min,k,t}_{\mathrm{NC},ap,x} = -\frac{\log(\varepsilon)}{\theta D^{\mathrm{Q_M},k,t}_{\mathrm{NC},ap,x}}. \tag{4.7}$$

To evaluate the performance of reserved resources in each AP for slices, the effective capacity, which characterizes the maximum accommodated service rate [11], is defined as

$$C^{k,t}_{ap,x} = -\frac{1}{\theta} \log\left(\mathbb{E}\left\{e^{-\theta \xi^{k,t}_{ap,x,g}}\right\}\right). \tag{4.8}$$

With a given effective capacity, the bounded queueing and transmission delay can be expressed as

$$D_{\mathrm{C},ap,x}^{\mathrm{Q},k,t} = D_{\mathrm{NC},ap,x}^{\mathrm{Q},k,t} = -\frac{\log(\varepsilon)}{\theta C_{ap,x}^{k,t}}. \tag{4.9}$$

According to effective capacity theory [10], satisfying the delay constraint requires

$$C_{ap,x}^{k,t} \geq A_{\mathrm{C},ap,x}^{k,t} \Leftrightarrow D_{\mathrm{C},ap,x}^{\mathrm{Q},k,t} \leq D_{\mathrm{C},ap,x}^{\mathrm{Q_M},k,t}, \tag{4.10}$$

$$C_{ap,x}^{k,t} \geq A_{\mathrm{NC},ap,x}^{k,t} \Leftrightarrow D_{\mathrm{NC},ap,x}^{\mathrm{Q},k,t} \leq D_{\mathrm{NC},ap,x}^{\mathrm{Q_M},k,t}, \tag{4.11}$$

for cached and non-cached files, respectively.

When the reserved communication resources are insufficient to satisfy these conditions or accommodate all required service demand, each AP can only fulfill a portion of the service demand. Let $\tilde{\lambda}_{ap,x,f}^{k,t}$ denote the accommodated service demand intensity of file f from AP ap in slice x, whose determination will be presented in Sect. 4.3. Note that terrestrial BSs only participate in the US, i.e., $\tilde{\lambda}_{ap,0,f}^{k,t} = 0$ for all $ap \in \mathcal{BS}$.

4.2 Problem Formulation and TLRS Scheme Design

In this section, we formulate the long-term resource slicing problem for HD map distribution in STVNs and design an efficient solution framework. Specifically, communication resource reservation, caching placement, multicast decisions, and slicing window length are tightly coupled and collectively affect the long-term system performance. To address these challenges, we first formulate the reservation-stage resource slicing problem as a long-term system cost minimization problem, and then propose a TLRS scheme to enable adaptive and low-complexity decision-making in dynamic STVNs.

4.2.1 Problem Formulation

Considering the spatiotemporal dynamics of service demand and the time-varying availability of satellite resources, we aim to minimize the long-term overall system cost while satisfying the service requirements of HD map distribution. The overall system cost accounts for resource consumption, service delay, slicing reconfiguration overhead, and penalties for unmet service demand.

(1) Resource Cost: The resource cost reflects the long-term consumption of communication and caching resources reserved for different slices across BSs and LEO

satellites. Specifically, the resource cost in slicing window k is defined as the time-averaged cost of all reserved resources from APs serving the target area, given by

$$H_k^{\mathrm{res}}(\omega_k, v_{ap,x}^k, u_{ap,f}^k) = \frac{1}{\omega_k}\sum_{t=1}^{\omega_k}\sum_{ap\in\mathcal{AP}^k} a_{ap}^{k,t}\left(\sum_{x\in\mathbf{x}}\alpha_{ap}^{\mathrm{cm}} v_{ap,x}^k B_{ap}^{\mathrm{cm}} + \alpha_{ap}^{\mathrm{ch}}\sum_{f\in\mathcal{F}} u_{ap,f}^k \kappa\right), \tag{4.12}$$

where $\alpha^r ap$ denotes the unit cost of resource type r at AP ap.

(2) Delay Cost: Although the delay requirement for HD map distribution is not extremely stringent, reducing service latency is still critical for improving the user experience of CVs. Therefore, we introduce a delay cost to capture the average service delay incurred by both slices under the reserved resources and multicast decisions. The delay cost in slicing window k is defined as the average delay weighted by the accommodated service demand intensity, given by

$$H_k^{\mathrm{d}}(\omega_k, m_{ap,f}^k, v_{ap,x}^k, u_{ap,f}^k) = \frac{1}{\omega_k}\sum_{t=1}^{\omega_k}\frac{\sum\limits_{f\in\mathcal{F}}\sum\limits_{ap\in\mathcal{AP}^k} a_{ap}^{k,t}\sum\limits_{x\in\mathbf{x}} D_{ap,x,f}^{k,t}\tilde{\lambda}_{ap,x,f}^{k,t}}{\sum\limits_{f\in\mathcal{F}}\sum\limits_{ap\in\mathcal{AP}^k} a_{ap}^{k,t}\sum\limits_{x\in\mathbf{x}}\tilde{\lambda}_{ap,x,f}^{k,t}}. \tag{4.13}$$

(3) Slice Reconfiguration Cost: At the beginning of each slicing window, the SDN controller may adjust communication resource reservation decisions to adapt to changing service demand and satellite availability. However, adjusting reserved resources incurs slice reconfiguration cost, such as processing overhead. Since releasing resources can be executed with negligible cost, only the cost associated with increasing reservations is considered. The slice reconfiguration cost in slicing window k is defined as

$$H_k^{\mathrm{slice}}(\omega_k, v_{ap,x}^k | v_{ap,x}^{k-1}) = \frac{1}{\omega_k}\sum_{ap\in\mathcal{AP}^{k-1}\cup\mathcal{AP}^k}\sum_{x\in\mathbf{x}}\left[v_{ap,x}^k - v_{ap,x}^{k-1}\right]^+, \tag{4.14}$$

where function $[\cdot]^+$ represents $\max\{\cdot, 0\}$.

(4) Service Demand Penalty: When reserved resources are insufficient to accommodate all service demands within the required delay bounds, a portion of the demand remains unmet. To this end, a penalty term is introduced to quantify the time-averaged unmet service demand intensity in each slicing window, given by

$$\begin{aligned} &H_k^{\mathrm{pen}}(\omega_k, m_{ap,f}^k, v_{ap,x}^k, u_{ap,f}^k) \\ &= \frac{1}{\omega_k}\sum_{t=1}^{\omega_k}\left[\lambda_f^{k,t} - \left(\sum_{ap\in\mathcal{BS}}\min\left\{\tilde{\lambda}_{ap,1,f}^{k,t}, \lambda_{ap,f}^{k,t}\right\} + \sum_{ap\in\mathcal{S}_k}\left(\tilde{\lambda}_{ap,0,f}^{k,t} + \tilde{\lambda}_{ap,1,f}^{k,t}\right)\right)\right]^+. \end{aligned} \tag{4.15}$$

Note that BSs can only serve the service demand within their coverage, while satellites can support all service demand in the target area.

By combining the above cost components, the overall system cost in slicing window k is given by

$$
\begin{aligned}
&H_k^{\text{sys}}(\omega_k, m_{ap,f}^k, v_{ap,x}^k, u_{ap,f}^k) \\
&\quad = \beta_1 H_k^{\text{res}}(\omega_k, v_{ap,x}^k, u_{ap,f}^k) + \beta_2 H_k^{\text{d}}(\omega_k, m_{ap,f}^k, v_{ap,x}^k, u_{ap,f}^k) \\
&\qquad + \beta_3 H_k^{\text{slice}}(\omega_k, v_{ap,x}^k | v_{ap,x}^{k-1}) + \beta_4 H_k^{\text{pen}}(\omega_k, m_{ap,f}^k, v_{ap,x}^k, u_{ap,f}^k),
\end{aligned}
\tag{4.16}
$$

where β_1, β_2, β_3, and β_4 reflect the relative importance of different components.

The resource slicing problem in STVNs, aiming at minimizing the long-term overall system cost, is formulated as

$$
\mathbf{P0} \min_{\substack{\omega_k, m_{ap,f}^k, \\ v_{ap,x}^k, u_{ap,f}^k}} \mathbb{E}\left[\lim_{K\to\infty} \frac{1}{K}\sum_{k=1}^{K} H_k^{\text{sys}}(\omega_k, m_{ap,f}^k, v_{ap,x}^k, u_{ap,f}^k)\right] \tag{4.17}
$$

$$
\text{s.t.} \quad \sum_{f\in\mathcal{F}} m_{ap,f}^k \le d_{ap}^k, \tag{4.17a}
$$

$$
\sum_{x\in\mathbf{X}} v_{ap,x}^k \le \mathbb{1}_{ap\in\mathcal{AP}^k}, \tag{4.17b}
$$

$$
\sum_{f\in\mathcal{F}} u_{ap,f}^k \kappa \le \mathbb{1}_{ap\in\mathcal{AP}^k} B_{ap}^{\text{ch}}, \tag{4.17c}
$$

$$
\omega_k \in \{1, ..., \omega_{\max}\}, v_{ap,x}^k \in [0, 1], \tag{4.17d}
$$

$$
m_{ap,f}^k \in \{0, 1\}, u_{ap,f}^k \in \{0, 1\}. \tag{4.17e}
$$

Constraint (4.17a) limits the number of HD map files that can be served via the MS at each AP, such that it does not exceed the maximum allowable number of multicast files d_{ap}^k, whose detailed expression is provided in Sect. 4.3. Constraints (4.17b) and (4.17c) guarantee the feasibility of resource reservation by ensuring that the total reserved communication resource ratio at each AP does not exceed 1, and that the total size of cached files remains within the available caching capacity when the AP is accessible during the slicing window. Constraint (4.17d) restricts the maximum slicing window length and enforces that communication resource reservation decisions take continuous values between zero and one. Finally, constraint (4.17e) specifies the binary nature of multicast selection and caching decisions.

4.2.2 Design of TLRS Scheme in STVNs

The formulated problem **P0** is a stochastic optimization problem due to the spatiotemporal dynamics of service demand and the time-varying availability of resources in STVNs. Moreover, the lack of future information, combined with the coexistence of continuous and discrete decision variables, makes the problem highly complex and intractable for conventional optimization approaches. Although RL provides a promising tool for decision-making under uncertainty, directly applying a fully data-driven RL solution to **P0** suffers from large action spaces, slow convergence, as well as potential hallucination caused by tightly coupled decisions across different resource dimensions.

By examining the system cost formulation in (4.16), we can observe that the inter-window coupling effect exists solely from the slice reconfiguration cost in (4.14), which depends on the slicing window length ω_k and the reserved communication resources $v^k_{ap,x}$, while the remaining cost components are confined within individual slicing windows. This structural property enables an equivalent decomposition of problem **P0** into a two-layer optimization framework as

$$\begin{aligned} &\min_{\omega_k, m^k_{ap,f}, v^k_{ap,x}, u^k_{ap,f}} \mathbb{E}\left[\lim_{K\to\infty} \frac{1}{K} \sum_{k=1}^{K} H^{\text{sys}}_k(\omega_k, m^k_{ap,f}, v^k_{ap,x}, u^k_{ap,f})\right] \\ &= \min_{\omega_k, v^k_{ap,x}} \mathbb{E}\left[\lim_{K\to\infty} \frac{1}{K} \sum_{k=1}^{K} O_k(\omega_k, v^k_{ap,x})\right], \end{aligned} \tag{4.18}$$

where

$$O_k(\omega_k, v^k_{ap,x}) = \min_{m^k_{ap,f}, u^k_{ap,f}} H^{\text{sys}}_k(\omega_k, m^k_{ap,f}, v^k_{ap,x}, u^k_{ap,f}). \tag{4.19}$$

Motivated by this decomposition, we propose a two-layer resource slicing (TLRS) scheme to efficiently address the multi-dimensional resource slicing problem in STVNs, as illustrated in Fig. 4.2. The TLRS scheme consists of the following two subproblems.

1. *Inner-layer subproblem: Caching and multicast file selection.* In the inner layer, the long-term impact induced by slice reconfiguration is isolated. Given the slicing window length $\hat{\omega}_k$ and the reserved communication resources $\hat{v}^k_{ap,x}$, we aim to minimize the system cost within slicing window k by optimizing caching and multicast decisions. This subproblem is formulated as

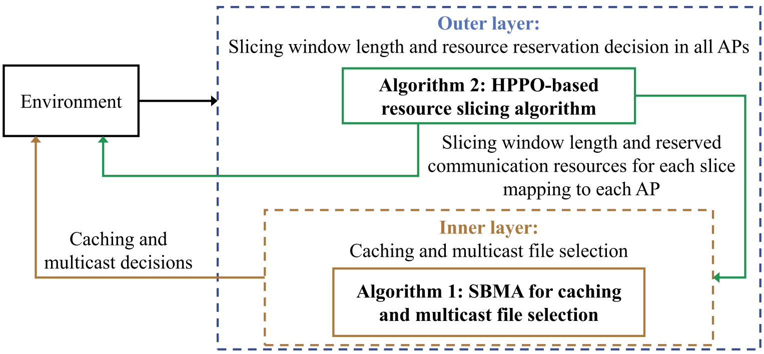

Fig. 4.2 Working diagram of the proposed TLRS scheme in STVNs

$$\mathbf{P1} \quad \min_{m^k_{ap,f}, u^k_{ap,f}} \quad H^{\text{sys}}_k(\omega_k, m^k_{ap,f}, v^k_{ap,x}, u^k_{ap,f}) \tag{4.20}$$

$$\text{s.t.} \quad \omega_k = \hat{\omega}_k, \tag{4.20a}$$

$$v^k_{ap,x} = \hat{v}^k_{ap,x}, \ \forall x \in \mathbf{x}, \forall ap \in \mathcal{AP}^k, \tag{4.20b}$$

$$(4.17\text{a}), (4.17\text{c}), (4.17\text{e}).$$

A matching-based algorithm is developed to efficiently solve this subproblem.

2. *Outer-layer subproblem: Slicing window length and communication resource reservation.* In the outer layer, we optimize the slicing window length and the reserved communication resources for both the MS and US, taking into account the long-term system performance under dynamic environments. The outer-layer subproblem is formulated as

$$\mathbf{P2} \quad \min_{\omega_k, v^k_{ap,x}} \mathbb{E}\left[\lim_{K\to\infty} \frac{1}{K} \sum_{k=1}^{K} H^{\text{sys}}_k(\omega_k, m^k_{ap,f}, v^k_{ap,x}, u^k_{ap,f})\right] \tag{4.21}$$

$$\text{s.t.} \quad (4.17\text{b}), (4.17\text{d}).$$

To address the mixed discrete–continuous decision space and capture long-term effects, an HPPO-based RL algorithm is designed for solving this subproblem.

By integrating RL-based adaptive slice management in the outer layer with model-based optimization for caching and multicast decisions in the inner layer, the proposed TLRS scheme effectively balances flexibility and computational efficiency, making it well-suited for the dynamic and heterogeneous characteristics of STVNs. In the following sections, we present the detailed algorithms for solving subproblems **P1** and **P2** in Sects. 4.3 and 4.4, respectively.

4.3 Matching-Based Caching and Multicast File Selection

In this section, we focus on the inner-layer subproblem **P1** in the proposed TLRS framework. We first derive the accommodated service demand intensity in different slices, which plays a critical role in evaluating the delay cost and service demand penalty in the system cost function. Based on this analysis, the joint caching and multicast file selection problem within each slicing window is reformulated as a many-to-many matching problem, capturing the mutual preferences between APs and HD map files under limited communication and caching resources. To efficiently solve the resulting combinatorial optimization problem, a swap-based matching algorithm is developed with computational complexity analysis.

4.3.1 Accommodated Service Demand Intensity Analysis

For the inner-layer subproblem **P1**, the system cost in each slicing window depends on how much service demand can be accommodated by the reserved communication and caching resources. In this subsection, we characterize the accommodated service demand intensity in different slices, which serves as the basis for evaluating the delay cost and service demand penalty.

For the MS established at satellite ap, if file f is selected for multicast, the satellite can simultaneously serve all CVs requesting this file within its coverage area. The accommodated service demand intensity at time slot (k, t) can be regarded as the total service demand intensity of file f in the target area, given by

$$\tilde{\lambda}_{ap,0,f}^{k,t} = \begin{cases} m_{ap,f}^{k}\lambda_f^{k,t}, & \text{if } D_{\mathrm{C},ap,0}^{\mathrm{Q},k,t} \le D_{\mathrm{C},ap,0}^{\mathrm{Q_M},k,t}, u_{ap,f}^{k} = 1, \\ & \text{or } D_{\mathrm{NC},ap,0}^{\mathrm{Q},k,t} \le D_{\mathrm{NC},ap,0}^{\mathrm{Q_M},k,t}, u_{ap,f}^{k} = 0, \\ 0, & \text{otherwise.} \end{cases} \tag{4.22}$$

For the US, both satellites and BSs can serve CVs through unicast transmissions, where the accommodated service demand is constrained by the reserved communication resources and statistical delay requirements. Based on effective capacity theory, the maximum service demand intensity that can be accommodated by AP ap at time slot (k, t) is given by [12]

$$\hat{\lambda}_{ap}^{k,t} = \frac{\theta C_{ap,1}^{k,t}}{e^{\theta} - 1}. \tag{4.23}$$

To satisfy the delay constraints for cached and non-cached files, the effective accommodated demand intensities are respectively given by

$$\hat{\lambda}_{\mathrm{C},ap}^{k,t} = \begin{cases} \hat{\lambda}_{ap}^{k,t}, & \text{if } D_{\mathrm{C},ap,1}^{\mathrm{Q},k,t} \le D_{\mathrm{C},ap,1}^{\mathrm{Q_M},k,t}, \\ 0, & \text{otherwise,} \end{cases} \text{ and } \hat{\lambda}_{\mathrm{NC},ap}^{k,t} = \begin{cases} \hat{\lambda}_{ap}^{k,t}, & \text{if } D_{\mathrm{NC},ap,1}^{\mathrm{Q},k,t} \le D_{\mathrm{NC},ap,1}^{\mathrm{Q_M},k,t}, \\ 0, & \text{otherwise.} \end{cases} \tag{4.24}$$

Since CVs within the coverage of an AP may request different HD map files, accurately determining the accommodated demand for each individual file under real-time scheduling is challenging, where a file can be delivered either from the local cache of an AP or retrieved from the content server. Therefore, for large timescale resource reservation, we focus on maximizing the total accommodated service demand intensity across all APs and files, given the reserved resources and caching decisions, and formulate a linear programming problem, given by

$$\mathbf{P3} \quad \max_{\tilde{\lambda}_{ap,1,f}^{k,t}} \sum_{ap \in \mathcal{AP}^k} \sum_{f \in \mathcal{F}} \tilde{\lambda}_{ap,1,f}^{k,t} \tag{4.25}$$

$$\text{s.t.} \quad \sum_{f \in \mathcal{F}} \tilde{\lambda}_{ap,1,f}^{k,t} \leq a_{ap}^{k,t} \hat{\lambda}_{ap}^{k,t}, \tag{4.25a}$$

$$\sum_{ap \in \mathcal{AP}^k} (\tilde{\lambda}_{ap,0,f}^{k,t} + \tilde{\lambda}_{ap,1,f}^{k,t}) \leq \lambda_f^{k,t}, \tag{4.25b}$$

$$\tilde{\lambda}_{ap,1,f}^{k,t} \leq u_{ap,f}^k \hat{\lambda}_{\mathrm{C},ap}^{k,t} + (1 - u_{ap,f}^k) \hat{\lambda}_{\mathrm{NC},ap}^{k,t}, \tag{4.25c}$$

where constraint (4.25a) limits maximum accommodated service demand intensity in each AP; (4.25b) constrains the service demand intensity request of each file; and (4.25c) regulates the maximum accommodated service demand intensity in each AP for a file. Since **P3** is a linear program problem, it can be efficiently solved using standard convex optimization tools such as CVX [13], to achieve the accommodated service demand intensity from the US in all APs under the given resource reservation and caching decisions.

4.3.2 Many-to-Many Matching Game Formulation

To solve subproblem **P1**, we optimize the multicast and caching decisions $m_{ap,f}^k$ and $u_{ap,f}^k$ for each AP within a slicing window. For notational simplicity, the slicing window index k is omitted in this subsection, as all decisions are made independently for each slicing window with given reserved communication resources and window length. Since each BS is assumed to have sufficient storage to cache all HD map files within its coverage area, we focus on the caching and multicast file selection decisions at LEO satellites for both multicast and unicast slices. Considering that each HD map file can be served by multiple satellites, and each satellite can simultaneously serve or cache multiple files under different transmission modes, subproblem **P1** can be reformulated as a graph-based many-to-many matching problem by constructing a bipartite graph $\mathcal{G} = (\Phi, \mathcal{F}, \mathcal{E})$, where $\Phi = \{(ap, m) \mid ap \in \mathcal{S}^k,\ m \in \{1, 2, 3, 4\}\}$ is the set of satellite service modes. Each element (ap, m) represents one service mode of satellite ap, corresponding to the combination of transmission mode and caching decision, where $m = 1$ is multicast with caching, $m = 2$ indicates multicast without caching, $m = 3$ represents unicast with caching, and $m = 4$ represents unicast without caching. A connected edge $(f, (ap, m)) \in \mathcal{E}$ indicates that file f is served by satellite ap using service mode m.

The objective is to determine a matching that minimizes the system cost within the slicing window.

Definition 4.1 Given the bipartite graph $\mathcal{G} = (\Phi, \mathcal{F}, \mathcal{E})$, a matching Ψ is a subgraph of $\mathcal{G}$ satisfying:

1. $\Psi((ap, m)) \subseteq \mathcal{F}$ and $\Psi(f) \subseteq \Phi$;
2. $|\Psi((ap, 1))| \leq d_{ap,1}$ and $|\Psi((ap, 2))| \leq d_{ap,2}$;
3. $|\Psi((ap, 1))| + |\Psi((ap, 3))| \leq \lfloor B_{ap}^{\mathrm{ch}} / \kappa \rfloor$;
4. $|\Psi(f)| = |\mathcal{S}^k|$;
5. $(ap, m) \in \Psi(f)$ if and only if $f \in \Psi((ap, m))$;

6. $\Psi((ap, m)) \cap \Psi((ap, m')) = \emptyset$, for $m \neq m'$.

Condition (1) specifies that each satellite service mode can be matched with a subset of files and each file can be matched with multiple satellite service modes. Condition (2) limits the maximum number of files that can be supported by multicast transmission at each satellite. Specifically, let $d_{ap,1}$ denote the maximum number of cached multicast files supported by satellite ap, given by

$$d_{ap,1} = \begin{cases} \min_t \left\{ \left\lfloor C^{k,t}_{ap,0} T^{\mathrm{M}} \right\rfloor \middle| a^{k,t}_{ap} = 1 \right\}, & \text{if } \exists t:\ D^{\mathrm{Q},k,t}_{\mathrm{C},ap,0} \leq D^{\mathrm{Q_M},k,t}_{\mathrm{C},ap,0}, \\ 0, & \text{otherwise}, \end{cases} \tag{4.26}$$

which represents the worst-case multicast file capacity over the slicing window considering satellite mobility. Multicast transmission for cached files is prioritized compared to non-cached files since it more easily satisfies the delay constraint. Therefore, in slicing window k, the maximum number of files d^k_{ap} served by MS in constraint (4.17a) is the same as $d_{ap,1}$ in this section. Accordingly, the maximum number of non-cached multicast files is given by

$$d_{ap,2} = \begin{cases} d_{ap,1} - |\Psi((ap, 1))|, & \text{if } \exists t:\ D^{\mathrm{Q},k,t}_{\mathrm{NC},ap,0} \leq D^{\mathrm{Q_M},k,t}_{\mathrm{NC},ap,0}, \\ 0, & \text{otherwise}. \end{cases} \tag{4.27}$$

Condition (3) enforces the shared caching capacity constraint between MS and US from each satellite. Condition (4) ensures that each file selects exactly one service mode at each satellite, where the size of $\Psi(f)$ should equal the satellite number $|\mathcal{S}^k|$ in the slicing window. This formulation allows a satellite to explicitly decide whether a file is multicast, unicast, or not effectively served (mode 4), which does not directly correspond to the accommodated service demand intensity. Condition (5) guarantees consistency of the matching, and Condition 6) ensures that each file selects only one service mode per satellite.

Given a matching Ψ, the corresponding multicast and caching decisions for satellite ap are obtained, where $(f, (ap, 1))$ corresponds to $m^k_{ap,f} = 1$ and $u^k_{ap,f} = 1$; $(f, (ap, 2))$ corresponds to $m^k_{ap,f} = 1$ and $u^k_{ap,f} = 0$; $(f, (ap, 3))$ corresponds to $m^k_{ap,f} = 0$ and $u^k_{ap,f} = 1$; and $(f, (ap, 4))$ corresponds to $m^k_{ap,f} = 0$ and $u^k_{ap,f} = 0$. Based on these decisions, the accommodated service demand intensities in both slices are computed by solving problem **P3**. The utility $H(\Psi)$ of a matching Ψ is then defined as $-H^{\mathrm{sys}}_k$ for slicing window k.

4.3.3 Swapping-Based Matching Algorithm

The formulated caching and multicast file selection problem constitutes a many-to-many matching game with externalities [14]. Specifically, the utility of a matching pair $(f, (ap, m))$ depends not only on the file f and the service mode (ap, m) itself,

Algorithm 1 SBMA for caching and multicast file selection

1: **Initialization Phase**
2: Let $\Psi = \emptyset$;
3: **for** $f \in \mathcal{F}$ **do**
4: Match f with the service mode $(ap, 4)$ of each satellite, $\Psi = \Psi \cup (f, (ap, 4))$;
5: **Swap Matching Phase**
6: **for** $ap \in \mathcal{S}^k$, $m \in \{1, 2, 3, 4\}$ **do**
7: Calculate $H(\Psi)$, set $\Psi_{\text{temp}} = \Psi$;
8: For a file $f \in \Psi((ap, m))$, the controller searches the satellite service mode $(ap', m') \in \Phi \setminus \{(ap, m)\}$ with $f' \in \Psi((ap', m'))$ for a swap operation;
9: **if** $H(\Psi^{ap,m,f}_{ap',m',f'}) > H(\Psi_{\text{temp}})$ **then**
10: Swap the pair according to **Definition** 4.2 and obtain Ψ' as new matching policy;
11: $\Psi_{\text{temp}} = \Psi'$, and go back to Line 8;
12: Update the matching with $\Psi = \Psi_{\text{temp}}$;
13: Go back to Line 6 and repeat until no swapping pairs can be found;
14: **Output:** Caching indicator $u^k_{ap,f}$ and multicast decision $m^k_{ap,f}$ in the slicing window according to matching policy Ψ;

but also on the service modes selected for other files at the same satellite. This coupling arises from shared communication and caching resources, as well as delay constraints that jointly affect multicast capacity and unicast performance. As a result, the preference relations of satellite service modes are dynamic and matching-dependent, making static preference lists unsuitable.

To address this challenge, we adopt a swap-based matching framework, which has been shown to be effective for many-to-many matching games with externalities. The key idea is to iteratively improve the system utility by swap operations, which allows two matching pairs to exchange their matches while keeping all other matching relationships unchanged [15].

Definition 4.2 (*Swap operation*) Given a matching Ψ and two matching pairs $(f, (ap, m))$ and $(f', (ap', m'))$ in Ψ, a swap matching is defined as

$$\begin{aligned}\Psi^{ap,m,f}_{ap',m',f'} = \Psi \setminus \{(f, (ap, m)), (f', (ap', m'))\} \\ \cup \{(f', (ap, m)), (f, (ap', m'))\}.\end{aligned} \tag{4.28}$$

The swap is feasible if the resulting matching satisfies all constraints in Definition 4.1, and the swap operation leads to a strict increase in the system utility.

Based on the above definition, we propose a swapping-based matching algorithm (SBMA) to solve subproblem **P1**, which is summarized in Algorithm 1. The algorithm iteratively searches for utility-improving swaps until no further improvement is possible, which consists of two phases. In the initialization phase, a baseline matching is constructed by assigning each file to the unicast, non-caching service mode $(ap, 4)$ at every satellite. This corresponds to a conservative strategy without multicast or caching. Then, in the swap matching phase, the controller iteratively explores possible swap operations. For a given matching pair $(f, (ap, m))$, the algorithm searches for another pair $(f', (ap', m'))$ such that swapping the two pairs increases the overall utility. Once a beneficial swap is found, the matching is updated and the search continues. The procedure terminates when no swap can further improve the utility.

Property 4.1 (Finite convergence of SBMA) *The proposed SBMA converges within a finite number of swap operations. Each accepted swap strictly increases the system utility $H(\Psi)$. Since $H(\Psi)$ is upper-bounded by the finite communication and caching resources available in the system, an infinite sequence of improving swaps is impossible. Therefore, the algorithm terminates after a finite number of iterations.*

Upon convergence, the obtained matching Ψ is swap-stable, meaning that no feasible swap operation can further improve the system utility under the given slicing window length and reserved communication resources. The resulting matching is mapped to caching and multicast decisions with the given slicing window length and reserved communication resources.

4.3.4 Computational Complexity Analysis

The proposed SBMA iteratively searches for utility-improving swap pairs to optimize caching and multicast file assignments within each slicing window. For each candidate swap, the algorithm evaluates whether the swap increases the system utility $H(\Psi)$. This evaluation requires recomputing the accommodated service demand intensities by solving subproblem **P3**, which is a structured linear programming problem with linear constraints and can be efficiently solved in polynomial time. In particular, by exploiting its flow-based structure, **P3** can be solved using algorithms such as Dinic's method, with a worst-case complexity of $O\left(T_\omega|\mathcal{AP}^k|F(|\mathcal{AP}^k|+F)^2\right)$. In the worst case, the number of candidate swap pairs examined in each iteration is upper-bounded by $|\mathcal{S}^k|L_{\max}L_{\text{tot}}$. Here, $L_{\max} = \min\{\max_{ap\in\mathcal{S}^k}(\lfloor B_{ap}^{\text{ch}}/\kappa\rfloor + d_{ap,1}), \frac{F-1}{2}\}$ denotes the maximum number of files eligible for swapping at a single satellite, and $L_{\text{tot}} = \sum_{ap\in\mathcal{S}^k}(\lfloor B_{ap}^{\text{ch}}/\kappa\rfloor + d_{ap,1})$ represents the total number of candidate swaps across all satellites in the slicing window. This quantity is an upper bound on the number of swap candidates explored per iteration. Let I denote the finite number of iterations required for the SBMA to converge. The overall computational complexity for determining caching and multicast decisions within a slicing window is given by $O(I|\mathcal{S}^k|L_{\max}L_{\text{tot}}\cdot T_\omega|\mathcal{AP}^k|F(|\mathcal{AP}^k|+F)^2)$.

Although the above expression represents a worst-case bound, the actual runtime of SBMA is significantly lower in practice. Specifically, the number of HD map files F in a target area is typically limited, and the number of visible satellites and accessible access points $|\mathcal{AP}^k|$ within a slicing window is moderate. Moreover, empirical observations show that SBMA converges within a small number of iterations, and only a fraction of candidate swaps lead to utility evaluations. As a result, the effective number of **P3** evaluations is far smaller than the theoretical upper bound. Since all computations are performed by a ground SDN controller with sufficient computational capability, the runtime of SBMA is well below the slicing window duration, which typically ranges from tens to hundreds of milliseconds. This confirms that the proposed SBMA is computationally feasible and suitable for practical implementation in STVNs.

4.4 HPPO-Based Slicing Window Length and Communication Resource Determination

In this section, we focus on determining the slicing window length and communication resource reservation decisions in the outer layer to solve subproblem **P2**. Considering the long-term impacts on sequential decision-making from the time-varying service demand and the adjustment of reserved resources, we reformulate the subproblem by leveraging the Markov decision process (MDP) and propose an RL algorithm to solve it.

4.4.1 Markov Decision Process Formulation

Due to the time-varying service demand and the coupling effect introduced by slicing reconfiguration costs across consecutive slicing windows, the optimization of slicing window length and communication resource reservation involves sequential decision-making. Conventional deterministic optimization approaches are inadequate to capture such long-term temporal dependencies. Therefore, we reformulate subproblem **P2** as an MDP to model the network dynamics and enable adaptive policy learning.

State: Let $\zeta^k = [\Lambda^k, P^k, \mathbf{v}^{k-1}] \in \mathfrak{S}$ denote the system state in slicing window k. Here, Λ^k represents the predicted service demand intensities for all HD map files over the next $\omega_{\max}$ time slots, P^k denotes the predicted positions and accessibility of APs during the next $\omega_{\max}$ time slots, and $\mathbf{v}^{k-1}$ is the communication resource reservation decision in the previous slicing window to capture the impact of slice reconfiguration costs, where $\mathbf{v}^k = \{v^k_{ap,x} \mid \forall ap \in \mathcal{AP}^k_{\max}, \forall x \in \mathbf{x}\}$.

Action: The action space is defined as the Cartesian product $\mathfrak{A} = \mathfrak{A}_1 \otimes \mathfrak{A}_2$, where $\mathfrak{A}_1$ denotes the discrete action space for slicing window length and $\mathfrak{A}_2$ denotes the continuous action space for communication resource reservation. Accordingly, the action taken in slicing window k is $\mathcal{A}^k = (\omega_k, \mathbf{v}^k)$, where $\omega_k \in \{1, \ldots, \omega_{\max}\}$ and $\mathbf{v}^k \in [0, 1]^{|\mathcal{AP}^k_{\max}|}$.

Reward: To align with the objective of minimizing the system cost, the immediate reward obtained by taking action $\mathcal{A}^k$ in state ζ^k is defined as the negative system cost in slicing window k, given by,

$$\mathcal{R}(\zeta^k, \mathcal{A}^k) = -H^{\text{sys}}_k. \tag{4.29}$$

Let $\mathbf{\Pi}$ denote the set of admissible policies mapping states to actions. By adopting a discounted reward formulation, the long-term optimization problem in subproblem **P2** can be approximated as

$$\mathbf{P2'} \quad \max_{\pi \in \mathbf{\Pi}} \mathbb{E}\left[\sum_{k=1}^{\infty} \gamma^k \mathcal{R}(\zeta^k, \mathcal{A}^k) \,\Big|\, \pi\right] \qquad (4.30)$$
$$\text{s.t.} \quad (4.17\text{b}), \ (4.17\text{d}).$$

4.4.2 Hybrid Proximal Policy Optimization-Based Algorithm

Considering the lack of state transition probability information of the formulated MDP, RL provides a suitable solution for solving subproblem **P2**′. However, the action space in **P2**′ is hybrid, consisting of an interdependent discrete action of slicing window length and high-dimensional continuous actions of communication resource reservation. Directly handling such non-homogeneous actions using a single policy network is challenging. Existing approaches attempt to unify discrete and continuous actions by discretizing continuous actions or converting discrete actions into continuous spaces [16]. Nevertheless, these methods may suffer from scalability issues or complicate the approximation and generalization of continuous action in piecewise-function action subspaces.

Motivated by recent advances in RL with parameterized action spaces for both discrete and continuous actions [17–19], we develop an HPPO-based algorithm to address the hybrid action structure and large-scale high-dimensional state space in STVNs. As illustrated in Fig. 4.3, two actor networks are employed to separately handle discrete and continuous decisions. Specifically, a discrete actor network first determines the slicing window length based on the current state. Conditioned on both the state and the selected slicing window length, a continuous actor network then

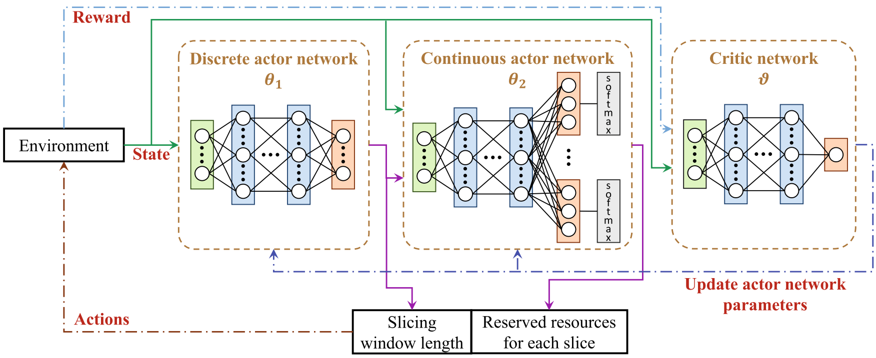

Fig. 4.3 Illustration of proposed HPPO-based algorithm

generates the communication resource reservation decisions for each AP. The two actor networks operate sequentially without parameter sharing and are optimized using task-specific gradients, which avoids unnecessary enlargement of the action space, while enhancing flexibility and specialization in decision-making. The overall action is obtained by combining the outputs of the two actor networks, and the joint policy is formulated as the product of the two policies, with the continuous policy conditioned on the discrete actor's decision. Additionally, a critic network as a state-value function is leveraged to generate state values for updating both discrete and continuous actor networks. This design effectively captures the interplay between slicing window length and resource reservation decisions to reach a better performance.

To accommodate the varying number of APs caused by satellite mobility, we adopt a fixed maximum number of APs, denoted by M, to standardize the dimensions of the state and action spaces. Let θ_1 and θ_2 denote the parameters of the discrete and continuous actor networks, respectively. To ensure that the output of the continuous actor satisfies the communication resource constraints in (4.17b) and (4.17d), we design a softmax-based output layer for the continuous actor network to regulate the output decisions. For each AP, the continuous actor outputs a 3-dimensional vector $\{v^k_{ap,0}, v^k_{ap,1}, v^k_{ap,2}\}$, representing the resource ratios allocated to the MS, US, and unreserved resources, respectively, and the overall output vector from the continuous actor network has a dimension of $3M$. By construction, $\sum_{x=0}^{2} v^k_{ap,x} = \mathbb{1}_{ap\in\mathcal{AP}^k}$, ensuring that the reserved resources in MS and US satisfy $\sum_{x=0}^{1} v^k_{ap,x} \le \mathbb{1}_{ap\in\mathcal{AP}^k}$.

The overall policy is parameterized by $\Theta = [\theta_1, \theta_2]$ and factorized as

$$\pi_\Theta(\mathcal{A} \mid \zeta) = \pi_{\theta_2}(\mathcal{A}_2 \mid \mathcal{A}_1, \zeta)\, \pi_{\theta_1}(\mathcal{A}_1 \mid \zeta), \tag{4.31}$$

where $\mathcal{A}_1$ and $\mathcal{A}_2$ denote the discrete and continuous actions, respectively.

To train the HPPO model, the goal is to maximize the clipped surrogate objective, given by

$$L^{\text{clip}}(\Theta) = \mathbb{E}\left[\min\left(\xi_\Theta A^{\pi_{\Theta_{\text{old}}}}, \text{clip}(\xi_\Theta, 1-\delta, 1+\delta) A^{\pi_{\Theta_{\text{old}}}}\right)\right], \tag{4.32}$$

where the policy update ratio based on the current policy for Θ is defined as

$$\xi_\Theta = \frac{\pi_\Theta(\mathcal{A}|\zeta)}{\pi_{\Theta_{\text{old}}}(\mathcal{A}|\zeta)} = \frac{\pi_{\theta_2}(\mathcal{A}_2|\mathcal{A}_1, \zeta)\pi_{\theta_1}(\mathcal{A}_1|\zeta)}{\pi_{\theta_{\text{old},2}}(\mathcal{A}_2|\mathcal{A}_1, \zeta)\pi_{\theta_{\text{old},1}}(\mathcal{A}_1|\zeta)}. \tag{4.33}$$

Here, $\pi_{\theta_{\text{old,i}}}$ is the old policy of actor network i. Moreover, $A^{\pi_{\Theta_{\text{old}}}}$ is the estimated advantage from policy $\pi_{\Theta_{\text{old}}}$, which can be expressed as

$$A^{\pi_{\Theta_{\text{old}}}}(\zeta^k, \mathcal{A}^k) = \mathcal{R}(\zeta^k, \mathcal{A}^k) + \gamma V_\vartheta(\zeta^{k+1}) - V_\vartheta(\zeta^k), \tag{4.34}$$

where $V_\vartheta(\zeta)$ denotes the state-value function estimated by a critic network with parameters ϑ, given by

Algorithm 2 HPPO-based slicing window length and communication resource determination

1: **Initialization:** Parameters $\Theta = [\theta_1, \theta_2]$ for policy, ϑ for state-value function, and buffer $\mathcal{B}$;
2: **for** $j \in \{1, 2, ..., J\}$ **do**
3: Obtain initial state ζ^1;
4: $k = 1$;
5: **while** $\sum_{l=1}^{k} \omega_l < T_{\text{all}}$ **do**
6: Select and execute action $\mathcal{A}^k$ based on $\pi_\Theta(\mathcal{A}^k|\zeta^k)$;
7: Compute reward $\mathcal{R}(\zeta^k, \mathcal{A}^k)$;
8: Obtain new state ζ^{k+1};
9: Record transition $(\zeta^k, \mathcal{A}^k, \mathcal{R}^k, \zeta^{k+1})$ into $\mathcal{B}$;
10: $k = k + 1$;
11: **for** $e \in \{1, 2, ..., E\}$ **do**
12: Sample a minibatch of $\mathcal{B}_N$ transitions from buffer $\mathcal{B}$;
13: Update parameters $\Theta \leftarrow \arg\max_\Theta L^{\text{clip}}(\Theta)$ and $\vartheta \leftarrow \arg\min_\vartheta L^{\text{critic}}(\vartheta)$;
14: Empty buffer $\mathcal{B}$;
15: **Output:** Parameters θ_1, θ_2;

$$V_\vartheta(\zeta^k) = \mathbb{E}\left[\sum_{l=0}^{\infty} \gamma^l \mathcal{R}(\zeta^{k+l+1}, \mathcal{A}^{k+l+1}) \mid \zeta^k\right]. \tag{4.35}$$

The clipping function clips the ratio ξ_Θ between $1 - \delta$ and $1 + \delta$ using a hyperparameter δ, preventing the new policy from deviating far from the old policy to improve the learning stability. The critic is trained by minimizing the mean squared error

$$L^{\text{critic}}(\vartheta) = \mathbb{E}\left[\left(\mathcal{R}^k + V_\vartheta(\zeta^{k+1}) - V_\vartheta(\zeta^k)\right)^2\right]. \tag{4.36}$$

The overall HPPO-based slicing window length and communication resource determination procedure is summarized in Algorithm 2, where J denotes the number of training episodes. To handle the variability of slicing window lengths, the episode duration is defined in terms of overall time slots rather than slicing windows. Specifically, the total number of time slots in each episode is set to T_{all}. When the cumulative number of time slots within a slicing window reaches or exceeds T_{all}, the last slot of that slicing window is treated as the final slot of the episode. This design ensures that each episode always ends at a slicing window boundary, thereby preserving the integrity of slicing decisions.

At the beginning of training, the discrete actor, continuous actor, and critic networks are initialized with parameters θ_1, θ_2, and ϑ, respectively. A replay buffer $\mathcal{B}$ is used to store the interaction transitions. During each slicing window, the controller observes the current state from the environment, selects the slicing window length and communication resource reservation according to the current policy π_Θ, executes the action, receives the corresponding reward, and observes the new state. The resulting transition $(\zeta^k, \mathcal{A}^k, \mathcal{R}^k, \zeta^{k+1})$ is stored in the buffer, as illustrated in Lines 6–9. At the end of each training episode, the collected transitions are used to update the policy and value networks. Specifically, the parameters θ_1 and θ_2 of the discrete and continuous actor networks are updated by maximizing the clipped surrogate objective in Eq. (4.32) via gradient ascent, while the critic network parameters ϑ are updated by minimizing the mean squared error loss via gradient descent, as shown in Line 13. To enhance training stability of policy updates, the parameters are updated for E times in each episode to take full use of the samples generated by the current strategy.

The training complexity of the HPPO-based algorithm is primarily determined by the dimensions of the state and action spaces. As the number of satellites increases, the state dimension grows due to the inclusion of additional satellite-related information. Similarly, the dimension of the continuous action space, corresponding to the communication resource reservation vectors of all APs, increases linearly with the number of satellites. Nevertheless, both the actor and critic networks are implemented with fixed numbers of hidden layers and neurons. As a result, the computational complexity of both training and inference scales approximately linearly with the number of satellites. Moreover, HPPO updates are performed on fixed minibatches sampled from the buffer, which prevents the number of training samples per update from increasing with the system scale. Consequently, the proposed HPPO-based algorithm remains computationally efficient and scalable for large-scale STVNs.

4.5 Performance Evaluation

In this section, extensive simulations are conducted to evaluate the effectiveness of the proposed TLRS scheme. We first describe the simulation setup and benchmark algorithms. Afterward, the simulation results are presented to demonstrate the effectiveness of our proposed scheme.

In the simulation scenario, we consider a target area with a radius of 15 km, centered at 30°N latitude and 82.5°W longitude. A total of eight HD map files are requested by CVs in the area, each with a size of 10 Mb. The satellite network follows the Starlink Phase 1 constellation, consisting of 72 orbits with 22 satellites per orbit, an inclination angle of 53°, and an altitude of 550 km. Unless otherwise specified, the minimum access elevation angle is set to 35°.

For terrestrial networks, BSs are deployed with a density of 0.1 km^{-2}, each covering a radius of 1 km. The unit costs of satellite communication and caching resources are both set to 0.1, while those of BSs are set to 0.02. The simulation lasts for 30 min, with each time slot being 20 s. The slicing window length ranges from 1 to 9 time slots. The delay requirement for HD map distribution is set to 2.5 s with a reliability constraint of 0.99, and the default multicast interval is 1.5 s.

In the HPPO-based model, both actor and critic networks consist of three fully connected hidden layers with [256, 256, 128] neurons. The tanh activation function is used in the hidden layers of both actor networks to facilitate stable training. Meanwhile, in the discrete actor network's output layer, we apply the softmax to produce a valid probability distribution. Furthermore, the Adam optimizer is adopted to train

Table 4.1 Simulation parameters

LEO satellite transmission power	40 dBm	LEO satellite carrier frequency	40 GHz
LEO satellite antenna gains	32 dBi	LEO satellite bandwidth	250 MHz
LEO satellite path-loss exponent	2.5	Noise power	−174 dBm/Hz
BS transmission power	32 dBm	BS carrier frequency	28 GHz
BS antenna gains	10 dBi	BS bandwidth	100 MHz
BS path-loss exponent	3.5	Parameters β_1, β_2, β_3, and β_4	0.01, 1, 0.5, 1.5

the network parameters. Additional communication parameters of satellites and BSs [20, 21] are summarized in Table 4.1.

We first evaluate the learning performance of the proposed TLRS scheme. The following three benchmark algorithms are considered: (1) *SBMA+Vanilla HPPO*: discrete and continuous actors are trained independently instead of feeding discrete decisions to the continuous actor [22], while the SBMA for the inner layer remains the same as in the proposed scheme; (2) *SBMA+PDQN*: parameterized DQN (PDQN) is used in the outer layer, which extends DQN to parameterized actions by learning a joint Q-function where each discrete action is associated with a continuous parameter vector [18], while the SBMA for the inner layer remains the same as in the proposed scheme; (3) *Vanilla HPPO*: all decisions are made directly by a single HPPO agent.

The convergence performance of the proposed TLRS scheme is shown in Fig. 4.4 to illustrate the average cost of each episode. First, Fig. 4.4a compares the convergence behavior of different algorithms, where the dark line shows the 50-episode moving average cost value and the shadowed lines are the average system cost of each episode. The proposed TLRS scheme converges within a small number of episodes and exhibits stable and convergent performance. In contrast, *SBMA+Vanilla HPPO* converges more slowly with greater fluctuations, as its continuous actor only learns a marginal policy across different discrete actions. *SBMA+PDQN* suffers from instability caused by the difficulty of approximating joint Q-functions over discrete actions and continuous parameters. *Vanilla HPPO* fails to converge, owing to the excessively large and highly coupled action space. These results demonstrate that, by decomposing the slicing window length and resource reservation into a structured matching process in the inner layer, our TLRS enables more efficient exploration of the optimal decisions in the outer layer, which significantly improves learning stability and convergence speed. In addition, the impact of learning rate is illustrated in Fig. 4.4b, where an identical learning rate is set for all actor and critic networks. All curves converge with increasing training episodes. While larger learning rates accelerate convergence, they may also introduce performance instability. Therefore, a learning rate of 5×10^{-5} for the HPPO-based algorithm is adopted for subsequent experiments.

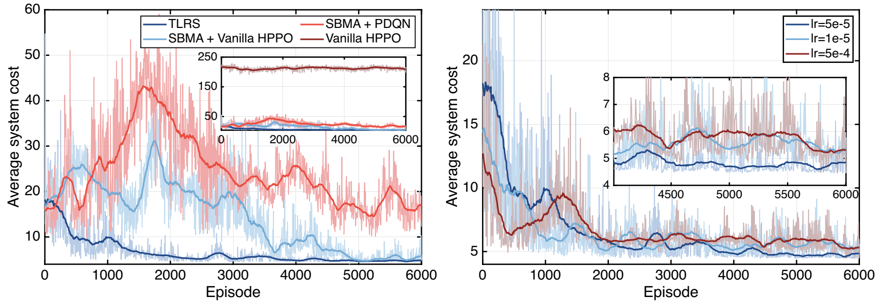

(a) Convergence of different algorithms. (b) Different learning rates.

Fig. 4.4 Convergence performances

Next, we investigate the impact of slicing window length determination. The proposed TLRS is compared with fixed-length slicing strategies (*Fix n*) with a fixed window length n time slots and a demand-driven dynamic strategy (*Dynamic*) based on service demand fluctuations such that the variance of the accumulative service demand intensity within each slicing window [23]. All benchmark algorithms use conventional PPO for resource reservation and SBMA for caching and multicast decisions.

The performances of different slicing window length determination policies are shown in Fig. 4.5, evaluating the slot performance of resource cost and slice reconfiguration, and showing the statistical performance of unsupported service demand and overall system cost. Figure 4.5a shows the cumulative distribution function (CDF) of resource cost per time slot. The resource cost of *Fix*3 achieves the lowest resource cost by adapting quickly to demand variations, while longer windows incur higher costs due to resource over-provisioning. While *Dynamic* policy is tailored to service demand variations, it overlooks the time-varying resource resulting from satellite mobility. Consequently, a long slicing window can lead to a high resource cost when reserving resources on satellites with limited communication capabilities, such as those at low elevation angles. The proposed TLRS achieves a comparable resource cost to *Fix*3 by adaptively adjusting slicing window length, which effectively accommodates dynamic service demand with efficient resource usage. The CDF of time-averaged slice reconfiguration cost is shown in Fig. 4.5b. Short slicing windows lead to frequent reconfiguration, which incurs larger slice reconfiguration cost, whereas longer or dynamic windows reduce reconfiguration overhead. Figure 4.5c presents the unsupported service demand in the target area. In the per-slot results, the proposed TLRS scheme and *Fix3* exhibit lower unsupported demand across most time slots, which achieve superior demand accommodation compared to the others. Although *Fix3* yields a slightly lower mean and variance of unsupported demand, it incurs a much higher slice reconfiguration cost as shown in Fig. 4.5b. By contrast, TLRS can adjust the slicing windows according to dynamic demand and available resources, thereby minimizing unsupported demand while maintaining a balanced tradeoff with

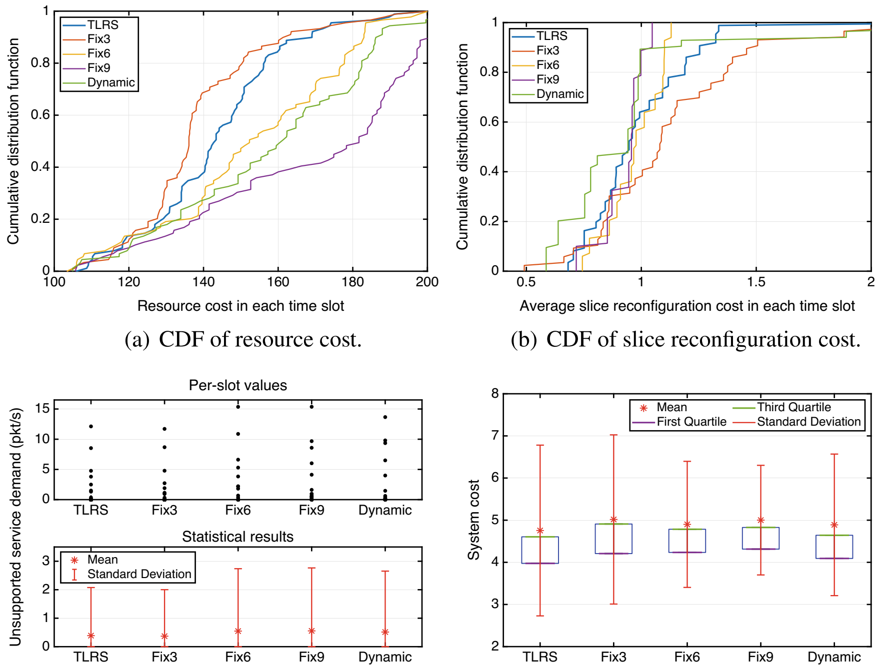

(a) CDF of resource cost.

(b) CDF of slice reconfiguration cost.

(c) Unsupported service demand.

(d) Overall system cost.

Fig. 4.5 Performance under different slicing window length determination policies

reconfiguration cost. Finally, Fig. 4.5d summarizes the overall system cost statistics within the entire simulation duration. TLRS consistently achieves the lowest mean system cost and quartile performance, which indicates that TLRS can achieve better performance in most time slots from its adaptation, demonstrating its robustness under dynamic service demand and satellite availability for a long-term optimum. In contrast, the *Dynamic* strategy has a higher mean cost, which ignores time-varying satellite resources and incurs occasional high costs due to unnecessary resource reservation and unsupported service demands. For the fixed slicing window policies, longer slicing windows result in smaller standard deviations, reflecting more consistent resource costs within each slicing window.

Figure 4.6 illustrates the average system cost under different minimum satellite elevation angles. When the minimum elevation angle is small, more satellites are visible to the target area, and the system cost becomes small due to sufficient resources enabling efficient resource reservation with adaptive slicing windows. In this case, the reconfiguration cost becomes a dominant component, and thus *Fix*3 yields a relatively higher cost due to frequent slice adjustments. As the minimum elevation angle increases, fewer satellites can serve the area, leading to reduced satellite availability and a higher overall cost. Specifically, when the elevation angle is large, satellite resources are insufficient to cover demand outside BS coverage, and the ser-

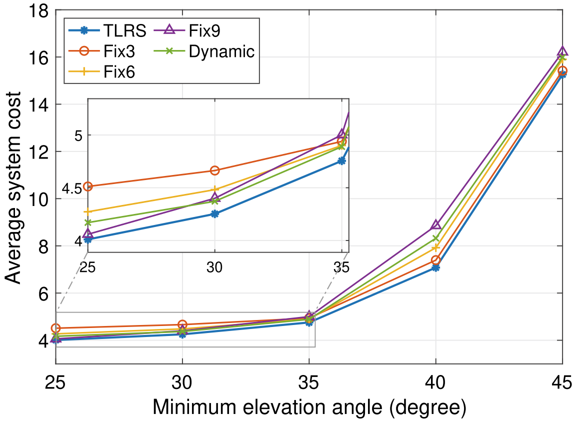

Fig. 4.6 Average system cost under different minimum elevation angles of LEO satellites

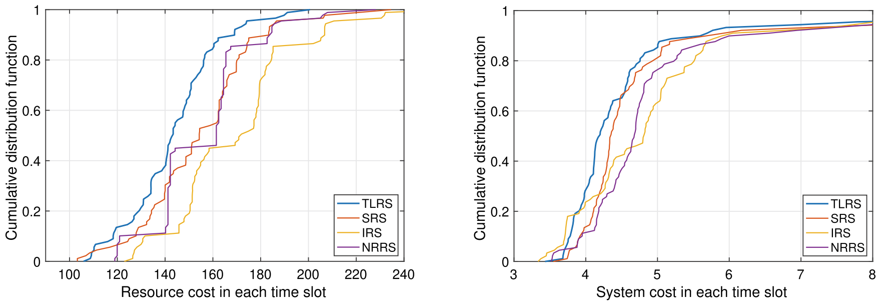

(a) CDF of resource cost. (b) CDF of system cost.

Fig. 4.7 Performance under different reservation strategies

vice demand penalty dominates the system cost. In this case, shorter slicing windows become beneficial because more frequent reconfiguration allows the controller to better adapt to time-varying satellite accessibility with less demand-violation penalties. Across all elevation settings, TLRS consistently achieves the lowest cost, demonstrating its robustness and adaptability across varying network conditions.

Next, we evaluate the effectiveness of the HPPO-based resource reservation strategy in the proposed TLRS framework. We consider three benchmark algorithms: (1) *SRS*, where resource reservation is determined separately for satellite and terrestrial networks and is identical across all satellites (and across all BSs) within each slicing window [24]; (2) *IRS*, where all APs share identical reservation decisions within each slicing window; and (3) *NRRS*, where reservation decisions are fixed over time and determined using the average resource availability and average demand. Both *SRS* and *IRS* policies adopt an HPPO-based algorithm, with reduced action dimensions compared to TLRS.

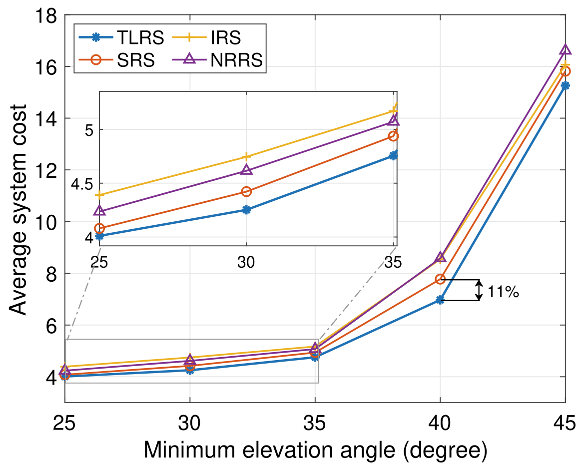

Fig. 4.8 Average system cost with different resource reservation policies

Figure 4.7 compares the CDFs of resource cost and overall system cost. The proposed TLRS scheme achieves the lowest system cost and efficient resource usage by enabling fine-grained reservation decisions at the AP level, which can capture both spatially heterogeneous demands and time-varying satellite accessibility. In contrast, *SRS* and *IRS* are constrained by their reduced action dimensions, which cannot fully exploit the spatiotemporal heterogeneity and satellite mobility in STVNs. *NRRS* performs the worst since it overlooks the changes in satellite resources and only considers the average service demand across all time slots, resulting in either resource waste or unsupported service demand.

Figure 4.8 further shows the average system cost of different resource reservation strategies under different minimum elevation angles. When the minimum elevation angle is small, our proposed TLRS scheme achieves a slight improvement in overall system cost with more efficient resource reservation, but the cost difference among strategies is limited due to abundant satellite resources for satisfying service demand with moderate resource usage. As the elevation angle increases, all strategies incur higher system cost due to reduced satellite accessibility, while TLRS exhibits a constant advantage. For example, at 40°, the proposed TLRS reduces the system cost by at least 11% compared with other benchmark strategies, benefiting from fine-grained adaptive reservation that better adapts to the service demand with constrained resource conditions.

Finally, we evaluate the SBMA-based caching and multicast decisions. We compare TLRS with three benchmark algorithms: (1) *UO+MBC* for unicast only with matching-based caching policy; (2) *MU+NC* for both multicast and unicast without caching; and (3) *MU+PAC* for both multicast and unicast with a popularity-aware caching policy.

In Fig. 4.9, we compare the performances of different caching and multicast policies in terms of unsupported service demand, average delay, and average system cost. Figure 4.9a shows that TLRS accommodates the highest service demand across

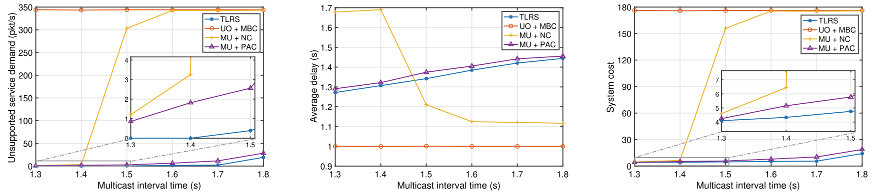

(a) Unsupported service demand. (b) Average delay. (c) Average system cost.

Fig. 4.9 Performance for different caching and multicast policies

different multicast intervals due to its efficient strategies at each satellite. When the multicast interval is short, multicast can efficiently serve popular files with limited reserved resources, enabling more files to benefit from multicast delivery. However, as the multicast interval increases, the limited transmission time of each file necessitates more resources within each multicast period to satisfy service requirements, which leads to increased unmet demand for all policies, while TLRS constantly performs the best. *MU+PAC* performs close to TLRS but remains inferior because it relies solely on file popularity and does not explicitly account for time-varying satellite availability and jointly leverage multicast and unicast capabilities of satellites. *MU+NC* degrades sharply with the increment of multicast intervals because the backhaul delay makes it difficult to satisfy the delay requirement without satellite caching, resulting in significant unmet service demand. *UO+MBC* yields the highest unmet service demand since unicast alone cannot efficiently support bursty HD map requests.

Figure 4.9b presents the average delay of accommodated service demand. *UO+MBC* has a relatively low delay because the multicast waiting time is absent. For *MU+NC*, when the multicast interval is small, the delay requirements can be easily met with the available resources, but the backhaul delay leads to a higher delay compared to other strategies. When the multicast interval increases, more multicast requests become infeasible. Only the accommodated demand, mainly through unicast transmission, is counted in the average delay statistic, resulting in decreased delay. When both multicast and caching are incorporated, the delay performance becomes stable, and TLRS achieves the lowest average delay, benefiting from SBMA for jointly optimizing multicast and caching decisions under time-varying environments.

Finally, the performance in Fig. 4.9c demonstrates that TLRS achieves the minimum system cost. The dominant factor contributing to the overall cost is driven by unsupported service demand. Thus *MU+PAC* approaches TLRS when caching and multicast are both available. In contrast, strategies without multicast or caching incur significant system costs, especially when the multicast interval is large. These results validate that TLRS provides adaptive and efficient resource slicing for HD map distribution in dynamic STVNs.

4.6 Summary

In this chapter, we have investigated multi-dimensional resource slicing for HD map distribution in STVNs. By exploiting the complementary characteristics of satellite and terrestrial infrastructures, we establish a novel slicing architecture supporting multicast and unicast transmissions. To cope with time-varying resource availability and spatiotemporal demand dynamics, a TLRS scheme was proposed, which jointly optimizes slicing window length, communication and caching resource reservation, and multicast decisions. Through a hybrid data–model co-driven design, TLRS achieves efficient resource utilization with low delay and reconfiguration overhead, which enables robust adaptation to STVN environments while satisfying service reliability requirements. Overall, the proposed scheme offers practical design insights for scalable and service-aware resource slicing in future STVNs.

References

1. Wu, F., Yang, W., Lu, J., Lyu, F., Ren, J., Zhang, Y.: RLSS: a reinforcement learning scheme for HD map data source selection in vehicular NDN. IEEE Internet Things J. **9**(13), 10777–10791 (2021)
2. He, M., Wu, H., Zhou, C., Shen, X.: Resource slicing with cross-cell coordination in satellite-terrestrial integrated networks. In: Proceedings of the IEEE ICC (2024)
3. Shen, X., Gao, J., Wu, W., Li, M., Zhou, C., Zhuang, W.: Holistic network virtualization and pervasive network intelligence for 6G. IEEE Commun. Surveys Tuts. **24**(1), 1–30 (2021)
4. He, M., Wu, H., Zhou, C., Hu, S., Shen, X., Zhuang, W.: Adaptive multi-dimensional resource slicing in cognitive satellite-terrestrial vehicular networks. IEEE Trans. Cogn. Commun. Netw. **12**, 3191–3208 (2026)
5. Wu, H., He, M., Shen, X., Zhuang, W., Dao, N., Shi, W.: Network performance analysis of satellite-terrestrial vehicular network. IEEE Internet Things J. **11**(9), 16829–16844 (2024)
6. Zhao, J., Wang, Y., Lu, H., Li, Z., Ma, X.: Interference-based QoS and capacity analysis of VANETs for safety applications. IEEE Trans. Veh. Technol. **70**(3), 2448–2464 (2021)
7. Ramakrishnan, N., Soni, T.: network traffic prediction using recurrent neural networks. In: Proceedings of the IEEE ICMLA (2018)
8. Lin, Y., Wang, M., Zhou, X., Ding, G., Mao, S.: Dynamic spectrum interaction of UAV flight formation communication with priority: a deep reinforcement learning approach. IEEE Trans. Cogn. Commun. Netw. **6**(3), 892–903 (2020)
9. He, M., Zhou, C., Wu, H., Shen, X.: Learning-based cache placement and content delivery for satellite-terrestrial integrated networks. In: Proceedings of the IEEE GLOBECOM, pp. 1–6 (2021)
10. Wu, D., Negi, R.: Effective capacity: a wireless link model for support of quality of service. IEEE Trans. Wireless Commun. **2**(4), 630–643 (2003)
11. He, M., Wu, H., Zhou, C., Hu, S., Tang, Z., W.: Zhuang: digital twin-assisted robust and adaptive resource slicing in LEO satellite networks. In: Proceedings of the IEEE GLOBECOM, pp. 3261–3266 (2024)
12. Chang, C.S.: Performance Guarantees in Communication Networks. Springer, London, U.K. (2000)
13. Grant, M., Boyd, S.: CVX: Matlab software for disciplined convex programming, version 2.1 (2014). https://cvxr.com/cvx/

14. Zhao, J., Liu, Y., Chai, K.K., Chen, Y., Elkashlan, M.: Many-to-many matching with externalities for device-to-device communications. IEEE Wireless Commun. Lett. **6**(1), 138–141 (2016)
15. Di, B., Song, L., Li, Y.: Sub-channel assignment, power allocation, and user scheduling for non-orthogonal multiple access networks. IEEE Trans. Wireless Commun. **15**(11), 7686–7698 (2016)
16. Tang, Y., Agrawal, S.: Discretizing continuous action space for on-policy optimization. In: Proceedings of the AAAI Artificial Intelligence (2020)
17. Masson, W., Ranchod, P., Konidaris, G.: Reinforcement learning with parameterized actions. In: Proceedings of the AAAI Artificial Intelligence (2016)
18. Xiong, J., Wang, Q., Yang, Z., Sun, P., Han, L., Zheng, Y., Fu, H., Zhang, T., Liu, J., Liu, H.: Parametrized deep Q-networks learning: reinforcement learning with discrete-continuous hybrid action space. arXiv:1810.06394 (2018)
19. Fan, Z., Su, R., Zhang, W., Yu, Y.: Hybrid actor-critic reinforcement learning in parameterized action space. In: Proceedings of the IJCAI (2019)
20. Leyva-Mayorga, I., Soret, B., Matthiesen, B., Röper, M., Wübben, D., Dekorsy, A., Popovski, P.: Non-geostationary orbit constellation design for global connectivity, chap. 10, pp. 237–267. IET (2024)
21. de Almeida, T.T., de Carvalho Gomes, L., Ortiz, F.M., Júnior, J.G.R., Costa, L.H.M.: Comparative analysis of a vehicular safety application in NS-3 and veins. IEEE Trans. Intell. Transp. Syst. **23**(1), 620–629 (2020)
22. Wang, T., Deng, Y., Yang, Z., Wang, Y., Cai, H.: Parameterized deep reinforcement learning with hybrid action space for edge task offloading. IEEE Internet Things J. **11**(6), 10754–10767 (2023)
23. Shen, H., Tian, Y., Wang, T., Bai, G.: Slicing-based task offloading in space-air-ground integrated vehicular networks. IEEE Trans. Mobile Comput. **23**(5), 4009–4024 (2023)
24. Liu, Y., Ma, T., Qin, X., Zhou, H., Shen, X.: Reconfigurable RAN slicing for ultra-dense LEO satellite networks via DRL. IEEE Trans. Cogn. Commun. Netw. **11**(1), 566–580 (2025)

Chapter 5
Cooperative Resource Scheduling for Environment Sensing in STVNs

Abstract In satellite–terrestrial vehicular networks (STVNs), efficient resource management is essential to support diverse vehicular services under dynamic network conditions. While long-term resource reservation provides a foundation for service provisioning, the real-time orchestration of reserved resources plays a critical role in achieving timely and reliable service performance. In this chapter, we investigate resource management for infrastructure-assisted environment sensing for connected vehicles (CVs) in STVNs at the operation stage, where low Earth orbit (LEO) satellites and roadside units (RSUs) cooperatively provide CVs with fresh sensing information. Due to the stringent information freshness requirements, satellite mobility, and heterogeneous network capabilities, real-time multi-dimensional resource scheduling in STVNs is highly challenging. To this end, we formulate a cooperative resource scheduling problem that jointly optimizes sensing intervals and real-time computing and communication resource allocation, and propose a cooperative satellite–terrestrial resource scheduling (CSTRS) scheme to satisfy service requirements with efficient resource utilization. CSTRS adopts a hybrid model–data co-driven design, which decomposes the complex scheduling problem into complementary subproblems. Specifically, by exploiting the multicast capability of LEO satellites, coalition game- and particle swarm optimization-based algorithms are developed to partition CVs into sensing groups and determine appropriate sensing intervals. Based on the resulting CV partition, a reinforcement learning-based algorithm is further designed to make real-time computing and communication resource allocation decisions. Simulation results demonstrate that the proposed CSTRS scheme outperforms benchmark methods in terms of resource efficiency and reliability under dynamic STVN conditions.

Keywords Cooperative resource scheduling · Infrastructure-assisted environment sensing · Coalition game · Proximal policy optimization

With the rapid growth of connected vehicles (CVs), the acquisition of real-time environment information becomes essential for route optimization, traffic safety enhancement, and intelligent driving control [1]. Specifically, each CV requires accurate and up-to-date environment information within its range of interest (RoI) to support safe and efficient driving. Although onboard sensors and processors enable CVs to per-

M. He et al., *Resource Management for Satellite-Terrestrial Vehicular Networks*, SpringerBriefs in Computer Science, https://doi.org/10.1007/978-3-032-24526-7_5

ceive and process surrounding environments to detect objects, such as non-connected vehicles, obstacles, etc., their sensing capability is inherently limited by sensing range and single-view constraints. As a result, augmenting sensing coverage and mitigating blocked areas are crucial for reliable perception. Infrastructure-assisted environment sensing, which leverages sensors deployed on network infrastructures, provides an effective solution by enabling large-scale and cooperative perception within the RoI of CVs [2]. By integrating sensing results from multiple infrastructures, CVs can obtain more reliable environment information. To ensure the effectiveness of such sensing services, the freshness and reliability of sensing results are critical, as outdated information may lead to incorrect decision-making and safety risks. Meanwhile, sensing information inevitably becomes stale over time, necessitating continuous updates with stringent freshness guarantees.

Currently, environment sensing is primarily supported by terrestrial infrastructures such as roadside units (RSUs), where sensors and edge servers are deployed to perceive the environment, process sensing data to generate sensing results, and deliver them to nearby CVs [3]. While RSU-assisted sensing can provide low-latency services, the high deployment cost of terrestrial infrastructures often leads to coverage gaps, especially in suburban and remote areas. To complement terrestrial networks, low Earth orbit (LEO) satellites offer ubiquitous coverage and enable seamless sensing services beyond terrestrial networks [4, 5]. Moreover, by equipping satellites with onboard edge servers, sensing data can be processed directly, avoiding the transmission of massive raw data to ground servers. Nevertheless, the inherent satellite mobility and high resource costs introduce new challenges, making it essential to jointly and efficiently coordinate satellite and terrestrial resources. Taking full advantage and complementarity of both satellites and RSUs, this chapter investigates cooperative resource scheduling in satellite–terrestrial vehicular networks (STVNs) to support infrastructure-assisted environment sensing with stringent data freshness requirements and efficient resource utilization [6].

However, cooperative resource scheduling in STVNs still encounters several challenges in supporting environment sensing. First, sensing data freshness depends jointly on the sensing interval and the infrastructure-induced delays in data processing and transmission, which leads to tightly coupled and multi-dimensional scheduling decisions in a dynamic STVN environment. Second, the mobility of LEO satellites and CVs causes time-varying network accessibility, propagation delays, and communication performance, resulting in highly dynamic resource demands from both satellite and terrestrial networks. Third, satellites and RSUs exhibit heterogeneous network characteristics in terms of coverage areas, connection durations, resource costs, and content delivery modes. As CVs may be served by satellites alone or by both satellite and terrestrial infrastructures, cooperative scheduling across heterogeneous networks becomes highly complex.

To address the abovementioned challenges, we propose a cooperative satellite–terrestrial resource scheduling (CSTRS) scheme, which jointly determines sensing intervals and allocates computing and communication resources in STVNs to satisfy stringent data freshness requirements with efficient resource usage. Specifically, a two-step scheduling framework is developed to find the optimal solutions. By exploiting the multicast capability of LEO satellites, large-timescale model-based algorithms are designed to partition CVs into sensing groups and determine appropriate sensing intervals, thereby reducing resource consumption and decision complexity. Based on the CV partitioning and sensing intervals, a reinforcement learning-based algorithm is further developed to perform real-time computing and communication resource allocation, enabling adaptive responses to dynamic network conditions. The main contributions of this chapter are summarized as follows:

- We investigate resource scheduling in STVNs for infrastructure-assisted environment sensing, where both LEO satellites and RSUs provide network services to CVs. The formulated cooperative resource scheduling problem jointly considers sensing interval determination, CV partitioning, and real-time computing and communication resource allocation under stringent data freshness requirements to satisfy data freshness requirements with efficient resource consumption.
- We propose the CSTRS scheme to solve the mixed-integer and sequential decision-making problem by decoupling the original problem into two subproblems operating on different timescales, thereby significantly reducing scheduling complexity. Specifically, CV partition and sensing interval decisions are adjusted on a large timescale, while resource allocation for each service group is determined on a small timescale.
- We design a particle swarm optimization (PSO)-based and a coalition formation game-based algorithm to optimize long-term sensing intervals and CV partitioning, and develop a proximal policy optimization (PPO)-based reinforcement learning algorithm for real-time computing and communication resource allocation in dynamic environments. Extensive experiments are conducted to demonstrate the effectiveness of the proposed CSTRS scheme by comparing multiple performance metrics, including resource cost and reliability.

The remainder of this chapter is organized as follows. Section 5.1 introduces the network scenario and system models. Section 5.2 presents the problem formulation and the design of the CSTRS scheme. Section 5.3 develops the PSO-based sensing interval optimization and coalition formation-based CV partitioning methods, while Sect. 5.4 presents the reinforcement learning-based real-time resource allocation algorithm. Simulation results are provided in Sect. 5.5, followed by the conclusions in Sect. 5.6.

5.1 Network Scenario and System Model

5.1.1 Scenario Description

The considered infrastructure-assisted environment sensing scenario in STVNs is illustrated in Fig. 5.1. Terrestrial RSUs provide sensing services for CVs within their coverage areas, while a LEO satellite equipped with steerable beams can

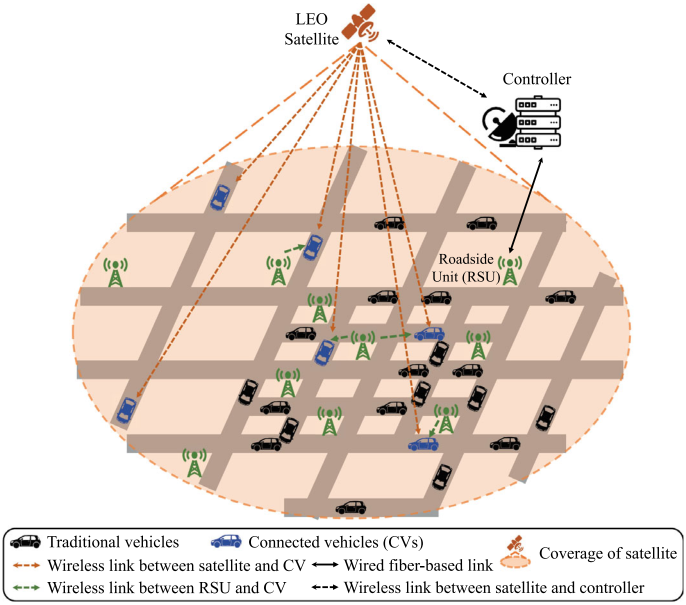

Fig. 5.1 Considered environment sensing scenario in STVNs

serve CVs across the entire target region. A ground central controller coordinates both RSUs and the satellite to support cooperative sensing for the target area. We consider a time-slotted system, where each time slot $t \in \mathcal{T} = \{1, 2, \ldots, T\}$ has duration τ. The length of T time slots corresponds to the continuous service period of the satellite for the target area determined by the minimum elevation angle constraint. The time-varying position of the satellite is characterized by $(r^{\mathrm{S}}, \alpha, \omega(t), \rho(t))$, representing the orbit radius, orbital inclination angle, longitude of ascending node of the orbit, and argument of periapsis, respectively. Accordingly, the satellite position in the Cartesian coordinate system at time slot t is $\mathbf{p}^{\mathrm{S}}(t) = (x^{\mathrm{S}}(t), y^{\mathrm{S}}(t), z^{\mathrm{S}}(t))$ [5]. Let $\mathcal{N} = \{1, 2, \ldots, N\}$ denote the set of RSUs, where each RSU has a fixed coverage radius of r^{T}. The coordinate of RSU n is $\mathbf{p}_n^{\mathrm{T}} = (x_n^{\mathrm{T}}, y_n^{\mathrm{T}}, z_n^{\mathrm{T}})$. Let $\mathcal{U} = \{1, 2, \ldots, U\}$ denote the set of CVs, and the position of CV u at time slot t is $\mathbf{p}_u^U(t) = (x_u^U(t), y_u^U(t), z_u^U(t))$. Due to the mobility of CVs, their connectivity to RSUs varies over time. Let $a_u^{\mathrm{T}}(t)$ represent the RSU accessibility indicator of CV u at time slot t, where $a_u^{\mathrm{T}}(t) = 1$ if at least one RSU can serve CV u, and $a_u^{\mathrm{T}}(t) = 0$ otherwise.

Consider that both LEO satellites and RSUs have the capability of data processing with the deployment of edge servers. To support environment sensing, infrastructures periodically sense the RoI of CVs, process sensing data, and deliver sensing results to CVs. However, independently sensing each CV's RoI leads to excessive computation and communication overhead due to the potential spatial overlap of RoIs among nearby CVs. To improve efficiency, we leverage the multicast capability of the LEO satellite to serve CVs into groups to enhance resource utilization. Specifically, multiple satellite service groups (SSGs) are formed, where each group contains a subset of CVs served simultaneously by the satellite. Let $\Omega^{\mathrm{S}}(t) = \{\mathbf{s}_0(t), \mathbf{s}_1(t), \ldots, \mathbf{s}_m(t)\}$ denote the set of SSGs, where $\mathbf{s}_i(t)$, $i \neq 0$ represents the i-th SSG, and $\mathbf{s}_0(t)$ indicates the set of CVs not served by the satellite at time slot t. For terrestrial sensing, each RSU serves one terrestrial service group (TSG) consisting of all CVs within its coverage. The set of TSGs is denoted by $\Omega^{\mathrm{T}}(t) = \{\mathbf{g}_1(t), \ldots, \mathbf{g}_n(t)\}$, where $\mathbf{g}_i(t)$ represents the CV set served by RSU i. Due to vehicle mobility, CVs in each TSG vary over time, while SSG partitioning is updated periodically every time interval, consisting of k time slots.

To satisfy data freshness requirements, each service group must determine an appropriate sensing interval. A small sensing interval enables real-time object tracking but incurs high processing and transmission resource consumption to satisfy stringent processing and transmission delay requirements. On the other hand, a large sensing interval reduces resource usage but may violate freshness constraints. Since sensing data originates from both satellite and RSUs, their sensing intervals must be jointly determined to minimize resource consumption and satisfy data freshness requirements. Let $I_{\mathbf{s}}^{\mathrm{S}}(t)$ and $I_{\mathbf{g}}^{\mathrm{T}}(t)$ denote the sensing intervals for SSG $\mathbf{s}$ and TSG $\mathbf{g}$ at time slot t, respectively.

5.1.2 Age of Information Model

To enable timely decision-making in dynamic environments for driving safety and efficiency, CVs require up-to-date sensing results. We adopt the age of information (AoI) to characterize the freshness of received sensing results, which measures the elapsed time since the latest successfully received sensing data was generated [7]. Each sensing result is timestamped at the moment of generation. For CV u, the AoI of sensing result originating from source $\mathbf{x}$ is given by

$$q_u^{\mathbf{x}}(t) = \begin{cases} q_u^{\mathbf{x}}(t-1) + 1, & \text{if no packet is received,} \\ t - \max_i\{t_u^{\mathbf{x}}(i) \mid t_u'^{\mathbf{x}}(i) \leq t\}, & \text{otherwise,} \end{cases} \tag{5.1}$$

where $t_u^{\mathbf{x}}(i)$ and $t_u'^{\mathbf{x}}(i)$ denote the generation time and reception time of the i-th sensing data and result for CV u, respectively, and $\mathbf{x} \in \{\mathrm{S}, \mathrm{T}\}$ represents that the sensing information originating from source satellite or RSUs. The AoI value increases linearly over time when no updated result is received by a CV, and drops to the elapsed time since the generation of the latest received sensing result once an update arrives.

Since CVs may receive sensing results from both the LEO satellite and RSUs, the latest effective information is determined by the freshest received data, as shown in Fig. 5.2. Therefore, the overall AoI of CV u is defined as

$$q_u(t) = \min\{q_u^{\mathrm{S}}(t),\ q_u^{\mathrm{T}}(t)\}. \tag{5.2}$$

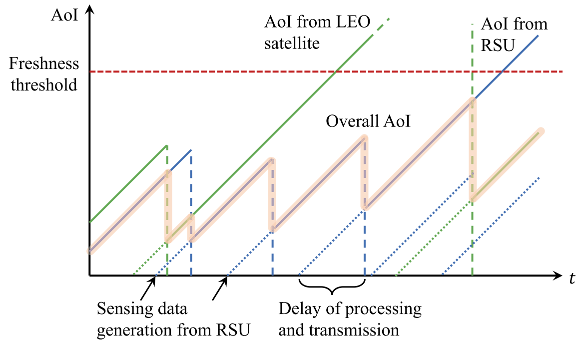

Fig. 5.2 AoI illustration of CV

If a fresher sensing result is received by the CV, outdated packets that have not yet been delivered are discarded. Meanwhile, if two sensing results are received at the same time, the formerly generated packet will be discarded.

To guarantee sensing reliability, the AoI must satisfy a probabilistic freshness constraint. Specifically, the probability that the AoI exceeds a freshness threshold T^{th} should be smaller than ε [8]. In this case, the AoI depends on the following two key factors: (1) the sensing interval of SGs, which determines how frequently new data is generated, and (2) the processing and transmission delay affected by computing and communication resource allocation. Therefore, satisfying the freshness requirement requires jointly optimizing sensing intervals and real-time resource allocation across satellite and terrestrial networks.

5.1.3 Computing and Communication Model

After sensing data for an SG is generated, it must be processed, and then the result should be transmitted to CVs. Therefore, the overall delivery delay of each sensing data consists of computing delay, transmission delay, and propagation delay for satellites, which directly affects the AoI evolution introduced in the previous subsection.

For SSG $\mathbf{s}$, sensing data with size $\nu_{\mathbf{s}}^{\mathrm{S}}(t)$ is generated at time slot t, which varies for different sensing areas. The generation time of the i-th sensing data is $K(t) + \Psi_{\mathbf{s}}^{\mathrm{S}}(t) + iI_{\mathbf{s}}^{\mathrm{S}}(t)$, where $K(t) = \max\{jk|jk \le t, \forall j\}$ denotes the initial time slot of the current interval for SSG adjustment, and $\Psi_{\mathbf{s}}^{\mathrm{S}}(t)$ is the delayed time of the first sensing for SSG $\mathbf{s}$ from $K(t)$.

Let $Q_{\mathbf{s}}^{\mathrm{S}}(t)$ denote the remaining data size for processing at time slot t, given by

$$Q_{\mathbf{s}}^{\mathrm{S}}(t) = \begin{cases} \nu_{\mathbf{s}}^{\mathrm{S}}(t), & t = K(t) + iI_{\mathbf{s}}^{\mathrm{S}}(t) + \Psi_{\mathbf{s}}^{\mathrm{S}}(t), \forall i, \\ \max\{Q_{\mathbf{s}}^{\mathrm{S}}(t-1) - \Delta\nu_{\mathbf{s}}(t-1), 0\}, & \text{otherwise.} \end{cases} \tag{5.3}$$

Here, the processed data amount at time slot t is $\Delta \nu_{\mathbf{s}}(t) = \min\{Q_{\mathbf{s}}^{\mathrm{S}}(t), \tau f^{\mathrm{S}} c_{\mathbf{s}}(t)/\gamma\}$, where $c_{\mathbf{s}}^{\mathrm{S}}(t)$ is the allocated computing resource for SSG $\mathbf{s}$ at time slot t, f^{S} is CPU frequency unit (in CPU cycles per second), and γ is the computation workload (in CPU cycles per bit). The computing resource allocation for SSG $\mathbf{s}$ at time slot t must satisfy

$$\sum\nolimits_{\mathbf{s}\in\Omega^{\mathrm{S}}(t)} c_{\mathbf{s}}^{\mathrm{S}}(t) \le c_{\max}^{\mathrm{S}}, \quad \forall t, \tag{5.4}$$

indicating the constraint on the computing resource capability, and

$$c_{\mathbf{s}}^{\mathrm{S}}(t) = c_{\mathbf{s}}^{\mathrm{S}}(t-1), \text{ if } 0 < Q_{\mathbf{s}}^{\mathrm{S}}(t) < Q_{\mathbf{s}}^{\mathrm{S}}(t-1), \tag{5.5}$$

representing that the computing resources cannot be adjusted during the processing.

After processing, sensing results with size $\beta_{\mathbf{s}}^{\mathrm{S}}(t)$ are multicast to CVs in SSG $\mathbf{s}$. The remaining data size for transmission in the queue evolves as

$$W_{\mathbf{s}}^{\mathrm{S}}(t) = \begin{cases} \beta_{\mathbf{s}}^{\mathrm{S}}(t), & \text{if } Q_{\mathbf{s}}^{\mathrm{S}}(t-1) > Q_{\mathbf{s}}^{\mathrm{S}}(t) = 0, \\ \max\{W_{\mathbf{s}}^{\mathrm{S}}(t-1) - \Delta\beta_{\mathbf{s}}(t-1), 0\}, & \text{otherwise.} \end{cases} \tag{5.6}$$

The transmitted data amount in time slot t is $\Delta\beta_{\mathbf{s}}(t) = \min\{W_{\mathbf{s}}^{\mathrm{S}}(t), \tau R_{\mathbf{s}}^{\mathrm{S}}(t)\}$, with transmission rate $R_{\mathbf{s}}^{\mathrm{S}}(t) = b_{\mathbf{s}}^{\mathrm{S}}(t) \log_2\left(1 + \frac{P^{\mathrm{S}} h_{\mathbf{s}}^{\mathrm{S}}(t)}{\sigma^2}\right)$. Here, $b_{\mathbf{s}}^{\mathrm{S}}(t)$ is the communication resources allocated to SSG $\mathbf{s}$ at time slot t, P^{S} is the transmit power of the LEO satellite, σ^2 is the noise power, and $h_{\mathbf{s}}^{\mathrm{S}}(t)$ is the channel gain. The communication resource allocation should satisfy

$$\sum_{\mathbf{s}\in\Omega^{\mathrm{S}}(t)} b_{\mathbf{s}}^{\mathrm{S}}(t) \le b_{\max}^{\mathrm{S}}, \quad \forall t, \tag{5.7}$$

constraining the available communication resources of the LEO satellite, and

$$b_{\mathbf{s}}^{\mathrm{S}}(t) = b_{\mathbf{s}}^{\mathrm{S}}(t-1), \text{ if } 0 < W_{\mathbf{s}}^{\mathrm{S}}(t) < W_{\mathbf{s}}^{\mathrm{S}}(t-1). \tag{5.8}$$

representing that the communication resources remain fixed during the transmission.

Due to the long distance of satellite communication, propagation delay cannot be ignored. The remaining propagation time for SSG $\mathbf{s}$ is

$$Z_{\mathbf{s}}^{\mathrm{S}}(t) = \begin{cases} T_{\mathbf{s}}^{\mathrm{prop}}(t), & \text{if } W_{\mathbf{s}}^{\mathrm{S}}(t-1) > W_{\mathbf{s}}^{\mathrm{S}}(t) = 0, \\ \max\{Z_{\mathbf{s}}^{\mathrm{S}}(t-1) - \tau, 0\}, & \text{otherwise.} \end{cases} \tag{5.9}$$

Here, $T_{\mathbf{s}}^{\mathrm{prop}}(t) = \sqrt{|\mathbf{p}^{\mathrm{S}}(t) - \mathbf{p}_{\mathbf{s}}^{\mathrm{SSG}}(t)|^2}/c$ is the propagation delay between SSG $\mathbf{s}$ and the satellite, where $\mathbf{p}_{\mathbf{s}}^{\mathrm{SSG}}(t)$ is the center coordination of SSG $\mathbf{s}$, and c is the light speed.

For each TSG, the processing and transmission procedures follow the same models and queueing dynamics. However, computing and communication resources c^{T} and b^{T} are dedicated and fixed for each RSU, and the propagation delay is negligible due to the short transmission distance.

5.2 Problem Formulation and CSTRS Scheme Design

5.2.1 Problem Formulation

In this section, we formulate the cooperative resource scheduling problem for infrastructure-assisted environment sensing in STVNs. The objective is to minimize the overall resource consumption while guaranteeing sensing freshness and reliability for all CVs. Specifically, according to the AoI model, sensing freshness depends on the sensing interval and the end-to-end delay, including computing, transmission, and propagation latency. A shorter interval enhances freshness but consumes more resources, while insufficient resources enlarge the delay and may violate the AoI requirement. Moreover, since multiple CVs may share overlapped RoIs, grouping CVs into SGs affects both sensing frequency and resource utilization. Hence, CV grouping, sensing interval determination, and resource allocation must be jointly optimized.

Let $\Omega^{\mathrm{S}} = \{\Omega^{\mathrm{S}}(t), \forall t \in \mathcal{T}\}$ denote the SSG partition, $\mathcal{I}^{\mathrm{S}} = \{I_{\mathbf{s}}^{\mathrm{T}}(t), \forall \mathbf{s} \in \Omega^{\mathrm{S}}(t), \forall t\}$ and $\mathcal{I}^{\mathrm{T}} = \{I_{\mathbf{g}}^{\mathrm{T}}(t), \forall \mathbf{g} \in \Omega^{\mathrm{T}}(t), \forall t\}$ represent sensing intervals of SSGs and TSGs, respectively, and $\mathcal{C}^{\mathrm{S}} = \{c_{\mathbf{s}}^{\mathrm{S}}(t), \forall \mathbf{s} \in \Omega^{\mathrm{S}}, \forall t\}$ and $\mathcal{B}^{\mathrm{S}} = \{b_{\mathbf{s}}^{\mathrm{S}}(t), \forall \mathbf{s} \in \Omega^{\mathrm{S}}, \forall t\}$ denote computing and communication resource allocation decisions from the satellite for all time slots, respectively. The resource cost of SSG $\mathbf{s}$ at time slot t is $\Upsilon_{\mathbf{s}}^{\mathrm{S}}(t) = \chi_1^{\mathrm{S}} c_{\mathbf{s}}^{\mathrm{S}}(t) + \chi_2^{\mathrm{S}} b_{\mathbf{s}}^{\mathrm{S}}(t)$, and the cost of terrestrial service group $\mathbf{g}$ is $\Upsilon_{\mathbf{g}}^{\mathrm{T}}(t) = \chi_1^{\mathrm{T}} c_{\mathbf{g}}^{\mathrm{T}}(t) + \chi_2^{\mathrm{T}} b_{\mathbf{g}}^{\mathrm{T}}(t)$, where χ_1^{S}, χ_2^{S}, χ_1^{T}, and χ_2^{T} are the unit cost of computing and communication resources from the satellite and RSUs, respectively. Due to heterogeneous resource unit costs and coverage capabilities, satellite and terrestrial resources should be jointly optimized in STVNs.

Accordingly, the cooperative resource scheduling problem is formulated as

$$\mathbf{P1} \min_{\substack{\Omega^{\mathrm{S}}, \mathcal{C}^{\mathrm{S}}, \\ \mathcal{B}^{\mathrm{S}}, \mathcal{I}^{\mathrm{S}}, \mathcal{I}^{\mathrm{T}}}} \sum_{t=1}^{\mathrm{T}} \left(\sum_{\mathbf{s} \in \Omega^{\mathrm{S}}} \Upsilon_{\mathbf{s}}^{\mathrm{S}}(t) + \sum_{\mathbf{g} \in \Omega^{\mathrm{T}}} \Upsilon_{\mathbf{g}}^{\mathrm{T}}(t) \right) \tag{5.10}$$

$$\text{s.t.} \quad \frac{\sum_{t'=1}^{t} \mathbb{1}_{q_u(t') \geq T^{\mathrm{th}}}}{t} < \varepsilon, \forall u \in \mathcal{U}, \forall t \in \mathcal{T} \tag{5.10a}$$

$$\mathbf{s}_i \cap \mathbf{s}_j = \emptyset, \forall \mathbf{s}_i, \mathbf{s}_j \in \Omega^{\mathrm{S}}(t), i \neq j, \tag{5.10b}$$

$$\cup_{\mathbf{s} \in \Omega^{\mathrm{S}}(t)} \mathbf{s} = \mathcal{U}, \tag{5.10c}$$

$$I_{\mathbf{s}}^{\mathrm{T}}(t), I_{\mathbf{g}}^{\mathrm{T}}(t) \in \{l\kappa | l \in \mathbb{N}\}, \tag{5.10d}$$

$$|\Omega^{\mathrm{S}}(t)| \leq M, \tag{5.10e}$$

$$(5.4), (5.5), (5.7), (5.8).$$

Constraint (5.10a) ensures that the AoI violation probability of each CV should be lower than the threshold ε over any accumulated period of t time slots. Constraints (5.10b) and (5.10c) constrain the partition of CVs into non-overlapping SSGs, and every CV should be included in one SSG. Note that $\mathbf{s}_0(t)$ indicates the set of CVs not served by the satellite at time slot t. Constraint (5.10d) constrains sensing interval granularity for each SG, with the minimum interval κ limited by sensing devices. Constraint (5.10e) restricts the number of concurrent SSGs to be less than M due to onboard computing capability [9].

5.2.2 Problem Decomposition and CSTRS Scheme Design

Problem **P1** is difficult to solve directly due to the coexistence of heterogeneous decision variables and dynamic environments of STVNs. Specifically, CV partitioning and sensing interval determination are large timescale structural decisions, while computing and communication resource allocation must be adapted in each time slot according to instantaneous dynamics, channel conditions, and queue states. Moreover, resource allocation decisions affect the AoI evolution over time, leading to a sequential decision-making problem. Consequently, **P1** is a mixed-integer stochastic optimization problem with coupled large timescale and real-time decisions.

Directly applying a model-free learning method to the original problem may exacerbate model convergence difficulties due to highly dynamic network environments and an extremely large action space. Observing the system operation and characteristics of the actions, group formation and sensing interval are adjusted infrequently and periodically according to mobility patterns, whereas resource allocation must react rapidly to instantaneous network conditions. This motivates a hierarchical decomposition.

Accordingly, we propose a cooperative satellite–terrestrial resource scheduling (CSTRS) scheme that separates decisions into two timescales. Specifically, a large timescale is used to determine CV partitioning and sensing intervals for SG, while a small timescale is used to perform real-time computing and communication resource allocation. In this case, we decouple the original problem into two subproblems: (1) CV partitioning and sensing interval decisions determined by the ground controller, and (2) real-time computing and communication resource allocation for SGs in the satellite and RSUs. Figure 5.3 shows the working diagram of the CSTRS scheme for environment sensing in STVNs in two steps.

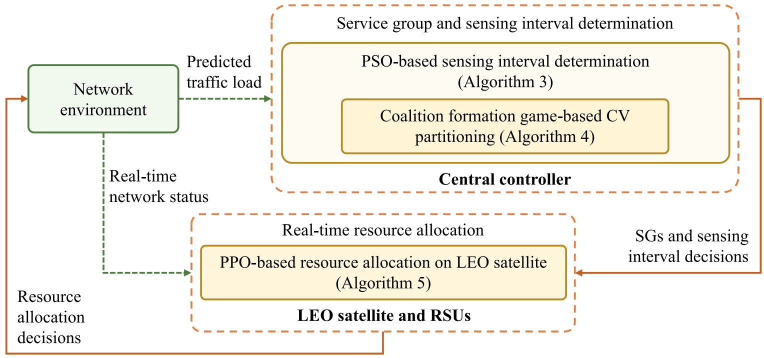

Fig. 5.3 Working diagram of the proposed CSTRS scheme for environment sensing

In the first problem, we aim to find the optimal CV partitioning and sensing intervals for each SG to minimize resource consumption in each time interval consisting of k time slots. Specifically, the average resource cost of each SG within each interval can be estimated through predicted processing and transmission workload according to the predicted CV trajectories.[1] The large timescale optimization problem is formulated as

$$\mathbf{P2} \min_{\Omega^{\mathrm{S}},\mathbf{I}^{\mathrm{S}},\mathbf{I}^{\mathrm{T}}} \sum_{\mathbf{s}\in\Omega^{\mathrm{S}}} C_{\mathbf{s}}^{\mathrm{S}} + \sum_{\mathbf{g}\in\Omega^{\mathrm{T}}} C_{\mathbf{g}}^{\mathrm{T}} \tag{5.11}$$

$$\text{s.t.} \quad (5.10\text{b}), (5.10\text{c}), (5.10\text{d}), (5.10\text{e}).$$

The average resource cost of SSG $\mathbf{s}$ is calculated by

$$C_{\mathbf{s}}^{\mathrm{S}} = \chi_1^{\mathrm{S}} \frac{k\tau\bar{v}_{\mathbf{s}}^{\mathrm{S}}\gamma}{I_{\mathbf{s}}^{\mathrm{S}} f^{\mathrm{S}}} + \chi_2^{\mathrm{S}} \frac{k\tau\bar{\beta}_{\mathbf{s}}^{\mathrm{S}}}{I_{\mathbf{s}}^{\mathrm{S}}\bar{R}_{\mathbf{s}}^{\mathrm{S}}}, \tag{5.12}$$

where $\bar{R}_{\mathbf{s}}^{\mathrm{S}}$ is the average transmission rate of unit bandwidth within the interval. We omit the notation t for the interval-based calculation. Let $\bar{v}_{\mathbf{s}}^{\mathrm{S}}$ and $\bar{\beta}_{\mathbf{s}}^{\mathrm{S}}$ denote the predicted processing and transmission workloads for each sensing of SSG $\mathbf{s}$ in the time interval, respectively. Similarly, the average resource cost for TSG $\mathbf{g}$ in a time interval is given by

$$C_{\mathbf{g}}^{\mathrm{T}} = \chi_1^{\mathrm{T}} \frac{k\tau\bar{v}_{\mathbf{g}}^{\mathrm{T}}\gamma}{I_{\mathbf{g}}^{\mathrm{T}} f^{\mathrm{T}}} + \chi_2^{\mathrm{T}} \frac{k\tau\bar{\beta}_{\mathbf{g}}^{\mathrm{T}}}{I_{\mathbf{g}}^{\mathrm{T}}\bar{R}_{\mathbf{g}}^{\mathrm{T}}}. \tag{5.13}$$

This step determines the sensing structure in STVNs and reduces the dimensionality of real-time scheduling.

[1] Here, the prediction method is not the primary focus and several algorithms have been studied, such as recurrent neural networks (RNN) [10] and long-short term memory (LSTM) [11].

Given CV partitioning and sensing intervals, we aim to find the optimal resource allocation under time-varying STVN conditions to minimize the overall resource cost based on the instantaneous network state, given as

$$\begin{aligned}
\mathbf{P3}\ \min_{\mathcal{C}^{\mathrm{S}},\mathcal{B}^{\mathrm{S}}} \quad & \sum_{t=1}^{\mathrm{T}} \left(\sum_{\mathbf{s}\in\Omega^{\mathrm{S}}(t)} \Upsilon_{\mathbf{s}}^{\mathrm{S}}(t) + \sum_{\mathbf{g}\in\Omega^{\mathrm{T}}(t)} \Upsilon_{\mathbf{g}}^{\mathrm{T}}(t) \right) \qquad (5.14)\\
\text{s.t.} \quad & (5.4), (5.5), (5.7), (5.8), (5.10a).
\end{aligned}$$

To solve these two subproblems, the proposed CSTRS scheme comprises two components: a CV partitioning and sensing interval determination algorithm presented in Sect. 5.3, and a real-time resource allocation algorithm, detailed in Sect. 5.4.

5.3 CV Partitioning and Sensing Interval Determination

To solve subproblem **P2**, we determine the SSGs and the sensing interval of each group. Specifically, we first derive the feasible sensing interval range for each CV according to the AoI requirement. Then, to achieve the minimum estimated average resource cost in each time interval, a particle swarm optimization (PSO)-based method is adopted to obtain the optimal sensing intervals. Based on the resulting sensing interval decisions, the SSGs are further determined by formulating a coalition formation game in each time interval.

5.3.1 PSO-Based Sensing Interval Determination

To determine the sensing interval of each service group (SG), we first derive the feasible sensing interval range for each individual CV according to the AoI freshness requirement, and then optimize the group-level sensing interval based on these feasible ranges. For each CV u, let T_u^{S} and T_u^{T} denote the sensing intervals from the LEO satellite and the associated RSU, respectively. Due to the hardware limitation of sensing devices, both intervals satisfy $T_u^{\mathrm{S}}, T_u^{\mathrm{T}} \in \{l\kappa \mid l \in \mathbb{N}\}$. As the decisions are updated in each time interval consisting of k time slots, the time index t is omitted for brevity.

Let $G = \gcd(T_u^{\mathrm{S}}, T_u^{\mathrm{T}})$ denote the greatest common divisor of the two sensing intervals.

Proposition 5.1 *If* $T_u^{\mathrm{S}} \neq T_u^{\mathrm{T}}$, *then* $|T_u^{\mathrm{S}} - T_u^{\mathrm{T}}| \geq G$.

Proof Since $T_u^{\mathrm{S}} = aG$ and $T_u^{\mathrm{T}} = bG$ for integers a, b, we have $|T_u^{\mathrm{S}} - T_u^{\mathrm{T}}| = |a - b|G \geq G$ because $a \neq b$. ∎

Let ψ_u^{S} denote the offset of the first satellite sensing relative to the beginning of the time interval, and $\hat{\psi}_u^{\mathrm{S}}$ is the set of feasible offsets for CV u, where the initial RSU sensing occurs at the beginning of the interval.

Proposition 5.2 (Feasible sensing interval pair for individual CVs) *A sensing interval pair $(T_u^{\mathrm{S}}, T_u^{\mathrm{T}})$ with offset ψ_u^{S} is feasible if the AoI threshold T^{th} can be guaranteed for CV u according to the following conditions:*

- *If CV u cannot always connect to RSUs during the time interval, i.e., $\exists t : a_u^{\mathrm{T}}(t) = 0$, then $T_u^{\mathrm{S}} < T^{\mathrm{th}}$ with $\psi_u^{\mathrm{S}} \in [0, T_u^{\mathrm{S}})$.*
- *If CV u can always connect to both satellite and RSUs, then one of the following conditions should be met:*
  - $T_u^{\mathrm{S}} < T^{\mathrm{th}}$ *with* $\psi_u^{\mathrm{S}} \in \hat{\psi}_u^{\mathrm{S}} = [0, T_u^{\mathrm{S}})$;
  - $T_u^{\mathrm{T}} < T^{\mathrm{th}}$ *with* $\psi_u^{\mathrm{S}} \in \hat{\psi}_u^{\mathrm{S}} = [0, T_u^{\mathrm{T}})$;
  - $T_u^{\mathrm{S}} = T_u^{\mathrm{T}} \in [T^{\mathrm{th}}, 2T^{\mathrm{th}})$ *with* $\psi_u^{\mathrm{S}} \in \hat{\psi}_u^{\mathrm{S}} = \{l\kappa \mid T_u^{\mathrm{T}} - T^{\mathrm{th}} < l\kappa < T^{\mathrm{th}}, l \in \mathbb{N}\}$.

Proof To satisfy the AoI requirement, the interval between two consecutive successfully received sensing results from either satellite or RSUs must be strictly smaller than T^{th}. There are three conditions.

(1) If RSU connectivity is unavailable during part of the interval, i.e., $a_u^{\mathrm{T}}(t) = 0$ for some t, freshness must be guaranteed solely by satellite updates. Therefore, $T_u^{\mathrm{S}} < T^{\mathrm{th}}$ is required, and any offset within one period is feasible with $\psi_u^{\mathrm{S}} \in [0, T_u^{\mathrm{S}})$.

(2) If both satellite and RSU connections are always available, freshness can be satisfied by a single source when either $T_u^{\mathrm{S}} < T^{\mathrm{th}}$ with $\psi_u^{\mathrm{S}} \in \hat{\psi}_u^{\mathrm{S}} = [0, T_u^{\mathrm{S}})$ or $T_u^{\mathrm{T}} < T^{\mathrm{th}}$ with $\psi_u^{\mathrm{S}} \in \hat{\psi}_u^{\mathrm{S}} = [0, T_u^{\mathrm{T}})$.

(3) Otherwise, when both sensing intervals $T_u^{\mathrm{S}}, T_u^{\mathrm{T}} \in [T^{\mathrm{th}}, 2T^{\mathrm{th}})$, both the satellite and RSUs should be involved for environment sensing, satisfying

$$\frac{1}{T_u^{\mathrm{S}}} + \frac{1}{T_u^{\mathrm{T}}} > \frac{1}{T^{\mathrm{th}}}. \tag{5.15}$$

In addition, the freshness requirement also depends on whether the sensing instants from the satellite and RSU can maintain a stable alternating pattern. Let RSU updates occur at $\{jT_u^{\mathrm{T}}\}$ and satellite updates at $\{kT_u^{\mathrm{S}} + \psi_u^{\mathrm{S}}\}$. By Bézout's identity, the relative phase $jT_u^{\mathrm{T}} - kT_u^{\mathrm{S}}$ can only change in integer multiples of G. As time evolves, the relative phase varies with granularity G. In this case, the freshness violation occurs if the relative phase difference falls into a region $\mathcal{L}$ that produces an update gap no smaller than T^{th}, given by

$$\mathcal{L} = [0, T_u^{\mathrm{T}} - T^{\mathrm{th}}] \cup [T^{\mathrm{th}}, T_u^{\mathrm{T}}] \cup [T_u^{\mathrm{T}} - T_u^{\mathrm{S}}, 0].$$

From Proposition 5.1, if $T_u^{\mathrm{S}} \neq T_u^{\mathrm{T}}$, the region $\mathcal{L}$ has width at least G. Since the relative offset moves in steps of G, it must fall inside $\mathcal{L}$ for any offset ψ_u^{S}, making freshness violation unavoidable.

On the other hand, when $T_u^{\mathrm{S}} = T_u^{\mathrm{T}}$, a feasible offset exists. In this case, the region width of $\mathcal{L}$ becomes $2(T_u^{\mathrm{T}} - T^{\mathrm{th}})$, which is smaller than $G = T_u^{\mathrm{S}} = T_u^{\mathrm{T}}$, leaving a feasible feasible offset $\psi_u^{\mathrm{S}} \in (T_u^{\mathrm{S}} - T^{\mathrm{th}}, T^{\mathrm{th}})$. ■

With the feasible ranges for individual CV sensing interval pairs and satellite sensing time offset given in **Proposition** 5.2, the sensing intervals of SGs can be optimized to minimize the estimated average resource cost in problem **P2**. Since determining optimal intervals for all CVs is a combinatorial optimization problem and finding a globally optimal solution is challenging [12].

To address this issue, we employ PSO, an evolutionary heuristic mechanism, to solve problem **P2**. A set of particles forms a particle swarm, where each particle represents a candidate sensing interval solution for all CVs, denoted by $\Lambda = [T_u^{\mathrm{S}}, T_u^{\mathrm{T}}]^{1\times|\mathcal{U}|}$.

Let $\mathcal{X}$ denote the set of particles. In each iteration, particles adjust their positions and speeds within the solution space to discover the corresponding values from the current positions [12]. For particle x in iteration y, its speed and position are updated by

$$p_x^{(y)} = \sigma p_x^{(y-1)} + \sigma_1 \left(\hat{\Lambda}_x - \Lambda_x^{(y-1)}\right) + \sigma_2 \left(\Lambda^* - \Lambda_x^{(y-1)}\right), \tag{5.16}$$

$$\Lambda_x^{(y)} = \Lambda_x^{(y-1)} + p_x^{(y-1)}. \tag{5.17}$$

Here $\hat{\Lambda}_x$ is the best historical position of particle x, and Λ^* is the global best position, while $\hat{\Xi}_x$ and Ξ^* are the corresponding values calculated based on Eq. (5.11) at those positions. In addition, σ is the inertia weight for each particle to keep its speed from the previous iteration, σ_1 and σ_2 are the cognitive coefficient and the social coefficient to control how much weight should be given to refining the search result of the particle itself and recognizing the search result of the swarm consisting of the randomness for exploration [13]. Since CVs within the same TSG share the same terrestrial sensing interval, the following constraint should be satisfied, given by

$$T_{u_1}^{\mathrm{T}} = T_{u_2}^{\mathrm{T}} = I_{\mathbf{g}}^{\mathrm{T}}, \forall u_1, u_2 \in \mathbf{g}. \tag{5.18}$$

For the PSO-based algorithm, each particle should explore the solution within the solution space $\Lambda \in \mathbb{F}$. If a particle violates Proposition 5.2 or 5.18, it is replaced by a new randomly selected position within $\mathbb{F}$, for the exploration in the solution space. Moreover, all sensing interval pairs should fulfill **Proposition** 5.2. After multiple iterations, the positions of all particles can converge to the same position, indicating the selected sensing interval pair for all CVs [13].

The details of the proposed PSO-based algorithm are given in **Algorithm** 3. Denote the maximum number of iterations by $y^{\max}$. The particles are initialized with the positions in the solution space $\mathbb{F}$ in Line 2. The position of each particle is updated in each iteration according to Lines 5 to 14. Specifically, with a given position, i.e., the sensing interval pair of each CV, SSGs Ω^{S} and the corresponding sensing interval $\mathbf{I}^{\mathrm{S}}$ can be obtained through the coalition game-based partitioning algorithm, which

Algorithm 3 PSO-based algorithm sensing interval determination

Input: $\Omega^T, \sigma, \sigma_1, \sigma_2, y^{\max}$;
Initialization: $y = 0$, $p_x^{(0)} = 0$, $\Lambda_x^{(0)} \in \mathbb{F}, \forall x \in \mathcal{X}$;
while $y \leq y^{\max}$ **do**
  for $x \in \mathcal{X}$ **do**
    if Proposition 5.2 and Eq. (5.18) are not satisfied **then**
      Replace the particle by a new $\Lambda_x^{(y)} \in \mathbb{F}$;
    Obtain sensing intervals $\mathbf{I}_x^{T,(y)}$ of TSGs according to Eq. (5.18);
    Determine $\Omega_x^{S,(y)}$ and $\mathbf{I}_x^{S,(y)}$ based on Algorithm 4 and calculate $\Xi_x^{(y)}$;
    if $\Xi_x^{(y)} < \hat{\Xi}_x$ **then**
      Update $\hat{\Lambda}_x \leftarrow \Lambda_x^{(y)}$, $\hat{\Xi}_x \leftarrow \Xi_x^{(y)}$;
    if $\Xi_x^{(y)} < \Xi^*$ **then**
      Update $\Lambda^* \leftarrow \Lambda_x^{(y)}$, $\Xi^* \leftarrow \Xi_x^{(y)}$;
    Update $p_x^{(y+1)}$ based on (5.16);
    Select $\Lambda_x^{(y+1)}$ based on (5.17);
Output: Ω^{S}, $\mathbf{I}^{\mathrm{S}}$, and $\mathbf{I}^T$

will be presented in Sect. 5.3.2. Finally, the outputs of the PSO-based algorithm are the solution of problem **P2** for each time interval.

5.3.2 Coalition Game-Based CV Partitioning Algorithm

Given the sensing interval candidates of individual CVs obtained from the PSO procedure, the SSGs still need to be determined, while the TSGs are pre-defined with the sensing interval according to Eq. (5.18). Since satellite sensing is performed in a multicast manner, all CVs within the same SSG must share a common sensing schedule, where the optimal SSGs and the corresponding sensing interval remain to be determined to solve problem **P2** with minimum resource costs. For each SSG $\mathbf{s}$, the group sensing interval and offset are determined based on the feasible sensing interval and offset of all CVs in the group as follows.

Proposition 5.3 (SSG sensing interval and offset) *Given the feasible sensing intervals and offset sets of CVs within SSG* $\mathbf{s}$*:*

- *If all CVs in* $\mathbf{s}$ *have the same satellite sensing interval and share a non-empty common feasible offset set, i.e.,*

$$T_{u_1}^{\mathrm{S}} = T_{u_2}^{\mathrm{S}}, \ \forall u_1, u_2 \in \mathbf{s}, \quad \bigcap_{u \in \mathbf{s}} \hat{\psi}_u^{\mathrm{S}} \neq \emptyset, \tag{5.19}$$

  then the SSG sensing interval and offset are

$$I_{\mathbf{s}}^{\mathrm{S}} = T_u^{\mathrm{S}}, \quad \Psi_{\mathbf{s}}^{\mathrm{S}} = \arg\max_{\varphi \in \hat{\Psi}_{\mathbf{s}}^{\mathrm{S}}} |T^{\mathrm{th}} - \varphi|, \tag{5.20}$$

where $\hat{\Psi}^{\mathrm{S}}_{\mathbf{s}} = \bigcap_{u \in \mathbf{s}} \hat{\psi}^{\mathrm{S}}_u$ *is the common feasible SSG sensing offset set;*

- *Otherwise, the SSG adopts the largest safe sensing interval*

$$I^{\mathrm{S}}_{\mathbf{s}} = \max\{l\kappa \mid l\kappa < T^{\mathrm{th}}, l \in \mathbb{N}^+\}, \quad \Psi^{\mathrm{S}}_{\mathbf{s}} = 0. \tag{5.21}$$

The first case enables efficient multicast sensing since all CVs can share a synchronized sensing schedule. The second case guarantees freshness even when sensing interval synchronization among CVs in the SSG is impossible.

Note that determining the optimal CV partition through a centralized exhaustive search approach encounters high complexity. Hence, we model the CV grouping problem as a coalition formation game to find the optimal SSGs [14].

Definition 5.1 (*Coalition partition*) A coalition partition $\Gamma^{\mathrm{S}} = \{\mathbf{s}_0, \mathbf{s}_1, \ldots, \mathbf{s}_m\}, 0 \le m \le M$, divides the CV set $\mathcal{U}$ into disjoint SSGs satisfying

$$\mathbf{s}_i \cap \mathbf{s}_j = \emptyset, \forall \mathbf{s}_i, \mathbf{s}_j \in \Gamma^{\mathrm{S}}, i \neq j, \text{ and } \bigcup_{i \le m} \mathbf{s}_i = \mathcal{U}.$$

Each coalition corresponds to a multicast sensing group. The utility of coalition $\mathbf{s}$ is defined as the negative estimated satellite resource cost in the time interval

$$\phi(\mathbf{s}) = -C^{\mathrm{S}}_{\mathbf{s}}. \tag{5.22}$$

The objective is to maximize the total utility

$$\phi(\Gamma^{\mathrm{S}}) = \sum_{\mathbf{s} \in \Gamma^{\mathrm{S}}} \phi(\mathbf{s}), \tag{5.23}$$

which is equivalent to minimizing satellite resource consumption. To enable coalition adjustment, each CV evaluates candidate coalitions based on a preference relation.

Definition 5.2 (*Preference relation*) For CV u, a preference relation is defined by $\succ_u$, where $\mathbf{s}_i \succ_u \mathbf{s}_j$ implies that CV u prefers joining coalition $\mathbf{s}_i$ rather than $\mathbf{s}_j$.

The preference is determined by the marginal utility improvement, given as

$$\mathbf{s}_i \succ_u \mathbf{s}_j \Leftrightarrow \phi(\mathbf{s}_i \cup \{u\}) + \phi(\mathbf{s}_j \setminus \{u\}) > \phi(\mathbf{s}_i \setminus \{u\}) + \phi(\mathbf{s}_j \cup \{u\}). \tag{5.24}$$

When CV u finds a more preferable coalition, the switch operation can be accepted only if it increases the overall utility.

Definition 5.3 (*Switch operation*) If CV u currently in $\mathbf{s}_1$ prefers coalition $\mathbf{s}_2$, the partition is updated as

$$\Gamma^{\mathrm{S}} = (\Gamma^{\mathrm{S}} \setminus \{\mathbf{s}_1, \mathbf{s}_2\}) \cup \{\mathbf{s}_1 \setminus \{u\}\} \cup \{\mathbf{s}_2 \cup \{u\}\}.$$

Algorithm 4 Coalition formation game-based algorithm for CV partitioning

1: **Input:** $\mathcal{U}$, Λ;
2: **Initialization:** The initial partition of CVs is $\Gamma^{\mathrm{S}}_{\mathrm{ini}}$, where CVs are partitioned into M coalitions;
3: **repeat**
4:   Randomly select CV u and choose another coalition $\mathbf{s} \in \Gamma^{\mathrm{S}}$;
5:   **if** CV prefers to join a new coalition **s and** $\mathbf{s} \cup \{u\} \notin \mathcal{H}(u)$ **then**
6:     Add $\mathbf{s} \cup \{u\}$ to the history set $\mathcal{H}(u)$;
7:     CV u detaches the current coalition and combines with the new coalition according to Definition 5.3;
8:     Update partition Γ^{S};
9: **until** Switch operation terminates with a stable partition
10: **Output:** Final SSGs $\Omega^{\mathrm{S}} = \Gamma^{\mathrm{S}}$, the sensing interval of all coalitions $\{I^{\mathrm{S}}_1, ..., I^{\mathrm{S}}_m\}$, and the offset $\{\Psi^{\mathrm{S}}_1, ..., \Psi^{\mathrm{S}}_m\}$ according to Proposition 5.3.

Definition 5.4 (*Nash stability*) A partition is Nash-stable if no CV can improve its preference by moving to another coalition [15].

Based on the above rules, we design a coalition formation game-based algorithm for CV partitioning. The main procedure is given in **Algorithm** 4. Initially, CVs are randomly divided into M coalitions. Then, as shown in lines 4 to 9, CVs iteratively perform switch operations based on **Definition** 5.3 for a higher utility until a stable partition is obtained as per **Definition** 5.4. Here, a set $\mathcal{H}(u)$ records the history of coalitions where CV u has previously joined to prevent repeated oscillations. Once the partition becomes stable, the final SSGs are determined by $\Omega^{\mathrm{S}} = \Gamma^{\mathrm{S}}$, and their sensing intervals and offsets are determined using Proposition 5.3.

5.3.3 Computational Complexity Analysis

In Algorithm 3, each particle represents a candidate sensing interval configuration, which encodes the satellite and RSU sensing intervals for every CV. Since CVs belonging to the same TSG share the same RSU sensing interval according to Eq. (5.18), the dimension of a particle is proportional to the number of CVs and RSUs. Thus, the particle dimension is $O(NU)$. During each PSO iteration, all particles update their speeds and positions once. Therefore, the computational complexity per iteration is $O(|\mathcal{X}|NU)$, where $|\mathcal{X}|$ is the number of particles. After obtaining sensing interval candidates, Algorithm 4 partitions CVs into SSGs using a coalition formation game. In each iteration, the maximum number of CV selections is UM. By considering the worst case, each CV is evaluated against $M - 1$ coalitions in each iteration. Hence, the complexity per iteration of the coalition formation process is $O(UM^2)$. Let L_1 and L_2 denote the number of iterations required for the PSO algorithm and coalition game to converge, respectively. Considering that the coalition formation is executed inside each PSO iteration, the overall computational complexity is $O(L_1|\mathcal{X}|(NU + L_2UM^2))$. Because both L_1 and L_2 are finite and typically small in practice, and the algorithms operate at a large timescale for CV partitioning, the proposed approach is computationally feasible for real-time STVN management.

5.4 PPO-Based Real-Time Resource Allocation

With the determined SSGs and sensing intervals, the satellite needs to allocate computing and communication resources for each SSG in real time for processing sensing data and transmitting sensing results to CVs in each service group. In this section, we reformulate problem **P3** as a Markov decision process (MDP) and develop a reinforcement learning-based algorithm to obtain adaptive real-time resource allocation decisions.

5.4.1 Markov Decision Process Formulation

Since the freshness and reliability constraint (5.10a) in **P3** is defined over a long-term time horizon, the resource allocation decision at each time slot cannot be optimized independently. Directly solving such a sequential constrained optimization problem is difficult due to the coupling between instantaneous decisions and long-term reliability performance. To handle this long-term impact, we adopt the Lyapunov optimization framework and introduce a virtual reliability queue for each CV [16], given by

$$H_u(t+1) = \max\{H_u(t) + \mathbb{1}_{q_u(t)>T^{\text{th}}} - \varepsilon, 0\}, \tag{5.25}$$

where $\mathbb{1}_{condition} = 1$ if $condition$ is true and $\mathbb{1}_{condition} = 0$ otherwise, and $H_u(1) = 0$. Specifically, the virtual queue $H_u(t+1)$ enlarges at time slot $t+1$ when the AoI requirement is violated at time slot t and decreases if a new sensing result is received within the freshness requirement. Therefore, stabilizing the virtual queue is equivalent to guaranteeing that the long-term violation probability satisfies the reliability constraint. To characterize the group-level reliability, we define the maximum virtual queue value in each SSG $\mathbf{s}$ as $H_{\mathbf{s}}^{\max}(t) = \max_{u\in\mathbf{s}} H_u(t)$. By incorporating the virtual queue into the objective function, problem **P3** can be transformed into

$$\begin{aligned}
\mathbf{P4}\ \min_{C^{\mathrm{S}},\mathcal{B}^{\mathrm{S}}} & \sum_{t=1}^{\mathrm{T}} \left(\sum_{\mathbf{s}\in\Omega^{\mathrm{S}}(t)} \left(\Upsilon_{\mathbf{s}}^{\mathrm{S}}(t) + \eta H_{\mathbf{s}}^{\max}(t)\right) + \sum_{\mathbf{g}\in\Omega^{\mathrm{T}}(t)} \Upsilon_{\mathbf{g}}^{\mathrm{T}}(t) \right) \\
\text{s.t.} \quad & (5.4), (5.5), (5.7), (5.8),
\end{aligned} \tag{5.26}$$

where the weight η balances resource cost and reliability performance.

The formulated computing and communication resource allocation problem **P4** is still difficult to solve using deterministic optimization because the channel condition and CV mobility are stochastic and time-varying. In this case, we reformulate problem **P4** by leveraging MDP to model the randomness of channels and CV mobility.

Let $\zeta_{\mathbf{s}}(t) = [\mathbf{p}_{\mathbf{s}}^{\mathrm{SSG}}(t), q_{\mathbf{s}}^{\max}(t), H_{\mathbf{s}}^{\max}(t), Q_{\mathbf{s}}^{\mathrm{S}}(t), W_{\mathbf{s}}^{\mathrm{S}}(t), c_{\mathbf{s}}^{\mathrm{S}}(t-1), b_{\mathbf{s}}^{\mathrm{S}}(t-1)]$ denote the state of SSG $\mathbf{s}$ at time slot t, where $q_{\mathbf{s}}^{\max}(t) = \max_{u\in\mathbf{s}}\{q_u(t)\}$. Since the number of SSGs varies over time, we adopt the maximum group number M to construct a fixed-dimension state. The overall system state is $\mathcal{S}(t) = [\zeta_{\mathbf{s}_1}(t), \ldots, \zeta_{\mathbf{s}_M}(t)] \in \mathfrak{S}$, where inactive groups are padded with zero vectors and $\mathfrak{S}$ is the state space with all possible states.

The action space consists of computing and communication resource allocation, given by $\mathcal{A}(t) = \{(c_{\mathbf{s}_1}^{\mathrm{S}}(t), b_{\mathbf{s}_1}^{\mathrm{S}}(t)), \ldots, (c_{\mathbf{s}_M}^{\mathrm{S}}(t), b_{\mathbf{s}_M}^{\mathrm{S}}(t))\} \in \mathfrak{A}$, where $\mathcal{A}(t) \in ([0,1] \times [0,1])^{1\times M}$. Here, $\mathfrak{A} = \mathfrak{A}^c \otimes \mathfrak{A}^b$ is the action space combining the computing and communication resource allocation actions, where $\otimes$ is the Cartesian product.

The reward function, obtained from taking action $\mathcal{A}(t)$ in state $\mathcal{S}(t)$, is defined as the negative system cost of a time slot, given by

$$\mathcal{R}(\mathcal{S}(t), \mathcal{A}(t)) = -\sum_{\mathbf{s}\in\Omega^{\mathrm{S}}(t)} \left(\Upsilon_{\mathbf{s}}^{\mathrm{S}}(t) + \eta H_{\mathbf{s}}^{\max}(t)\right) - \sum_{\mathbf{g}\in\Omega^{\mathrm{T}}(t)} \Upsilon_{\mathbf{g}}^{\mathrm{T}}(t). \tag{5.27}$$

Let $\mathbf{\Pi}$ denote the policy set mapping states in $\mathfrak{S}$ to actions in $\mathfrak{A}$. To estimate the expected return of the current decision-making, a discounted cumulative reward function is considered. The long-term objective is given by

$$\max_{\pi\in\mathbf{\Pi}} \mathbb{E}\left[\sum_{t=1}^{\mathrm{T}} \iota^t \mathcal{R}(\mathcal{S}(t), \mathcal{A}(t)) \middle| \pi\right] \tag{5.28}$$

where $\iota \in (0, 1)$ is the discount factor reflecting the importance of future rewards compared with immediate rewards.

5.4.2 PPO-Based Algorithm for Resource Allocation

Considering that the state transition probabilities are unknown due to stochastic channel conditions and vehicle mobility, combined with the continuous action space, the value-iteration or dynamic programming methods are not applicable for solving the formulated MDP problem. Policy gradient–based reinforcement learning provides a suitable solution as it directly learns a mapping from states to actions and updates the policy to maximize the total reward without requiring transition probabilities. Considering the learning stability and efficiency, we adopt a PPO-based algorithm [17], which can reuse the historical samples and handle a large-scale problem to find the optimal policy.

Algorithm 5 PPO-based resource allocation algorithm

Initialization: Parameters θ and ϑ for policy and state-value function, and buffer $\mathcal{B}$;
for $j \in \{1, 2, ...\}$ **do**
  Obtain initial state $\mathcal{S}(1)$;
  for $t \in \{1, 2, ..., T\}$ **do**
    Execute action $\mathcal{A}(t)$ based on the policy π_θ;
    Compute reward $\mathcal{R}(\mathcal{S}(t), \mathcal{A}(t))$ and observe new state $\mathcal{S}(t+1)$;
    Record transition $(\mathcal{S}(t), \mathcal{A}(t), \mathcal{R}(t), \mathcal{S}(t+1))$ into buffer $\mathcal{B}$;
    if $t \mod k = 0$ **then**
      Run **Algorithm 3** to adjust sensing interval and CV partition;
  for $e \in \{1, 2, ..., E\}$ **do**
    Sample a minibatch of transitions $\mathcal{B}_N$ from buffer $\mathcal{B}$;
    Update policy parameter $\theta \leftarrow \arg\max_\theta \frac{1}{|\mathcal{B}_N|} \sum_{t_N \in \mathcal{B}_N} L^{\text{clip}}(\theta)$;
    Update state-value function parameter
    $\vartheta \leftarrow \arg\min_\vartheta \frac{1}{|\mathcal{B}_N|} \sum_{t_N \in \mathcal{B}_N} (\mathcal{R}(t_N) + V_\vartheta(\mathcal{S}(t_N+1)) - V_\vartheta(\mathcal{S}(t_N)))^2$
  Empty buffer $\mathcal{B}$ for a new training episode;
Output: Parameter θ;

Specifically, PPO constrains the policy update within a constrained region using a clipped surrogate objective, preventing sudden policy changes between consecutive updates. The goal is to find the optimal parameter θ for policy π_θ that maximizes the clipped surrogate objective

$$L^{\text{clip}}(\theta) = \mathbb{E}\{\min(\xi_\theta A^{\pi_{\theta_{\text{old}}}}, \text{clip}(\xi_\theta, 1-\delta, 1+\delta) A^{\pi_{\theta_{\text{old}}}})\}. \tag{5.29}$$

Here,

$$\xi_\theta = \frac{\pi_\theta(\mathcal{A}|\mathcal{S})}{\pi_{\theta_{\text{old}}}(\mathcal{A}|\mathcal{S})} \tag{5.30}$$

is the probability ratio between the new policy and the old policy. The clipping operator restricts ξ_θ to the interval $[1-\delta, 1+\delta]$, which prevents excessively large policy updates and improves training stability. The advantage function quantifies the advantage of the selected action over the expected return of the current state, defined as

$$A^{\pi_{\theta_{\text{old}}}}(\mathcal{S}(t), \mathcal{A}(t)) = \mathcal{R}(\mathcal{S}(t), \mathcal{A}(t)) + \iota V_\vartheta(\mathcal{S}(t+1)) - V_\vartheta(\mathcal{S}(t)), \tag{5.31}$$

where $V_\vartheta(\mathcal{S}(t))$ is the state-value function parameterized by ϑ, given by

$$V_\vartheta(\mathcal{S}(t)) = \mathbb{E}\left\{\sum_{i=0}^{\infty} \iota^i \mathcal{R}(\mathcal{S}(t+i+1), \mathcal{A}(t+i+1)) \mid \mathcal{S}(t)\right\}. \tag{5.32}$$

A positive advantage encourages increasing the probability of selecting this action, while a negative advantage suppresses it.

Table 5.1 Simulation parameters

LEO satellite transmission power	40 dBm	LEO satellite path-loss exponent	2.5
LEO satellite antenna gains	32 dBi	LEO satellite bandwidth	250 MHz
CPU frequency in LEO satellite	1 Gcycles/s	CPU frequency in RSU	1 Gcycles/s
RSU transmission power	32 dBm	RSU path-loss exponent	3
RSU antenna gains	10 dBi	RSU bandwidth	100 MHz
Noise power σ^2	−174 dBm/Hz	CV antenna gains	10 dBi
Unit costs $\chi_1^{\mathrm{S}}, \chi_2^{\mathrm{S}}, \chi_1^{\mathrm{T}}, \chi_2^{\mathrm{T}}$	0.5, 2.5, 0.1, 0.5	Data processing workload	25 cycles/bit

Algorithm 5 describes the overall learning procedure, where E is the number of training times in each episode to update the network parameters through different minibatches and the buffer $\mathcal{B}$ is used to store transitions resulting from interactions with the environment. During each time slot, the controller observes the network state, allocates resources based on the current policy, and stores the transition samples, as shown in Lines 5 to 7. After one episode, the collected samples are reused multiple times to update the policy and value networks based on Lines 11 to 13, which significantly improves sample efficiency. Meanwhile, the large-timescale sensing interval and CV partition decisions are periodically updated every k slots.

5.5 Performance Evaluation

In this section, simulations are conducted to evaluate the effectiveness of the proposed CSTRS scheme. The simulated area corresponds to the beam coverage of a steerable LEO satellite with an orbital altitude of 550 km and a velocity of 7.56 km/s. CVs and RSUs are randomly distributed in the area, with the radius of the coverage area of each RSU being 500 m. The target area consists of both urban and rural areas, where different areas have different densities of RSUs and CVs. Urban areas have densities of 10 RSUs/km^2 and 40 CVs/km^2, while rural areas have densities of 2 RSUs/km^2 and 20 CVs/km^2. CVs move with stochastic speed and direction. The freshness threshold of sensing data is 100 ms and the reliability requirement is 0.99. Each time slot lasts $\tau = 5$ ms, and the SSG adjustment interval is 10 s. The minimum sensing interval from infrastructures is $\kappa = 20$ ms. More communication and computing parameters of the satellite and RSUs are summarized in Table 5.1 [18, 19].

For the PPO-based reinforcement learning algorithm, the deep neural network consists of three fully connected hidden layers with (128, 128, 64) neurons and ReLU activation to realize a nonlinear approximation. Each training episode contains 8000

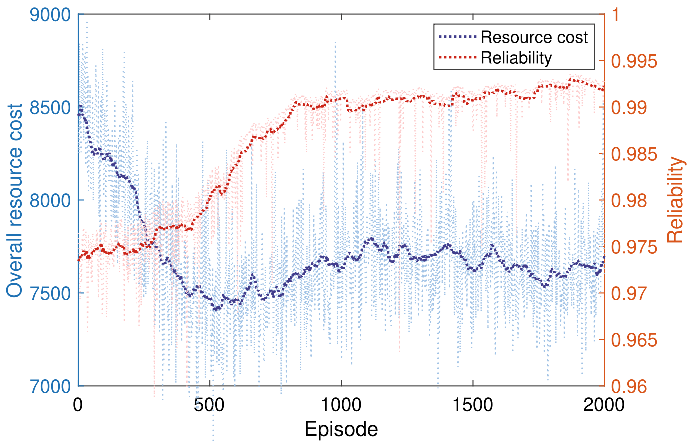

Fig. 5.4 Convergence performance of training process

time slots with CVs and RSUs randomly reset at the beginning of each episode. The training lasts 2000 episodes with a learning rate of 3×10^{-4} and a clipping ratio of 0.3. The convergence behavior is shown in Fig. 5.4 in terms of resource cost and reliability in each episode, where the performances converge after around 1100 episodes.

Then, we evaluate the real-time resource allocation strategy with the following three benchmark algorithms for resource allocation [20], namely (1) *FCFS*-based allocation: LEO satellite adopts the first-come-first-serve policy by allocating all available resources to the first requesting SSG; (2) *Random* allocation: LEO satellite randomly allocates computing and communication resources for each SSG; and (3) *Average* allocation: LEO satellite equally allocates computing and communications resources to each SSG. For *FCFS*-based resource allocation algorithm, if multiple SSGs start to process or transmit sensing data at the same time, all available resources will be equally allocated to SSGs.

Figure 5.5 shows the performance under different CV densities in rural areas. When traffic density is low, both *FCFS* and the proposed CSTRS schemes can satisfy reliability, whereas the resource cost differs significantly. The proposed scheme allocates resources according to urgency reflected by AoI and queue states, reducing unnecessary resource consumption. As the CV density increases, the difference becomes more pronounced. *FCFS* prioritizes early arrivals rather than urgent sensing tasks, leading to insufficient resources for other groups and degraded reliability. Meanwhile, random and average allocation ignore the stringent data freshness requirements of different CVs, resulting in low reliability performances. In contrast, the proposed scheme maintains reliability by dynamically prioritizing groups with higher freshness risk, demonstrating the necessity of adaptive allocation in dynamic STVNs.

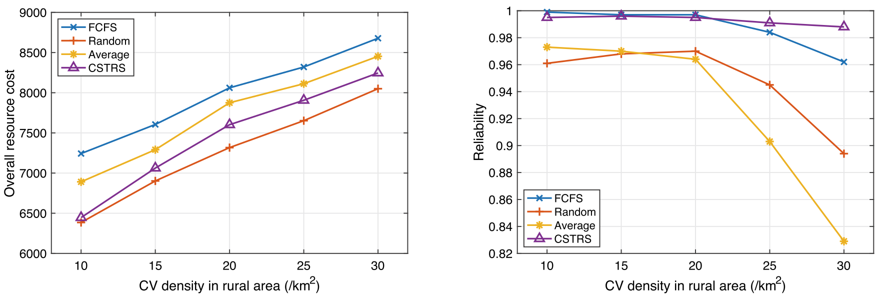

(a) Resource cost performance. (b) Reliability performance.

Fig. 5.5 Performance of different resource allocation algorithms

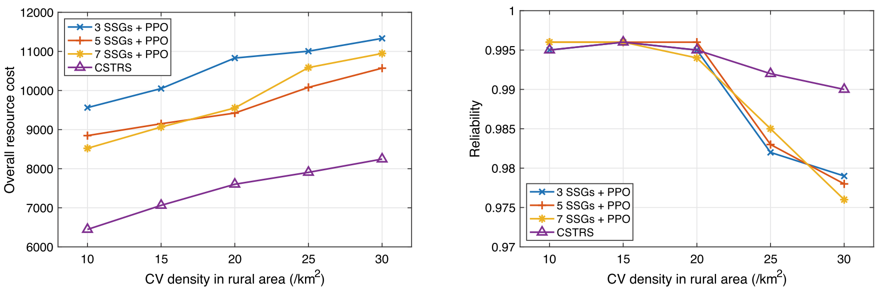

(a) Resource cost performance. (b) Reliability performance.

Fig. 5.6 Performance of different CV partition policies

Next, we evaluate the effectiveness of the large-timescale PSO-assisted sensing interval and CV partition algorithm in our proposed CSTRS scheme. The benchmark algorithms are *fixed-number SSG* with a predetermined SSG number and *k*-means algorithm for clustering, which is solely based on CV positions at the beginning of each time interval. The sensing interval of each SG is determined through **Algorithm** 3, while the communication and computing resources are allocated by adopting the PPO-based algorithm.

Figure 5.6 compares the resource cost and reliability performances of different CV partition methods with different CV densities in rural areas. The proposed CSTRS scheme with adaptive grouping significantly reduces resource cost compared with other methods in dynamic STVN environments by jointly considering both LEO satellite and terrestrial network capability. When CV density increases, *fixed-number SSG* strategies face challenges in effectively utilizing terrestrial and satellite resources due to improper CV partitioning and sensing intervals. Particularly, the reliability of *fixed-number SSG* strategies cannot be fully guaranteed with a high CV density due to inefficient resource allocation. In contrast, the proposed partition adapts the sensing interval and grouping simultaneously, consistently maintains a low level of resource cost, while satisfying reliability requirements.

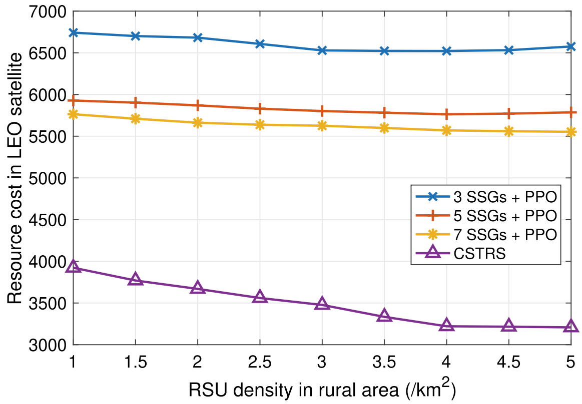

Fig. 5.7 Resource cost in LEO satellite under different RSU densities in rural area

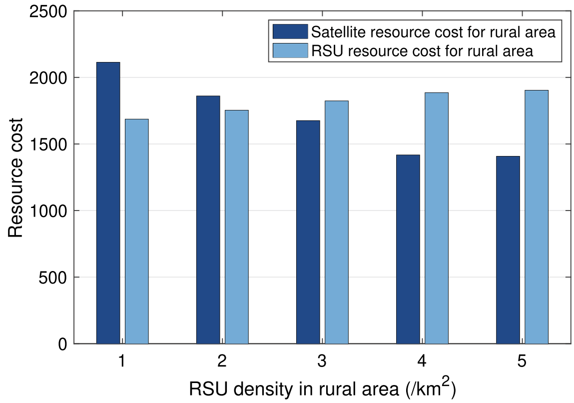

Fig. 5.8 Resource cost in rural areas from terrestrial and LEO satellite networks

We further investigate the cooperation between satellite and RSU infrastructure by comparing the LEO satellite resource cost of different CV partition strategies with different RSU densities in the rural area. Figure 5.7 shows that increasing RSU density significantly reduces satellite resource consumption through the CSTRS scheme. Specifically, the proposed CSTRS scheme adaptively shifts sensing responsibility toward available terrestrial infrastructure, while *fixed-number SSG* strategies struggle to exploit the spatial diversity across satellite and terrestrial networks. In this case, despite increased RSU densities, the sensing interval remains small for SSGs, resulting in a high resource cost.

Finally, Fig. 5.8 illustrates the resource cost for CVs in rural areas from the LEO satellite and terrestrial RSUs. We can observe that when RSU density increases, the RSU resource cost rises, while the satellite resource cost decreases more substantially for CVs. This is because the unit cost of satellite resources is higher than that of RSU resources, and RSU can effectively serve more CVs with the same cost. Therefore, cooperative resource scheduling from satellite and terrestrial networks minimizes the total cost by preferentially utilizing low-cost terrestrial resources while maintaining satellite coverage for sparse regions.

5.6 Summary

In this chapter, we investigated a joint communication and computing resource scheduling problem for infrastructure-assisted environment sensing in STVNs at the operation stage. To cope with the dynamic network environment and stringent freshness and reliability requirements, we proposed the CSTRS scheme, which is a hybrid model–data co-driven approach that jointly determines CV partitioning, sensing intervals, and real-time resource allocation decisions. By enabling cooperative scheduling between satellite and terrestrial networks, the proposed scheme effectively exploits their complementary characteristics, achieving reliable sensing performance with reduced resource consumption. Simulation results demonstrated that the CSTRS scheme significantly improves resource efficiency while maintaining high reliability compared with benchmark schemes. Beyond long-term reservation-stage resource management, real-time orchestration of heterogeneous resources is essential for supporting delay-critical vehicular services, thereby completing the slicing-based two-stage resource management framework for STVNs from reservation to operation.

References

1. Chen, Q., Xie, Y., Guo, S., Bai, J., Shu, Q.: Sensing system of environmental perception technologies for driverless vehicle: a review of state of the art and challenges. Sens. Actuators, A Phys. **319**, 112566 (2021)
2. 5GAA: C-V2X Use Cases Volume II: Examples and Service Level Requirements. White paper (2020)
3. Arnold, E., Dianati, M., de Temple, R., Fallah, S.: Cooperative perception for 3D object detection in driving scenarios using infrastructure sensors. IEEE Trans. Intell. Transp. Syst. **23**(3), 1852–1864 (2020)
4. Liu, X., Ma, T., Tang, Z., Qin, X., Zhou, H., Shen, X.: Ultrastar: a lightweight simulator of ultra-dense LEO satellite constellation networking for 6G. IEEE/CAA J. Autom. Sinica **10**(3), 632–645 (2023)
5. Wu, H., He, M., Shen, X., Zhuang, W., Dao, N., Shi, W.: Network performance analysis of satellite-terrestrial vehicular network. IEEE Internet Things J. **11**(9), 16829–16844 (2024)
6. He, M., Wu, H., Shen, X., Zhuang, W.: Cooperative resource scheduling for environment sensing in satellite-terrestrial vehicular networks. IEEE Internet Things J. **12**(6), 6734–6748 (2025)
7. Kaul, S., Yates, R., Gruteser, M.: Real-time status: how often should one update? In: Proceedings of the IEEE INFOCOM, pp. 2731–2735 (2012)
8. ETSI, Intelligent Transport Systems (ITS), Vehicular Communications; Basic Set of Applications: Part 2: Specification of cooperative awareness basic service, document v1.4.1. European Standard EN 302 637–2 (2019)

9. Teng, H., Li, Z., Cao, K., Long, S., Guo, S., Liu, A.: Game theoretical task offloading for profit maximization in mobile edge computing. IEEE Trans. Mobile Comput. **22**(9), 5313–5329 (2022)
10. Ramakrishnan, N., Soni, T.: Network traffic prediction using recurrent neural networks. In: Proceedings of the IEEE ICMLA, pp. 187–193 (2018)
11. Zhang, Y., Wang, S., Chen, B., Cao, J., Huang, Z.: Trafficgan: network-scale deep traffic prediction with generative adversarial nets. IEEE Trans. Intell. Transp. Syst. **22**(1), 219–230 (2019)
12. Cygan, M., Kowalik, Ł, Wykurz, M.: Exponential-time approximation of weighted set cover. Inf. Process. Lett. **109**(16), 957–961 (2009)
13. Clerc, M., Kennedy, J.: The particle swarm-explosion, stability, and convergence in a multidimensional complex space. IEEE Trans. Evol. Comput. **6**(1), 58–73 (2002)
14. Saad, W., Han, Z., Debbah, M., Hjorungnes, A., Basar, T.: Coalitional game theory for communication networks. IEEE Signal Process. Mag. **26**(5), 77–97 (2009)
15. Bogomolnaia, A., Jackson, M.O.: The stability of hedonic coalition structures. Games Econ. Behav. **38**(2), 201–230 (2002)
16. Neely, M.J.: Stochastic network optimization with application to communication and queueing systems. Synth. Lectures Commun. Netw. **3**(1), 1–211 (2010)
17. Schulman, J., Wolski, F., Dhariwal, P., Radford, A., Klimov, O.: Proximal policy optimization algorithms (2017). arXiv:1707.06347
18. de Almeida, T.T., de Carvalho Gomes, L., Ortiz, F.M., Júnior, J.G.R., Costa, L.H.M.: Comparative analysis of a vehicular safety application in NS-3 and veins. IEEE Trans. Intell. Transp. Syst. **23**(1), 620–629 (2020)
19. Tan, K., Feng, L., Dán, G., Törngren, M.: Decentralized convex optimization for joint task offloading and resource allocation of vehicular edge computing systems. IEEE Trans. Veh. Technol. **71**(12), 13226–13241 (2022)
20. Bittencourt, L.F., Diaz-Montes, J., Buyya, R., Rana, O.F., Parashar, M.: Mobility-aware application scheduling in fog computing. IEEE Cloud Comput. **4**(2), 26–35 (2017)

Chapter 6
Summary and Future Directions

Abstract In this chapter, we summarize the main contributions of this monograph and discuss some future research directions for resource management in STVNs.

Keywords Satellite-terrestrial vehicular networks · User-centric service provisioning · Agent-based intelligence · Autonomous resource management

6.1 Summary

In this monograph, we have developed a unified framework for resource management in STVNs. By jointly considering satellite communication characteristics and vehicular service requirements, a two-stage slicing-based management has been investigated, integrating theoretical performance modeling, long-term resource reservation, and real-time resource allocation. The proposed framework enables coordinated utilization of communication, computing, and caching resources across satellite and terrestrial networks, providing reliable connectivity, efficient resource usage, and adaptive service provisioning for diverse CV applications. The main contributions of this monograph are summarized as follows:

1. A tractable analytical framework has been developed to characterize satellite–terrestrial communication considering satellite mobility, constellation configuration, and terrestrial deployment strategies. Based on analytical models, key performance metrics can be evaluated, including service availability, outage probability, and system throughput. The results reveal the joint impact of satellite coverage dynamics and ground infrastructure deployments on network reliability and capacity, providing theoretical insights for STVNs and guidelines for resource management mechanisms.
2. Building upon the analysis, a slicing-based two-stage resource management framework has been proposed to coordinate communication, computing, and caching resources across satellite and terrestrial segments, which can reduce decision complexity while maintaining responsiveness to dynamic environments. At the reservation stage, we have studied HD map distribution in STVNs and proposed a TLRS scheme. By exploiting the heterogeneous characteristics of multicast and unicast transmission modes, communication and caching resources

M. He et al., *Resource Management for Satellite-Terrestrial Vehicular Networks*, SpringerBriefs in Computer Science, https://doi.org/10.1007/978-3-032-24526-7_6

are jointly reserved across satellite and terrestrial networks. A hybrid data–model co-driven design has been developed, where reinforcement learning determines slicing window length and communication resource reservation, and a matching-based algorithm optimizes multicast and caching decisions. The proposed scheme can effectively balance resource utilization, delay performance, and slice reconfiguration overhead under time-varying service demand and satellite availability.

3. At the operation stage, we have investigated cooperative environment sensing and the proposed CSTRS scheme. By leveraging the multicast capability of satellites with dynamic connectivity conditions, CVs are grouped according to mobility and sensing requirements, and sensing intervals are adaptively determined using coalition formation and particle swarm optimization methods. Based on the resulting grouping structure, a reinforcement learning-based algorithm has been developed for real-time communication and computing resource allocation to satisfy freshness and reliability requirements under highly dynamic connectivity conditions.

Overall, this monograph establishes a unified theoretical and practical framework for resource management in STVNs. The proposed methodologies demonstrate how the complementary characteristics of satellite and terrestrial infrastructures can be exploited to enable reliable and adaptive service provisioning for CVs. The developed theoretical modeling and resource management schemes can also provide design guidelines for the evolution of resilient, scalable, and intelligent transportation systems, and supporting innovations in integrated satellite–terrestrial networks.

6.2 Future Research Directions

The evolution of STVNs toward connected and intelligent vehicles reshapes service provisioning, task inference, and network management. For future research, several promising directions are outlined as follows.

1. **User-centric service provisioning in STVNs:** In STVNs, CVs may prefer satellite or terrestrial connectivity depending on latency, coverage, and service characteristics. However, unlike conventional heterogeneous networks, such preferences evolve along mobility and connectivity availability. A link that maximizes instantaneous performance may degrade the overall experience due to short connection durations, frequent handovers, or unstable availability along the driving trajectory. Moreover, even for the same application, users exhibit diverse Quality of Experience (QoE) requirements, such as different tolerance to delay, jitter, or interruption, which cannot be adequately captured by slice-level QoS guarantees. These characteristics motivate user-centric service provisioning in STVNs, where resource orchestration is guided by the evolution of user experience rather than instantaneous service performance. By leveraging spatiotemporal information, including trajectory prediction and future visibility windows, the network can

proactively maintain high QoE performance through adaptive access selection, transmission pacing, and service continuity control. Realizing such provisioning requires scalable mechanisms that transform predicted network dynamics into user experience control while balancing personalization and overall resource efficiency, forming user-centric STVN management.

2. **Resource management for intelligent agents in STVNs:** CVs are evolving from data consumers to intelligent agents capable of perception, reasoning, and collaborative decision-making, forming connected autonomous vehicles (CAVs). Unlike traditional applications that request predefined data services, agent-based driving relies on continuous state interaction, cooperative inference, and distributed decision execution. Consequently, network traffic is no longer externally generated but emerges during iterative perception–decision cycles, resulting in runtime-evolving execution graphs and consequently non-stationary workloads. Specifically, each intermediate observation during the inference may trigger replanning, tool invocation, or model escalation. This leads to a tightly coupled system in which agent behaviors reshape resource demand while network conditions simultaneously influence agent strategies. Such interaction requires intention-aware transmission, inference-oriented scheduling, and coordinated computing across satellite and terrestrial infrastructures, rather than conventional latency- or throughput-driven resource orchestration. Therefore, supporting distributed intelligence requires a new resource management paradigm while controlling resource consumption and ensuring service reliability for future STVN resource management.
3. **Agent-based autonomous management of STVNs:** STVNs operate over a large-scale and highly dynamic environment, where satellite mobility, intermittent visibility, and geographically shifting demand make globally synchronized or fully centralized control difficult and time-consuming in practice. A promising direction is to move toward agent-based autonomous management, where distributed agents embedded in network entities act on behalf of the operator through intent-driven closed loops, supported by enhanced observability, knowledge representations, and digital twins for pre-execution validation. Specifically, agents can exploit multi-source yet underutilized information, including predictable orbital trajectories, beam coverage schedules, satellite visibility windows, and multi-domain load states, to proactively coordinate reservation, access selection, and operation-stage scheduling. Enabling such operation requires network management to evolve from periodic optimization toward continuous decision loops where network entities maintain local situational awareness and coordinate actions through information exchange. In this case, new mechanisms are required for STVN management, such as semantic observability that exposes intent-relevant state, coordination for distributed decision alignment, and digital-twin-assisted evaluation for validating candidate actions before deployment. These capabilities establish the foundation for agent-based autonomous management in STVNs, allowing the network to operate as an intent-driven, predictive, and self-regulating system.